Dissertations, Theses, and Masters Projects   Theses, Dissertations, & Master Projects

2020

The Role Of Suspended Sediment In Assessing Coastal Wetland Vulnerability

Daniel J. Coleman

William & Mary - Virginia Institute of Marine Science, djcoleman@vims.edu

Follow this and additional works at: https://scholarworks.wm.edu/etd

Part of the Geomorphology Commons

The Role of Suspended Sediment in Assessing Coastal Wetland Vulnerability

—————

A Dissertation

Presented to

The Faculty of the School of Marine Science

The College of William & Mary

In Partial Fulfillment

of the Requirements for the Degree of

Doctor of Philosophy

—————

by

Daniel J. Coleman

May 2020

APPROVAL PAGE

This dissertation is submitted in partial fulfillment of

the requirements for the degree of

Doctor of Philosophy

Daniel J. Coleman

Approved by the Committee, May 2020

Matthew L. Kirwan, Ph.D.
Committee Chair / Advisor

Carl T. Friedrichs, Ph.D.

Christopher J. Hein, Ph.D.

David S. Johnson, Ph.D.

Glenn R. Guntenspergen, Ph.D.
United States Geological Survey
Duluth, Minnesota

TABLE OF CONTENTS

ACKNOWLEDGEMENTS

I would like to thank my advisor, Dr. Matt Kirwan, for his support, enthusiasm, and dedication. He compassionately and respectfully pushed me to become a better scientist. I owe him a debt of gratitude for shaping my academic experience into the rewarding venture it has been.

My committee members have been of great value throughout my dissertation. Through insightful comments on my research, well-taught classes, and a friendly and supportive demeanor, they have helped me achieve my academic goals. Additionally, I would like to thank the many collaborators who have been vital for enhancing the quality of my dissertation. I would especially like to thank Dr. Kerrylee Rogers who served as my mentor for Chapter 3, as well as a thoughtful host for my time spent in Australia. I could not have conducted international research without her scientific and personal support.

The Kirwan lab has been a continuously evolving, supportive group of scientists. The scientifically stimulating conversation held in lab meetings have shaped my dissertation into what it is. Their contributions to field and lab work was invaluable. Just without their help grinding sediment, I would have been in graduate school another three years.

My family and friends have, of course, been a huge part of my success during graduate school. The emotional support they provided made my goal of achieving a Ph.D. tenable. Beyond the quality-of-life improvements they provided, my friends and family where often roped into fieldwork in uninviting conditions, in-depth conversation about statistics over coffee, and late-night lab work. While many of them may never read my dissertation—or at least not enjoy doing so—they have played a crucial part in its fruition.

Finally, I would like to thank my fiancé, Matt Guenther. Matt is a constant source of love and support that has helped me face the numerous challenges on the path to a Ph.D. Having him by my side has made this journey not only possible, but worthwhile.

ABSTRACT PAGE

Coastal wetlands sequester carbon, attenuate waves and storm surge, filter out nutrients and pollutants, and act as nursery habitat for important fisheries. The value of these ecosystems is underscored by their vulnerability to climate change, especially sea level rise. To persist under the threat of rising sea level, coastal wetlands must build elevation vertically. Delivery of sediment to the marsh during tidal flooding is a key component in the ecogeomorphic feedbacks that lead to elevation gain. Despite the importance of suspended sediment to assessing coastal wetland vulnerability, many questions remain unanswered. This dissertation addresses the impact of suspended sediment concentration on wetland geomorphology from fine-scale processes to global patterns and from thriving systems to those experiencing significant environmental change. In Chapter I, I explore alterations to sediment transport and geomorphology caused by an acute vegetation disturbance in a Georgia saltmarsh. My results showed that the loss of vegetation was reversed the trajectory of the site from a prograding marsh to an eroding marsh. In Chapter II, I investigate how suspended sediment travels across the marsh platform using high frequency, long-term measurements in the Plum Island Estuary, Massachusetts. In contrast to the current paradigm, I found that sediment supply in the marsh interior is largely decoupled from channel sediment supply. Chapter III focuses on the role of sediment transport in mangrove encroachment into salt marshes in Australia. My work suggests that mangroves do not inhibit the ability of salt marsh to accrete vertically and that the removal of mangroves to preserve salt marsh would be ineffective. In Chapter IV, I analyze the relationship between suspended sediment concentration, tidal range, and accretion in salt marshes from around the world. My work emphasizes the importance of mineral accretion and marsh elevation when making predictions about marsh response to sea level rise. These results help bridge the gap between numerical models which predict marshes are capable of surviving high rates of relative sea level rise and field studies which suggest drowning at much lower rates. As a whole, my dissertation demonstrates that physical processes and the ways in which biology mediate these processes are critical to the ability of coastal wetlands to persist. As the rate of sea level rise continues to accelerate, it is increasingly important to understand the controls on vertical elevation growth in coastal wetlands at the scale of several meters to thousands of kilometers and in pristine systems to degraded environments.

The Role of Suspended Sediment in Assessing Coastal Wetland Vulnerability

CHAPTER I

The Effect of a Small Vegetation Dieback Event on Salt Marsh Sediment

Transport

Coleman, D.J., & Kirwan, M.L., (2019). The effect of a small vegetation dieback event on salt marsh sediment transport. *Earth Surface Processes and Landforms 44*(4), 944-952, https://doi.org/10.1002/esp.4547

Abstract

Vegetation is a critical component of the ecogeomorphic feedbacks that allow a salt marsh to build soil and accrete vertically. Vegetation dieback can therefore have detrimental effects on marsh stability, especially under conditions of rising sea levels. Here, we report a variety of sediment transport measurements associated with an unexpected, natural dieback in a rapidly prograding marsh in the Altamaha River Estuary, GA. We find that vegetation mortality led to a significant loss in elevation at the dieback site as evidenced by measurements of vertical accretion, erosion, and surface topography compared to vegetated reference areas. Belowground vegetation mortality led to reduced soil shear strength. The dieback site displayed an erosional, concave-up topographic profile, in contrast to the reference sites. At the location directly impacted by the dieback, there was a reduction in flood dominance of suspended sediment concentration. Our work illustrates how a vegetation disturbance can at least temporarily reverse the local trajectory of a prograding marsh and produce complex patterns of sediment transport.

Introduction

Ecogeomorphology—the study of geomorphic processes, ecological factors, and their interactions—is required to understand the evolution of numerous systems (Murray et al. 2008; Reinhardt et al. 2010). Such interactions dominate the topographic evolution of hill slopes (Saco et al. 2007, Pawlik et al. 2007), river floodplains (Steiger et al. 2005), beach dunes (Duran and Moore 2013), and salt marshes (Fagherazzi et al. 2004). Salt marshes are one of the classical ecogeomorphic systems, where two-way interactions shape the landscape and play a primary role in marsh stability (Redfield 1972, Reed 1995, Kirwan and Megonigal 2013, D'Alpaos and Marani, 2016). For example, elevation in the tidal frame is a major control on type and abundance of vegetation, which in turn promotes sediment deposition and thus affects elevation (Morris et al. 2002, Temmerman et al. 2003, Kirwan et al. 2010, Fagherazzi et al. 2012 and references therein). Animal activity also impacts marsh geomorphology; for example, grazing pressure from crabs can reduce vegetation and lead to sediment erosion (Hughes et al. 2009, Smith 2009, Smith and Green 2015).

Vegetation disturbances, or diebacks, are common in salt marshes, occurring throughout the world and affecting all elevations and geomorphic settings (Alber et al. 2008). Prominent examples include marshes from the Gulf Coast (DeLaune et al. 1994, Lindstedt et al. 2006, Day et al. 2011), southeastern (Silliman et al. 2005, Ogburn and Alber 2006, Alber et al. 2008, Li and Pennings

2016), and northeastern (Bertness and Ellison 1987, Holdredge et al. 2009, Smith 2009, Alteiri et al. 2013) regions of the U.S Atlantic Coast. For instance, in Louisiana in 2001, a statewide dieback reached 126,000 acres of marsh (Lindstedt et al. 2006). In Georgia, dieback affected 2,000 acres of marsh in 2001-2002 (Ogburn and Alber 2006), and the region continues to experience smaller scale events (Alber et al. 2008). *Spartina alterniflora* is the most common species to die back, but a host of other salt marsh plants can as well (Alber et al. 2008). Similarly, all geomorphic features of the marsh such as the creek edge and interior exhibit such events (Alber et al. 2008).

The variety of sites impacted likely stems from the variety of causes of dieback. Vegetation dieback is often linked in part to drought (Silliman et al., 2005; Alber et al., 2008), but can also be caused by herbivory (Smith and Green, 2015; Silliman et al. 2005; Holdredge et al. 2009), salt stress (Hughes et al. 2012), soil toxicity (Mckee et al. 2004), oil spills (Silliman et al. 2012, Lin et al. 2016), wrack deposits (Fischer et al. 2000), and other factors. In some cases, a marsh can recover from a dieback (Ogburn and Alber 2006, Angelini and Silliman 2012, Alteiri et al. 2013). The 2001 Louisiana dieback shrank to approximately 13% its original size after two years, indicating significant recovery (Lindstedt et al. 2006). However, diebacks can also be permanent, especially if the marsh experiences erosion (Lottig and Fox 2007, Silliman et al. 2012), such that the marsh elevation becomes too low for vegetation to grow (Wang and Temmerman 2013; van Belzen et al. 2016).

Vegetation loss often causes erosion, through the combination of enhanced flow velocities and weaker soils (Temmerman et al. 2012, Lin et al. 2016). For example, oil-induced vegetation mortality that extended to the belowground parts of the plant resulted in increased edge erosion (Silliman et al. 2012). This erosion however, may act as a source of sediment for the surrounding marsh, enhancing overall resiliency to sea level rise (Mariotti and Carr 2014, Hopkinson et al. 2018). For example, the rapidly eroding marsh complex of the Blackwater River (Maryland) had higher suspended sediment concentrations (SSC) and vertical accretion rates than a more stable adjacent system (Ganju et al. 2015).

Here, we study sediment transport before and after a small dieback event at a previously prograding marsh. We find that vegetation loss led to significant erosion and a local reversal of rapid marsh progradation.

Methods

Study Site and Approach

This study was conducted in a *Spartina alterniflora* marsh within the Altamaha River estuary system in Georgia, USA (31°17'59"N 81°24'24"W) (Figure 1). The lower Altamaha has a 2m tidal range and is characterized by expansive brackish and saline marshes (GCE LTER, https://gce-lter.marsci.uga.edu). Average salinities range from 5-20 PSU and average plant biomass ranges from approximately 1700-1000 g/m², respectively (Wieski et al.

2010). Our study site is a rapidly accreting, youthful salt marsh (<30 years old based off of aerial photography) located along a small tidal channel west of Little Broughton Island (Figure 1). The site ranges from approximately -0.8 m to +0.3 m mean sea level, based off the nearby vertical benchmark on St. Simon's Island. Proximate dredging in the early 1970s led to channel network reorganization (Hardisky 1978), and progradation of marsh into an infilling channel at our site. Analysis of 8 historical photographs (earthexplorer.usgs.gov) indicates significant marsh progradation, reducing open water area from over 650,000 m^2 to less than 125,000 m^2 between 1975 and 2013 (Figure 2). As a result, the site is characterized by a smooth topographic profile from channel to marsh platform without a scarp or levee, typical of concave-down, prograding marshes (Mariotti and Fagherazzi 2010).

The initial goal of this study was to monitor how seasonal vegetation growth influenced sediment transport across the marsh. We monitored sediment deposition rates, turbidity, and biomass along a transect from the channel to the marsh interior for an entire year. However, two months into the study, in early August 2016, vegetation began to die in a narrow band adjacent and parallel to the channel edge. By December 2016, the dieback reached its maximum spatial extent—over 6m in shore length and over 2m in width—and demonstrated erosive features such as exposed roots, gullies, and undercut equipment (Figure 3). The size of the dieback remained relatively constant through spring 2017 until there was some indication of recovery in early summer 2017. This unexpected event prevented us from evaluating the role of seasonal vegetation growth on

suspended sediment dynamics, but allowed us to address how a dieback event influences marsh sediment transport and surface elevation. To address the impact of the dieback, we supplemented our seasonal monitoring with one time measures of soil shear strength, rhizome mortality, and elevation profiles.

Seasonal monitoring of sediment transport

We measured turbidity and sediment deposition along a transect from channel to marsh interior for 1 year, beginning in June 2016. We measured turbidity (NTU) with optical back scatter sensors to quantify sediment transport from the channel across the marsh. The transect consisted of three turbidity sensors in a shore normal transect, with one in the channel (YSI 6600), and two on the marsh surface (referred to as the channel sensor and marsh sensors, respectively). The "marsh edge sensor" was 2.4m from the channel edge (Seapoint, RBR Solo) and the "marsh interior sensor" was 18m from the edge (Seapoint, RBR Duo; Figure 1c). The sensors measured every 15 minutes and were equipped with automatic wipers to reduce biofouling. Sensors were cleaned and maintained and the data downloaded on approximately bimonthly site visits. Following retrieval, the turbidity time series data was filtered to remove any erroneous points and times when the sensors were fouled or exposed (Ganju et al. 2005).

Turbidity data was converted to suspended sediment concentration (SSC) via a combination of in situ field sampling and laboratory calibrations using sediment collected from the site. In the field, we measured turbidity with an

additional sensor at various locations around the site and at different tidal stages, and collected a water sample in conjunction with each reading. In the lab, we created sediment-water slurries with a range of SSC and used a turbidity sensor to measure the slurries while they were kept in constant motion to avoid sediment settling. We compared sensor turbidity measurements to total suspended solid measurements obtained via vacuum filtration of water samples from the site and lab-created water-sediment slurries. The y-intercept value was set to zero, resulting in the equation SSC (mg/L) =1.33*Sensor Turbidity (NTU) (R^2=0.9345, n=26, p<<0.001). The data was then divided into pre-dieback (June 1, 2016-August 31, 2016) and post-dieback (September 1, 2016-April 18, 2017) periods. We calculated the average SSC for each sensor when all sensors were flooded for both time periods. The channel sensor also recorded water pressure which we converted to water depth by adjusting for barometric pressure. We then separated the turbidity time series into flooding (increasing depth) and ebbing (decreasing depth) tidal phases and calculated the difference in SSC on the flood versus ebb tide over both time periods. We computed and compared 95% confidence intervals for all SSC values.

Sediment deposition on top of ceramic titles and plastic grids was measured to quantify spatial gradients in accretion rates across the marsh (see Pasternack and Bush 1998). The sediment tiles and grids were installed in June 2016 in two shore parallel transects centered on the marsh turbidity sensors (Figure 1c). Five replicates of both the sediment tiles and grids were deployed at each of these transects. The sediment tiles were drawer-liner paper (to give a

rough surface) glued to the top of a 15.5cm x 15.5cm ceramic tile affixed to a PVC stake (Figure 3c). The stakes were pushed into the sediment so that the top of tile was flush with the surface. We cut 14.5cm x 14.5cm squares from fluorescent tube lighting covers which were plastic grids with 1.5cm^2 openings. The grids were then staked flush to the initial marsh surface. The openings in the grids allowed vegetation to grow through them, giving a natural surface.

The use of these sediment tiles and grids allowed for the calculation of mass accumulation rates and cumulative surface changes, respectively. All of the sediment accumulated on sediment tiles was scraped off during each subsequent visit, dried and weighed. This resulted in a mass of sediment per amount of time between visits, i.e. a mass accumulation rate. The sediment tiles were reinstalled flush with the marsh surface after each collection. The plastic grids function similarly to marker horizons. The difference between the sediment surface and grid surface was measured at each subsequent visit. A positive difference represents net deposition, while a negative difference represents net erosion. The difference between the sediment tile surface and sediment surface was only measured after the surface dropped below the tile. We averaged the cumulative vertical change in sediment surface height for each turbidity sensor location (edge or interior) for each site visit.

Post-dieback Measurements

In response to the unexpected dieback event, we made a variety of other measurements in spring 2017 to better quantify the dieback and its impact. All post-dieback measurements were collected at three sites: the dieback area, a

north reference area, and a south reference area. The dieback area refers to the site where initial monitoring began. The north reference area and the southern reference area are both vegetated reference sites approximately 10 and 20m from the dieback area, respectively (Figure 1c), where vegetation dieback did not occur. The north reference site is approximately 10 m from a small creek to the north.

To address the changes in elevation and marsh surface profiles associated with the dieback, we measured elevation along shore-normal transects using a Topcon RTK GPS system. We measured elevation along two transects for each the north reference area and the south reference area, totaling four "vegetated" topographic profiles. We measured along three transects through the dieback area, one along the turbidity sensor transect, and two intersecting the north and south ends of the sediment tile and grid transects (Figure 1c). All elevations were recorded relative to NADV88. Individual profiles were linearly interpolated between measured points to calculate an average topographic profile for vegetated and dieback areas.

To quantify the differences in shape between the average dieback profile and the average vegetated profile, we calculated the presence/location of any inflection points. A concave up marsh topographic profile implies erosion whereas a concave down profile implies deposition (Kirby 2000, Wilson and Allison 2008, Mariotti and Fagherazzi 2010). For this we first performed a coarse smoothing spline and then calculated the second derivative. The presence and

location of inflection points was defined as the location where the second derivative is equal to zero.

We calculated a loss of elevation in the dieback area by comparing the dieback topographic profile to the vegetated profile. We calculated the average difference in elevation between the vegetated profile and the portion of the dieback profile without living plants to determine a magnitude of elevation loss. From this value, we subtracted any measured erosion from the sediment tiles and plastic grids to produce an upper bound of possible subsidence. To approximate the volume of sediment lost we performed a low and high-end estimate. For the low-end estimate, we determined what volume of sediment would be required to fill the topographic concavity that was evident in the region of dead vegetation. For the high-end estimate, we assumed the topographic profiles were initially similar, and then determined the amount of sediment required to fill in the dieback profile so that it would not be statistically different than the vegetated profile

We collected sediment cores to determine if the vegetation death extended to belowground components of the plant. Specifically, we collected five cores (5cm diameter by 15cm length) from each area (i.e. the dieback area, north reference, and south reference areas). We washed each core over a 1mm sieve to extract belowground biomass. Rhizomes were collected and classified as living or dead based on color, turgor pressure, and attachment to other living material. The total number of live and dead were pooled for each of the three

locations. We conducted a z-score test for population proportions for the percent of living rhizomes to determine significance (α=0.05).

We measured in situ soil shear strength with a shear vein to determine the role the dieback may have played in affecting soil erodibility. The 50.8 x 101.6 mm head of a Humboldt H-4227 shear vein was inserted completely into the soil and was turned until the soil broke, giving a strength reading that represents the top 10 cm of the soil (after Howes et al. 2010). We performed this test with 15 replicates in the area affected by the dieback, and corresponding locations in the north reference, and south reference sites. We averaged results for each location and compared them with an ANOVA (α=0.05) to determine significance.

Results

Suspended Sediment Concentration

Measurements of SSC differ slightly from before versus after the dieback (Figure 4). The magnitude of SSC after the dieback is marginally significantly higher than before the dieback at the creek and interior locations (Figure 4a). Prior to the dieback, SSC was 41.2mg/L ± 2.45, 37.7 mg/L ± 1.00, and 22.8 mg/L ± 0.68 respectively for the creek, edge, and interior (mean and 95% confidence interval). After the dieback the SSC was 45.7 mg/L ± 1.85, 39.0 mg/L ± 1.27, and 24.7 mg/L ± 0.71 respectively for the creek, edge, and interior. SSC decreases with distance into the marsh both pre- and post-dieback.

The difference between flood tide SSC and ebb tide SSC, or flood-ebb differential, also differs before and after the dieback. The flood-ebb differentials

were all small in magnitude and positive, with most not being statistically different than zero. The flood-ebb differential was smaller after the dieback than before the dieback, but only significantly different at the marsh edge location (Figure 4b).

Deposition and Erosion.

Our seasonal measurements of sediment deposition and erosion indicate that the dieback event is contemporaneous with a switch from rapid deposition to rapid erosion at the marsh edge. For the first two months of measurement, both the marsh edge (Figure 5a) and interior sites (Figure 5b) experienced net positive changes in surface elevation measured over the plastic grids totaling 19.2mm ± 12.1 (mean ± 1σ) and 7.5mm ± 2.5 of deposition, respectively. Both sites also had positive mass accumulation measured with the sediment tiles (a maximum of 0.72g/day ± 0.41 at the edge and 0.25g/day ± 0.25 at the interior). Immediately following the dieback in December 2016, the edge site lost elevation compared to the initial elevation (-4.4mm ± 14.4) whereas the undisturbed interior site continued to gain elevation (8.7mm ± 3.1 in December 2016, totaling 24.0mm ± 6.8 by the end of May 2017). Similarly, the mass accumulation rate at the edge site quickly decreased to near zero following the dieback whereas the undisturbed interior maintained positive mass accumulation (a maximum of 0.73g/day ± 0.35 by the end of May 2017, Figure 5c-d). The change from accretion to erosion at the edge site meant that the sediment tiles were no longer useful in measuring mass accumulation, but could be used to quantify erosion by measuring the gap between the sediment surface and the sediment tile. We

14

found consistent patterns between the sediment tiles and plastic grids. The maximum elevation loss at the edge, as evidenced by the difference between the August surface elevation and the late-spring, is -33.5 mm ± 27.5 based off the sediment tiles and -28.5 mm ± 13 based off the plastic grids. Following a late-spring minimum, there was an increase in surface elevation at the edge, evidenced by both the sediment tiles and plastic grids.

Elevation profiles through the dieback and reference areas also reveal impacts of vegetation mortality on sediment deposition and erosion (Figure 6). The vegetated profile and the region of the dieback profile with living plants are both concave down, indicating deposition (Mariotti and Fagherazzi 2010). However, the profile through the portion of the dieback area with dead plants is concave up, consistent with an erosional profile (Kirby 2000, Wilson and Allison 2008). The average elevation difference between the vegetated profile (green) and the area of the dieback without living plants (blue dashed line) was 39.1 cm ±4.1.

To calculate an amount of sediment absent from the dieback topographic profile, we calculated low and high-end estimates. For the low-end estimate of sediment missing from the dieback profile, we drew the longest line possible within the devegetated zone such that the line was always above the profile (thin black line, Figure 6b). The difference in area between this line and a high-order polynomial approximation of the dieback curve was 0.15 m^3/meter of shoreline, which represents the minimum amount of sediment that would be required to eliminate the concave up nature of the dieback profile. For the high-end estimate,

we calculated the average amount of sediment needed to eliminate statistical differences between the dieback and vegetated profiles. We calculated the area between a high-order polynomial approximation of the average vegetated profile and one for the dieback profile. We set horizontal bounds to this area at the creek edge and at the maximum distance from the creek for which the vegetated curve was still statistically different from dieback curve. This maximum distance was approximately where the confidence bands begin to overlap, farther inland than the concave up region used to calculate the low-end estimate (Figure 6b). Assuming the dieback profile was originally similar to the vegetated profile, we calculate that 1.62 m^3/meter of shoreline of sediment is missing. If the dieback profile was initially lower than the vegetated profiles, this would represent an overestimation.

Soil Characteristics

Rhizome mortality and soil strength measurements demonstrate that the effect of the vegetation dieback included subsurface soil properties. The dieback area had a significantly lower proportion of living rhizomes (2.6%, n=39) than the north reference area (32%, n=38) and the south reference area (39%, n=23) (p<0.001 for both; Figure 7a). There was no significant difference in rhizome mortality between the two reference areas (p=0.55). Rhizomes were found in all cores, and each area had some cores without any living rhizomes. The dieback area shear strength was 1.45 kPa ± 1.18, the north reference area was 3.38 kPa ± 1.25, and the south reference area was 3.53 ± 1.17 (Figure 7b). The dieback area had significantly weaker soil than the reference areas (ANOVA p<0.0001),

and there was no significant difference in soil shear strength between the reference areas (p=0.73).

Discussion

Salt mash dieback can be caused by a number of factors including drought (Alber et al. 2008), herbivory (Holdredge et al. 2009, Smith 2009, Smith and Green 2015), salt stress (Hughes et al. 2012), soil toxicity (Mckee et al. 2004), human-induced disturbances, such as oil spills (Silliman et al. 2012, Lin et al. 2016), wrack deposits (Fischer et al. 2000), and interactions between these factors (Silliman et al., 2005). Although it is difficult to determine the initial cause of a dieback after it has occurred (Ogburn and Alber 2005), wrack deposition is a common source of dieback in the region (Li and Pennings 2016). The dieback size (e.g. 10s of meters) and creek-adjacent location, is consistent with wrack-induced diebacks elsewhere in the Altamaha estuary. (Lottig and Fox 2007). Our site was located near a drainage creek which suggests multidirectional flow, making it particularly vulnerable to wrack deposits (Li and Pennings 2016). However, we did not observe wrack during site visits meaning that any wrack deposits would have been short-lived, and perhaps insufficient to cause the dieback.

Regardless of the initial cause, the dieback affected above and belowground biomass, leading to a weakening of the soil. The site lost over 12 m^2 of marsh plants above ground and the rhizome analysis shows extensive belowground mortality (Figures 3a and 7a). The death of the rhizomes is thought

17

to be necessary for soil weakening (Silliman et al. 2012). Our results support that interpretation, where areas with high rhizome mortality had a significantly lower soil shear strength (Figure 7).

At our site, the loss of vegetation and soil strength led to erosion and possibly subsidence. Previous work in the system suggests diebacks that occur late in the growing season (i.e. September, like this event) produce the greatest plant mortality and loss of biomass (Li and Pennings 2017). We measured approximately 3 cm of erosion based off the sediment tiles and plastic grid measurements (Figure 5a and b), whereas the elevation profile of the dieback area was approximately 40 cm below the reference vegetated sites (Figure 6). If we assume the dieback area and the reference areas began at the same height, and the dieback experienced 3 cm of erosion, then the area would have experienced a maximum of 37 cm of subsidence. However, it is possible that the dieback area was initially lower than the reference areas before the death of the plants. Therefore, 37 cm of subsidence represents an extreme upper bound. An initial low elevation may have even contributed to the dieback location since the likelihood of wrack deposition increases with decreasing marsh elevation (Bertness and Ellison 1987).

Both erosion and subsidence have been observed in other marsh dieback events (Hughes et al. 2009, Baustian et al. 2012, Wilson et al. 2012). Studies of vegetation death in Bayou Chitigue, LA USA, found an elevation decrease of about 8 cm during a timeframe comparable to ours (DeLaune et al. 1994, Day et al. 2011). No erosion was observed during the first year and all of the change in

elevation was attributed to subsidence caused by root decomposition and a loss of turgor pressure (DeLaune et al. 1994, Day et al. 2011). Monitoring for a second year discovered ~7 cm additional elevation loss, 2-3 cm of which was erosion (Delaune et al. 1994). A study in Bayou Lafourche, LA USA found that even with marginal surface vertical accretion of 0.2 cm/year, an unvegetated dieback area still lost elevation at nearly 1 cm/year (Baustian et al. 2012). In a study in Cape Romain, SC USA, vegetation dieback area at the head of expanding creeks were 60cm lower than the vegetated platform, caused by both subsidence and erosion (Hughes et al. 2009). This severe elevation loss occurred at the bottom of an incipient channel (Hughes et al. 2009) and likely represents an extreme and specific example. The erosion at our site (3 cm) is therefore consistent with values from similar settings presented in the literature, and the upper bound of possible subsidence (37 cm) likely represents an overestimation.

Our results offer some limited support to the idea that sediment eroded from the marsh edge becomes a source of sediment to other areas of the marsh. This marsh cannibalization process, which is found in some numerical and conceptual models, has been suggested to enhance overall marsh resiliency to SLR (Mariotti and Carr 2014, Currin et al. 2015, Hopkinson et al. 2018). Field evidence to support this hypothesis is limited. One study in Blackwater, MD USA found that marshes with high edge erosion had a higher SSC and vertical accretion than stable areas (Ganju et al. 2015). In Plum Island, MA USA, SSC increased further upstream eroding channels (Cavatorta et al. 2003), which could

mean erosion increases sediment availability. Additionally, recent geochemical analysis and sediment budgeting suggests marsh edge erosion is an important factor in maintaining elevation relative to sea level rise in Plum Island (Hopkinson et al. 2018). In our study, we found only a small increase in SSC associated with vegetation dieback and erosion (Figure 4), likely because of the small spatial scale of the dieback and relatively sparse spatial sampling. Previous work suggests dieback events intensify ebb tidal flows and lead to scour (Hughes et al. 2009). Intensified ebb transport is difficult to detect via the marsh interior sensor as it is higher in the tidal frame than the dieback or via the channel sensor as the large volume of water and sediment in the channel would dilute the signal. Nevertheless, the marsh edge sensor had a significant reduction in positive flood-ebb differential, which is consistent with net erosion (Figure 4). Marsh cannibalization is therefore plausible but remains understudied.

Conclusions

Our study adds to the large body of evidence highlighting the importance of vegetation in maintaining marsh vertical accretion and limiting lateral erosion. In our study, the marsh was rapidly accreting and prograding prior to the dieback event. In the first two months of our study, the vegetated marsh edge accreted nearly 2 cm of sediment. Above and belowground vegetation mortality led to lower soil shear strength, a switch from positive to negative elevation change, and the development of an erosional topographic profile. Our work therefore

demonstrates that vegetation mortality can reverse the local elevation trajectory of an otherwise rapidly prograding marsh.

Acknowledgements

References

Alber, M., Swenson, E.M., Adamowicz, S.C. and Mendelssohn, I.A., 2008. Salt
marsh dieback: an overview of recent events in the US. Estuarine, Coastal
and Shelf Science, 80(1): 1-11.

Altieri, A.H., Bertness, M.D., Coverdale, T.C., Axelman, E.E., Herrmann, N.C.
and Szathmary, P.L., 2013. Feedbacks underlie the resilience of salt
marshes and rapid reversal of consumer-driven die-off. Ecology,
94(7):1647-1657.

Angelini, C. and Silliman, B.R., 2012. Patch size-dependent community recovery
after massive disturbance. Ecology, 93(1): 101-110.

Baustian, J.J., Mendelssohn, I.A. and Hester, M.W., 2012. Vegetation's
importance in regulating surface elevation in a coastal salt marsh facing
elevated rates of sea level rise. Global Change Biology, 18(11): 3377-
3382.

Bertness, M.D. and Ellison, A.M., 1987. Determinants of pattern in a New
England salt marsh plant community. Ecological Monographs, 57(2): 129-
147.

Cavatorta, J.R., Johnston, M., Hopkinson, C. and Valentine, V., 2003. Patterns of
sedimentation in a salt marsh-dominated estuary. The Biological
Bulletin, 205(2): 239-241.

Currin, C., Davis, J., Baron, L.C., Malhotra, A. and Fonseca, M., 2015. Shoreline
change in the New River estuary, North Carolina: rates and
consequences. Journal of Coastal Research, 31(5): 1069-1077.

D'Alpaos, A. and Marani, M., 2016. Reading the signatures of biologic–geomorphic feedbacks in salt-marsh landscapes. Advances in water resources, 93: 265-275.

Day, J.W., Kemp, G.P., Reed, D.J., Cahoon, D.R., Boumans, R.M., Suhayda, J.M. and Gambrell, R., 2011. Vegetation death and rapid loss of surface elevation in two contrasting Mississippi delta salt marshes: The role of sedimentation, autocompaction and sea-level rise. Ecological Engineering, 37(2): 229-240.

DeLaune, R.D., Nyman, J.A. and Patrick Jr, W.H., 1994. Peat collapse, ponding and wetland loss in a rapidly submerging coastal marsh. Journal of Coastal Research, 1021-1030.

Duran, O.V., Moore, L. 2013. Vegetation controls on the maximum size of coastal dunes. Proceedings of the National Academy of the Sciences. 110(43): 17217–17222

Fagherazzi, S., Marani, M. and Blum, L.K., 2004. The ecogeomorphology of tidal marshes. American Geophysical Union: Washington D.C.

Fagherazzi, S., Kirwan, M.L., Mudd, S.M., Guntenspergen, G.R., Temmerman, S., D'Alpaos, A., van de Koppel, J., Rybczyk, J.M., Reyes, E., Craft, C., Clough, J., 2012. Numerical models of salt marsh evolution: Ecological, geomorphic, and climatic factors. Review of Geophysics 50(1): doi/10.1029/2011RG000359

Fischer, J.M., Reed-Andersen, T., Klug, J.L., Chalmers, A.G., 2000. Spatial

    pattern of localized disturbance along a Southeastern salt marsh tidal

    creek. Estuaries and Coasts 23(4): 565–571

Ganju, N.K., Schoellhamer, D.H. and Bergamaschi, B.A., 2005. Suspended

    sediment fluxes in a tidal wetland: Measurement, controlling factors, and

    error analysis. Estuaries, 28(6): 812-822.

Ganju N. K., Kirwan M. L., Dickhudt P. J., Guntenspergen G. R., Cahoon D. R.,

    Kroeger K. D., 2015. Sediment transport-based metrics of wetland

    stability. Geophysical Research Letters 42(19): 7992-8000.

Hardisky, M., 1978. Marsh restoration on dredged material, Buttermilk Sound,

    Georgia. In Proceedings of the 5th Annual Conference of the Restoration

    and Creation of Wetlands, 136-151.

Holdredge, C., Bertness, M.D. and Altieri, A.H., 2009. Role of crab herbivory in

    die-off of New England salt marshes. Conservation Biology, 23(3): 672-

    679.

Hopkinson, C.S., Morris, J.T., Fagherazzi, S., Wollheim, W.M., Raymond, P.A.,

    2018. Lateral marsh edge erosion as a source of sediments for vertical

    marsh accretion. Journal of Geophysical Research: Biogeosciences

    123(8): 2444-2465

Howes, N.C., FitzGerald, D.M., Hughes, Z.J., Georgiou, I.Y., Kulp, M.A., Miner,

    M.D., Smith, J.M. and Barras, J.A., 2010. Hurricane-induced failure of low

    salinity wetlands. Proceedings of the National Academy of

    Sciences, 107(32): 14014-14019.

Hughes, A.L.H., Wilson, A.M., Morris, J.T., 2012. Hydrologic variability in a salt
marsh: Assessing the links between drought and acute marsh dieback.
Estuaries, Coast, and Shelf Science. 111(1): 95-106.

Hughes, Z.J., FitzGerald, D.M., Wilson, C.A., Pennings, S.C., Więski, K. and
Mahadevan, A., 2009. Rapid headward erosion of marsh creeks in
response to relative sea level rise. Geophysical Research Letters, 36(3):
doi:10.1029/2008GL036000

Kirby, R., 2000. Practical implications of tidal flat shape. Continental Shelf
Research, 20(10-11): 1061-1077.

Kirwan, M. L., Guntenspergen, G. R., D'Alpaos, A., Morris, J. T., Mudd, S. M.,
Temmermen, S., 2010. Limits on the adaptability of coastal marshes to
rising sea level. Geophysical Research Letters 37(23): doi
10.1029/2010GL045489

Kirwan, M. L., & Megonigal, J. P. 2013. Tidal wetland stability in the face of
human impacts and sea-level rise. Nature 504(7478): 53-60.

Li, S. and Pennings, S.C., 2016. Disturbance in Georgia salt marshes: variation
across space and time. Ecosphere, 7(10): dx.doi.org/10.1002/ecs2.1487

Li, S. and Pennings, S.C., 2017. Timing of disturbance affects biomass and
flowering of a saltmarsh plant and attack by stem-boring
herbivores. Ecosphere, 8(2): 01675. 10.1002/ecs2.1675

Lin, Q., Mendelssohn, I.A., Graham, S.A., Hou, A., Fleeger, J.W. and Deis, D.R.,
2016. Response of salt marshes to oiling from the Deepwater Horizon

spill: Implications for plant growth, soil surface-erosion, and shoreline

stability. Science of the Total Environment, 557: 369-377.

Lindstedt, D.M., Swenson, E.M., Reed, D., Twilley, R. and Mendelssohn, I.A.,

2006. The case of the dying marsh grass. Report submitted to the

Louisiana Department of Natural Resources, Baton Rouge, LA.

Lottig, N.R. and Fox, J.M., 2007. A potential mechanism for disturbance-

mediated channel migration in a southeastern United States salt

marsh. Geomorphology, 86(3-4): 525-528.

Mariotti G., Carr J., 2014. Dual role of salt marsh retreat: Long term loss and

short-term resilience. Water Resources Research 50(4): 2963-2974.

Mariotti G., Fagherazzi S. 2010. A numerical model for the coupled long-term

evolution of salt marshes and tidal flats. Journal of Geophysical Research

115(F1): doi:10.1029/2009JF001326

McKee, K.L., Mendelssohn, I.A. and D Materne, M., 2004. Acute salt marsh

dieback in the Mississippi River deltaic plain: a drought-induced

phenomenon? Global Ecology and Biogeography, 13(1): 65-73.

Morris J. T., Sundareshwar P. V., Nietch C. T., Kjerfve B., Cahoon D. R. 2002.

Responses of coastal wetlands to rising sea level. Ecology 83(10): 2869-

2877.

Murray, A.B., Knaapen, M.A.F., Tal, M. and Kirwan, M.L., 2008.

Biomorphodynamics: Physical-biological feedbacks that shape

landscapes. Water Resources Research, 44(11):

doi/10.1029/2007WR006410

Ogburn, M.B. and Alber, M., 2006. An investigation of salt marsh dieback in Georgia using field transplants. Estuaries and Coasts, 29(1): 54-62.

Pasternack, G.B. and Brush, G.S., 1998. Sedimentation cycles in a river-mouth tidal freshwater marsh. Estuaries, 21(3): 407-415.

Pawlik, L., Phillips, J.D., Šamonil, P., 2012. Roots, rock, and regolith: Biomechanical and biochemical weathering by trees and its impact on hillslopes—A critical literature review. Earth-Sciences Reviews 159: 142-159.

Redfield, A.C., 1972. Development of a New England salt marsh. Ecological monographs, 42(2): 201-237.

Reed, D.J., 1995. The response of coastal marshes to sea-level rise: Survival or submergence? Earth Surface Processes and Landforms, 20(1): 39-48.

Reinhardt, L., Jerolmack, D., Cardinale, B.J., Vanacker, V. and Wright, J., 2010. Dynamic interactions of life and its landscape: feedbacks at the interface of geomorphology and ecology. Earth Surface Processes and Landforms, 35(1): 78-101.

Saco, P.M., Willgoose, G.R. and Hancock, G.R., 2007. Eco-geomorphology of banded vegetation patterns in arid and semi-arid regions. Hydrology and Earth System Sciences Discussions, 11(6): 1717-1730.

Silliman, B. R., van de Koppel, J., Bertness, M. D., Stanton, L. E., & Mendelssohn, I. A. 2005. Drought, snails, and large-scale die-off of southern US salt marshes. Science, 310(5755): 1803-1806.

Silliman, B.R., van de Koppel, J., McCoy, M.W., Diller, J., Kasozi, G.N., Earl, K.,

    Adams, P.N. and Zimmerman, A.R., 2012. Degradation and resilience in

    Louisiana salt marshes after the BP–Deepwater Horizon oil

    spill. Proceedings of the National Academy of Sciences, 109(28): 11234-

    11239.

Smith, S.M., 2009. Multi-decadal changes in salt marshes of Cape Cod, MA:

    photographic analyses of vegetation loss, species shifts, and geomorphic

    change. Northeastern Naturalist, 16(2), pp.183-208.

Smith, S.M. and Green, C.W., 2015. Sediment suspension and elevation loss

    triggered by Atlantic mud fiddler crab (Uca pugnax) bioturbation in salt

    marsh dieback areas of southern New England. Journal of Coastal

    Research, 31(1): 88-94.

Steiger, J., Tabacchi, E., Dufour, S., Corenblit, D. and Peiry, J.L., 2005.

    Hydrogeomorphic processes affecting riparian habitat within alluvial

    channel–floodplain river systems: a review for the temperate zone. River

    Research and Applications, 21(7): 719-737.

Temmerman, S., Govers, G., Wartel, S. and Meire, P., 2003. Spatial and

    temporal factors controlling short-term sedimentation in a salt and

    freshwater tidal marsh, Scheldt estuary, Belgium, SW Netherlands. Earth

    Surface Processes and Landforms, 28(7): 739-755.

Temmerman S., Bouma T. J., Govers G., Wang Z. B., De Vries M. B., Herman P.

    M. J. 2005. Impact of vegetation on flow routing and sedimentation

patterns: Three-dimensional modeling for a tidal marsh. Journal of

    Geophysical Research 110(F4): doi: 10.1029/2005JF000301

Temmerman, S., Moonen, P., Schoelynck, J., Govers, G. and Bouma, T.J., 2012.

    Impact of vegetation die-off on spatial flow patterns over a tidal

    marsh. Geophysical Research Letters, 39(3): doi/10.1029/2011GL050502

van Belzen, J., van de Koppel, J., Kirwan, M.L., van der Wal, D., Herman, P.M.,

    Dakos, V., Kéfi, S., Scheffer, M., Guntenspergen, G.R. and Bouma, T.J.,

    2017. Vegetation recovery in tidal marshes reveals critical slowing down

    under increased inundation. Nature communications, 8, p.ncomms15811.

Wang, C. and Temmerman, S., 2013. Does biogeomorphic feedback lead to

    abrupt shifts between alternative landscape states?: An empirical study on

    intertidal flats and marshes. Journal of Geophysical Research: Earth

    Surface, 118(1): 229-240.

Wieski, K, H. Guo, C.B. Craft, S.C. Pennings 2010. Ecosystem functions of tidal

    fresh, brackish, and salt marshes on the Georgia Coast. Estuaries and

    Coasts 33(1):161-169.

Wilson, C.A. and Allison, M.A., 2008. An equilibrium profile model for retreating

    marsh shorelines in southeast Louisiana. Estuarine, Coastal and Shelf

    Science, 80(4): 483-494.

Wilson, C.A., Hughes, Z.J., FitzGerald, D.M., 2012. The effects of crab

    bioturbation on Mid-Atlantic saltmarsh tidal creek extension: Geotechnical

    and geochemical changes. Estuarine, Coastal and Shelf Science, 106:33-
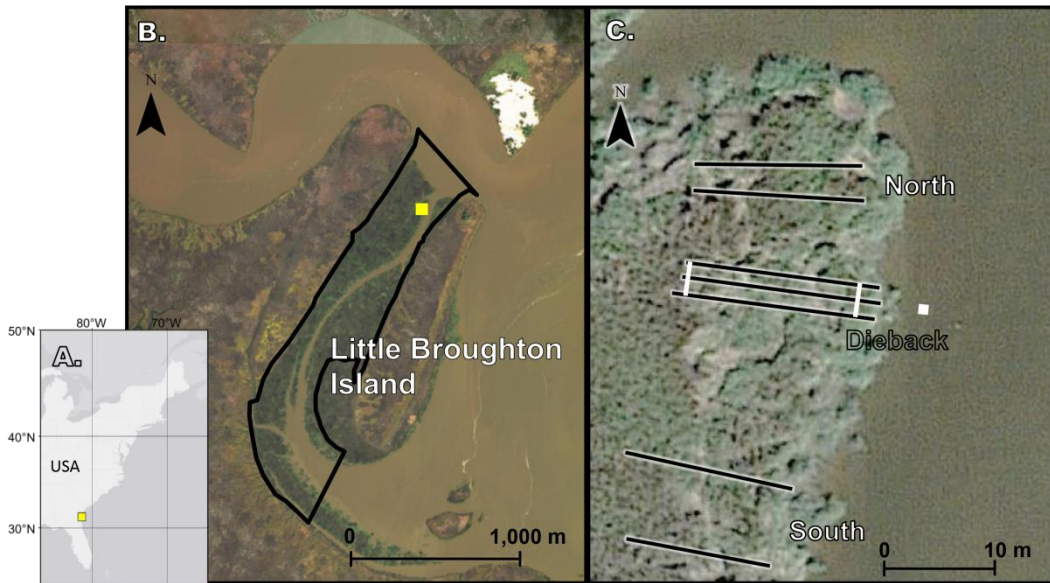
    44

Figure 1: A. Map of U.S. east coast with study site shown in yellow square. B. Regional scale site map, with a thick black line that outlines the area of open water in 1975. For all subsequent years, the 1975 polygon is used as a boundary and open water area within it is calculated. The yellow square marks the specific study site, detailed in C. Shore-normal black lines indicate topographic profiles and shore-parallel white lines indicate sediment tile and grid transects. The middle black line in the dieback zone is the sensor transect. The creek sensor is located at the white square, the marsh sensors are located at the intersections of the sediment tile and grid transects and the sensor transect
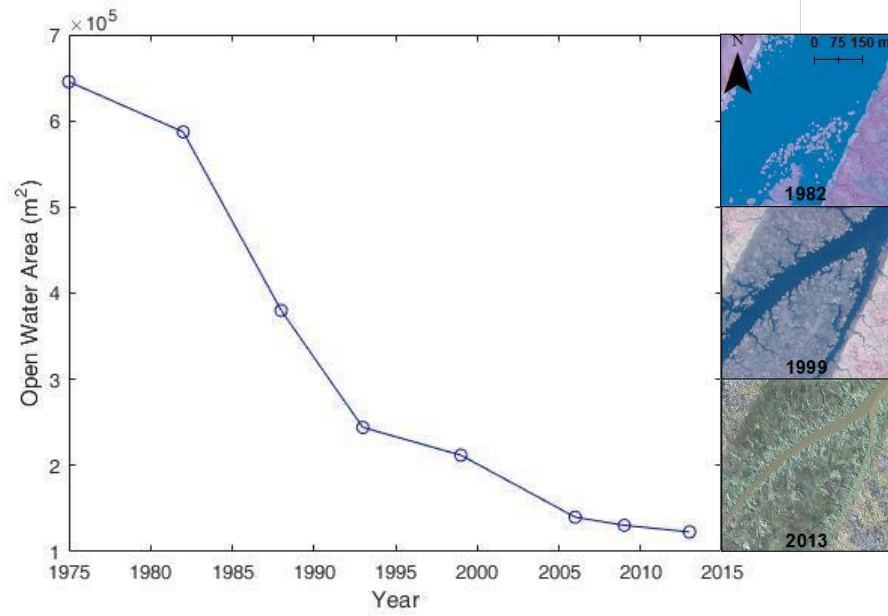
Figure 2: Area of open water within the study area (Figure 1b) was inferred from aerial photography from 1975 to 2013. Sample photos from 1982, 1999, and 2013 demonstrate the decrease in open water is attributable to lateral marsh expansion

Figure 3: A. The site at maximum dieback extent in March 2017. Short, dead plant stems mark the former extent of tall, living vegetation at beginning of the study. B. Exposed rhizomes of *Spartina alterniflora* from late-spring 2017. C. Undercut sediment tile and exposed *S. alterniflora* roots from late-spring 2017.

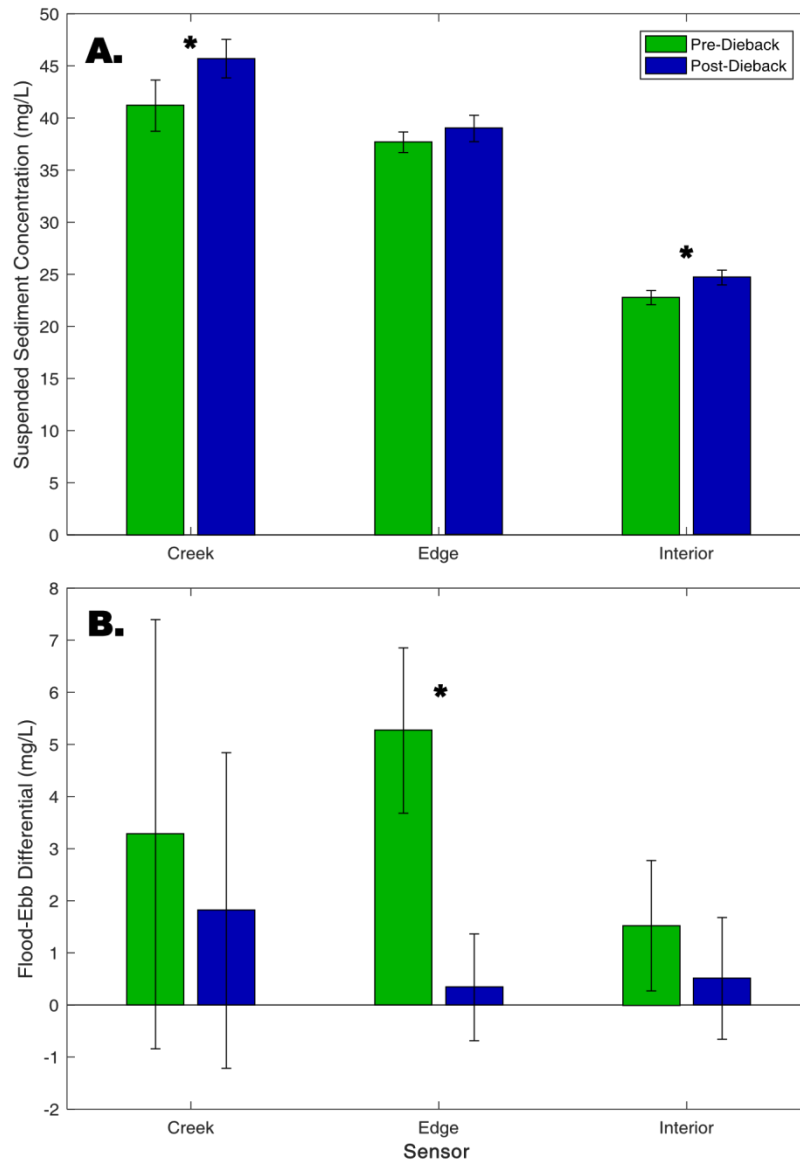Figure 4: A. Average suspended sediment concentration of the flooded marsh before (green) and after (blue) the dieback. B. Flood-ebb differential before (green) and after (blue) the dieback, with positive values indicating higher SSC on the flood tide. Asterisks indicate locations in which the 95% confidence interval (black error bars) from before the dieback does not overlap with the interval from after the dieback.
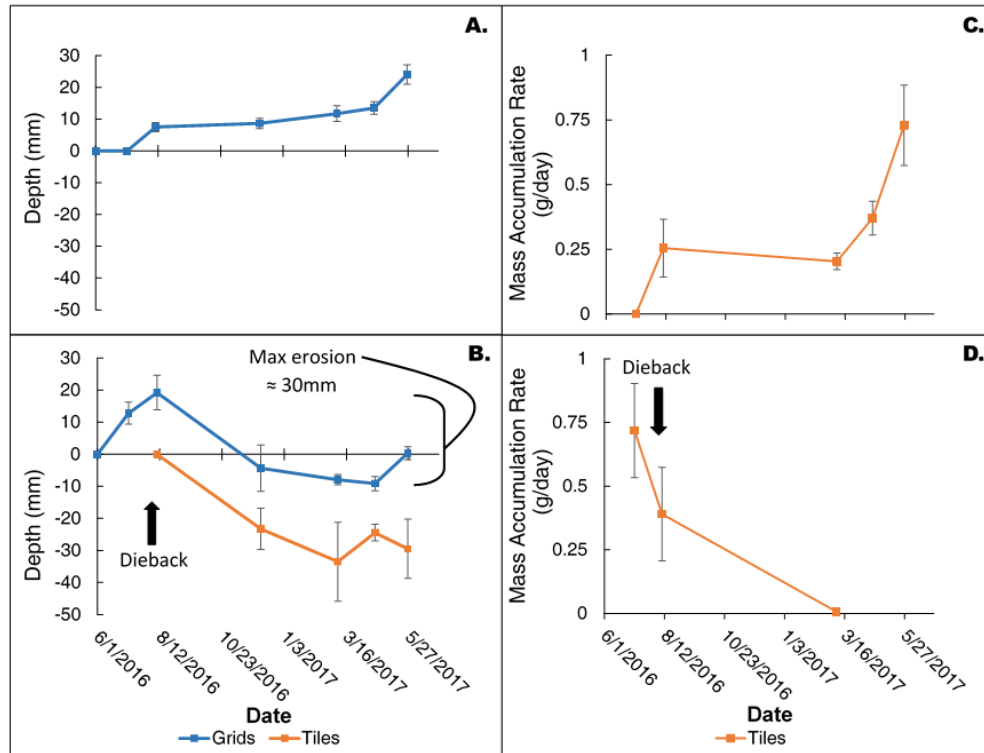
Figure 5: A. and B. Cumulative measures of elevation change, with initial values of zero and increasing values indicating accretion on the plastic grid (blue) or sediment tiles (orange). Decreasing values indicate erosion. C. and D. Mass accumulation rate of sediment on top of the sediment plates calculated per days since last collection. Top panels are the interior while the bottom panels are the edge which directly experienced the dieback. Error bars represent standard error of the mean. The approximate time of the dieback is indicated. Tiles at the edge (B. and D.) were used to measure mass accumulation until the dieback, when they were then used to measure sediment depth.
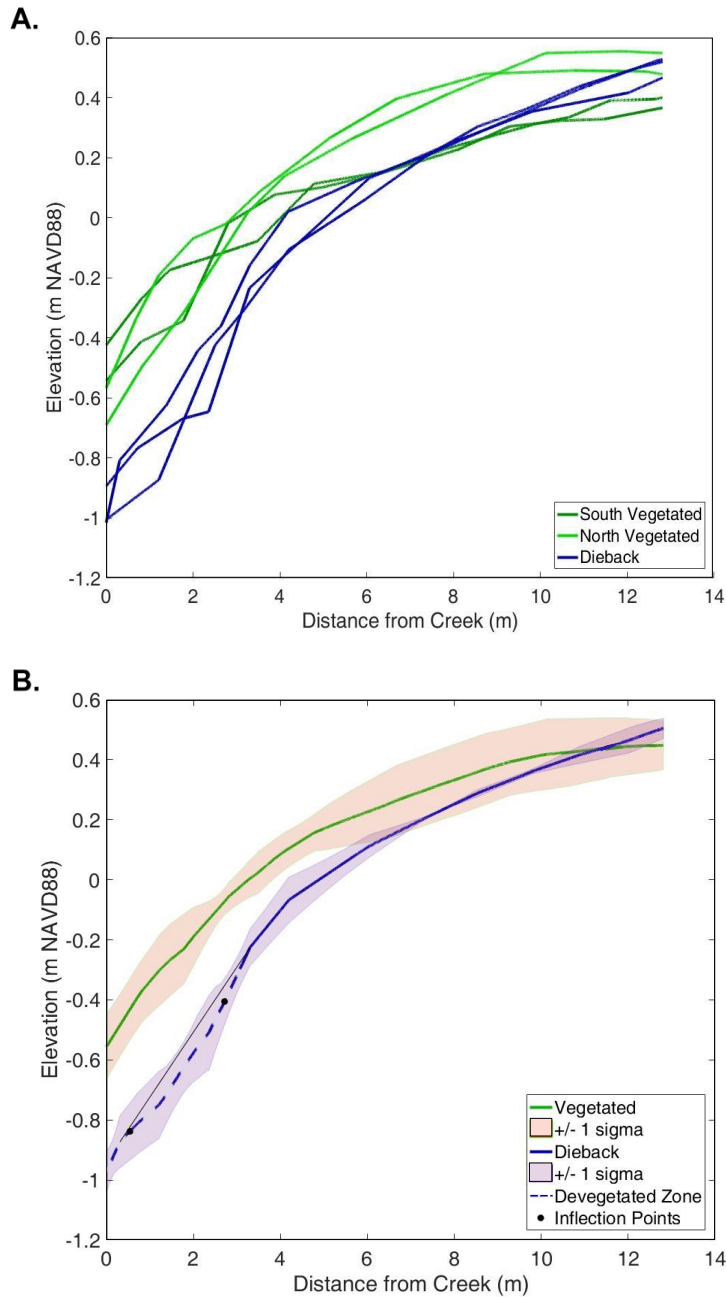
Figure 6: A. Individual elevation profiles for the South Reference (dark green), North Reference (light green) and Dieback (blue) sites. B. Average elevation profiles (± 1 standard deviation) for the vegetated (green line) and dieback areas (blue line). Black points represent inflection points used to quantify differences in curve shape. The dashed component of the dieback line indicates area without vegetation. The line used for the low-end sediment volume loss calculation is represented by the thin black line.
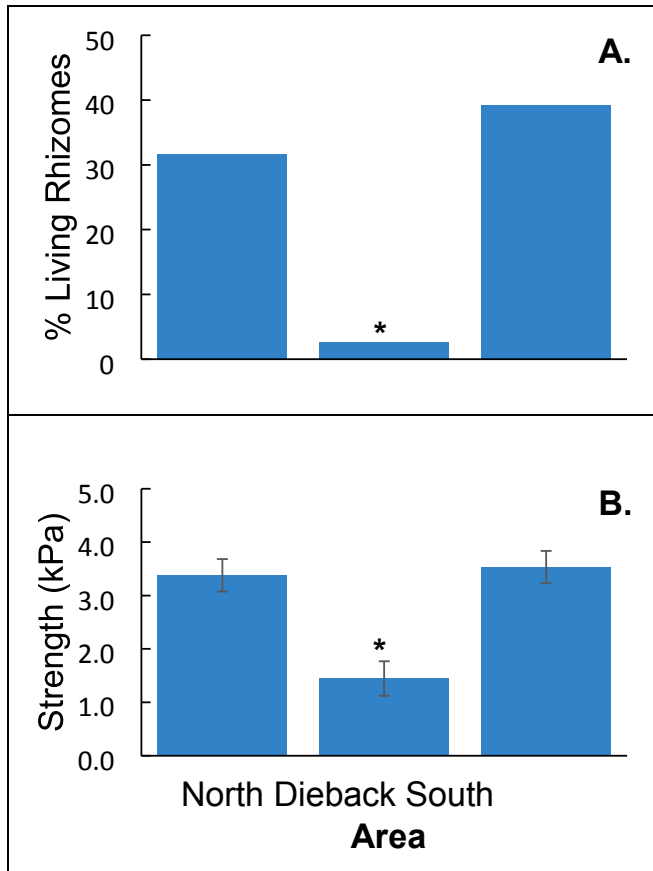
Figure 7: A. Pooled percentage of living rhizomes for each area. B. Average soil shear strength for each area. The error bars represent standard error of the mean and the asterisks indicate significantly lower values.

CHAPTER II

Sediment Delivery to a Tidal Marsh Platform is Minimized by Source Decoupling

and Flux Convergence

Key Points

1. We used an array of turbidity sensors to develop the highest resolution record of tidal marsh suspended sediment concentration to date.

2. Flux convergence indicates minimal interior sediment delivery is caused by sediment trapping near the edge rather than infrequent flooding.

3. Decoupling of marsh and channel sediment supplies indicates the marsh platform is insensitive to changes in channel concentration.

Abstract

Sediment supply is a primary driver of marsh resilience to sea level rise and is typically characterized by high resolution measurements of suspended sediment concentrations (SSC) from adjacent tidal channels. However, understanding sediment transport across the marsh itself remains limited by discontinuous measurements of SSC over individual tidal cycles. Here, we use an array of optical turbidity sensors to build a long-term, continuous record of SSC across a marsh platform and adjacent tidal channel. We find that channel and marsh concentrations are correlated (i.e. coupled) within tidal cycles, but are largely decoupled over longer timescales. We also find that net sediment fluxes decline to near zero within 10m of the marsh edge. An analysis of common environmental drivers of SSC further highlights dissimilarities between channel and marsh concentrations. Together, these results suggest that large sections of the marsh platform receive minimal sediment independent of flooding frequency

or channel sediment supply. Marsh-centric, as opposed to channel-centric, measures of sediment supply may better characterize marsh platform vulnerability.

Plain Language Summary

Coastal marshes are important for storm surge protection, water filtration, and habitat for wildlife. These environments are at risk of drowning by sea level rise and therefore must build elevation to survive. The material for building elevation can come as sediment suspended in the water, which then settles on the surface of the marsh. We often predict how much elevation a marsh can build by the amount of sediment in the associated tidal channel. However, we found sediment concentration in the channel to actually be a poor indicator of the amount of sediment reaching the marsh, especially farther from the marsh edge. External forces, like wind speed and precipitation, influence the sediment concentration more in the channel than on the marsh. This is partly because the channel and marsh are decoupled, meaning as the amount of sediment in the channel increases, the amount reaching the marsh does not necessarily increase. We suggest that sediment concentration should be measured directly in the water atop the flooded marsh to best predict how a marsh will survive into the future.

Introduction

Accelerating sea level rise (SLR) and decreased sediment supply threaten coastal ecosystems throughout the world, where many deltas, marshes, mangroves, and barrier islands rely on sediment to survive rising sea level (Blum and Roberts, 2009; Ellison and Stoddart, 1991; Fitzgerald et al., 2004; Syvitski et al., 2009; Weston 2014). Marsh formation and collapse have both been linked to changes in sediment supply (Day et al., 2007; Gunnell et al., 2013; Kirwan et al., 2011; Tommasini et al., 2019; Tweel and Turner, 2012), making coastal marshes a striking example of a system dependent on mineral sediment availability. Sediment supply is a primary factor influencing vertical accretion rates (Jankowski et al., 2017) and lateral changes in marsh size (Ganju et al., 2017), which affect marsh vulnerability to SLR (Kirwan et al., 2010). Organic accretion is unlikely to allow marshes to survive rapid SLR (Morris et al., 2016), which is consistent with extensive interior marsh loss far from sediment sources (D'Alpaos and Marani, 2016; Schepers et al., 2016; Zhang et al., 2019). Quantifying sediment supply to the marsh platform is therefore crucial in determining salt marsh response to SLR.

How best to characterize sediment supply, however, remains unclear. Numerical models often parameterize sediment supply with an average suspended sediment concentration (SSC) measured in the adjacent tidal channel (Fagherazzi et al., 2012; Kirwan et al., 2010; Ratliff et al., 2015). However, conditions for sediment entrainment often differ from those necessary for over-marsh transport (Duvall et al., 2019). The sediment reaching the marsh may also

differ in magnitude and grain characteristics from what is found in the channel (Poirier et al., 2017). For example, sediment concentration can vary by several orders of magnitude over a single tidal cycle (Christiansen et al., 2000). The pattern of flocculation and grain size varies with tidal stage and on longer timescales both in the channel and across the marsh platform (Chen et al., 2005; Murphy and Voulgaris, 2006; Poirier et al., 2017; Voulgaris and Meyers, 2004a). Furthermore, a marsh can succumb to SLR and wave erosion even if the SSC in the channel is high (Ganju et al., 2015). Although tidal channels are the ultimate source of sediment to most tidal marshes (Friedrichs and Perry, 2001; Reed et al., 1999) and are often measured continuously, measurements on the marsh itself are almost entirely collected through bottle sampling (e.g. Christiansen et al., 2000; Leonard and Reed, 2002; Moskalski and Sommerfield, 2012; Poirier et al., 2017; Wang et al., 1993). In this method, a water sample is collected either by hand or a type of automated sampler at some depth in the water column and taken to the lab for analysis of total suspended sediments, often through vacuum filtration. In part because bottle sampling is labor intensive, samples are typically collected over only a small number of individual tidal cycles. Therefore, it remains uncertain how well marsh sediment availability can be predicted from measurements in channels alone.

Here, we continuously measure SSC over two growing seasons (8 months total) across a marsh platform and adjacent tidal channel in the Plum Island Estuary. We find that channel and marsh SSC are largely decoupled through time and that sediment fluxes decline with distance from the marsh edge.

Ultimately, our findings suggest that measurements of SSC directly on the marsh platform may be required to characterize sediment supply.

Methods

Study area and approach

This study was conducted at a mixed *Spartina patens-S. alterniflora* salt marsh in the Plum Island Estuary, a Long Term Ecological Research site in Massachusetts, USA (PIE LTER; Figure 1). The system is dammed along the major tributaries and typically has low SSC (median = 15.6mg/L), which increase to 30-40mg/L at the estuarine turbidity maximum (Cavatorta et al., 2003; Hopkinson et al., 2018). Sediment budgets for marsh accretion indicate that oceanic input and tidal flat erosion are the largest sources of sediment, followed by marsh edge erosion and then river inputs (Hopkinson et al., 2018). Mean sea level (MSL) and mean higher high water (MHHW) are located at -0.09 m and 1.25 m NAVD88, respectfully (Milette et al., 2010). The average tidal range is 2.9m and approximately 75% of marshes are high marsh (Milette et al., 2010). Real-time kinematic global position satellite (RTK GPS) surveys indicate our site was located between 1.19m and 1.70m NAVD88, which corresponds with the transition from low to high marsh in this system (Figure 2, Milette et al., 2010). In many locations, including our site, there is a large marsh escarpment which regularly exceeds 2 meters in height (Figure 2). The study site floods from the marsh-channel (West Creek) edge to the marsh interior (Law's Point; Figure 1).

We quantified spatial and temporal patterns of suspended sediment transport over two growing seasons (May-November, 2016; June-September, 2017) using an array of optical-backscatter turbidity sensors) equipped with automatic anti-fouling wipers. We were not able to collect measurements or draw conclusions during the winter months when sediment transport is influenced by ice rafting, rather than simple advection of SSC (Argow et al. 2011). We deployed the sensors across the marsh platform and adjacent tidal channel in a shore-normal transect. Based on direct observations of flooding, we concluded the sensor transect was parallel to the direction of initial marsh flooding. The sensor in the channel (RBR Duo equipped with Seapoint turbidity probe) was located 35cm above the bed and 3m from the edge of the marsh. Sensors were fastened to rigid grates for deployment on the marsh, with the grid flush with the marsh soil surface and the actual sensor window located 7cm above the surface. The sampling point is 5cm in front of the sensor window. To minimize interference with plants, we removed vegetation from within this distance and placed a ceramic tile on the ground to prevent regrowth directly in front of the sensor window. In 2016, sensors were placed at 2.7m and 17m from the marsh edge (RBR Solo and RBR Duo, respectively). In 2017, five sensors were installed on the marsh surface at 1.25 m (RBR Solo), 2.7 m (RBR Duo), 9.3 m (RBR Duo), 17 m (YSI 6600), and 24 m (YSI Exo) from the marsh edge (Figure 1). The sensor located 17 m into the marsh in 2017 malfunctioned and did not record data. All other sensors measured turbidity every 15 minutes for the entire deployment, totaling nearly 100,000 measurements, with select sensors also

43

measuring pressure (see Figure 1). The sensor error in turbidity measurements is <2% and significant sensor drift is uncommon (http://seapoint.com/pdf/stm_ds.pdf).

Suspect data points were removed from the time series record following Ganju et al., 2005. We used a recursive filter to remove points which were greater than 10 NTU higher than adjacent time steps. The record was visually analyzed to ensure points being removed represented values anomalously higher than surrounding values. These removed data points represent times when a sensor was obstructed, fouled, or not submerged. Tidal stage and flooding durations were determined by measurements of water level by the sensors themselves (see Figure 2). Specifically, sensors measure pressure which is then corrected for atmospheric pressure obtained from the PIE LTER (Giblin, 2017; Giblin; 2018). These measurements of water level include astronomical tides and any other environmental drivers affecting water level, e.g. wind. We removed data points recorded by a sensor when it was not submerged by comparing the depth record in the channel to the elevation of the sensor. Data points were removed when the water level (in NADV88) was below the sensor elevation (in NADV88). Additionally, we divided the record into flooding tides (increasing water level) and ebbing tides (decreasing water level). We calculated the flood-ebb differential for each sensor by taking the average of all points that occurred during the flooding tide and subtracting the average of all points that occurred during the ebbing tide.

Turbidity data was converted to SSC via laboratory calibrations using sediment collected from the site and in situ field sampling. In the lab, we created sediment-water slurries with a range of SSC and measured them with an additional turbidity sensor. In the field, we measured turbidity with an additional sensor at various locations around the site and at different tidal stages. We collected a water sample in conjunction with each turbidity measurement. This ensures that the calibration is accurate to the average sediment characteristics from across the site. We compared sensor turbidity measurements to total suspended solid measurements obtained via vacuum filtration of water samples and sediment-water slurries. The y-intercept value was set to zero, resulting in the equation SSC (mg/L) $=2.26$*Sensor Turbidity (NTU) ($R^2=0.98$, n=35, p<<0.001; Supplementary Figure 2). There were no outliers which suggests the various locations sampled had sediment of similar optic properties. All field sensors were in turn individually calibrated to the sensor used in the lab via turbidity standards. In other words, all turbidity sensors were calibrated to one sensor which was then used to calibrate to SSC. Full SSC time series can be found in Figure 3.

Analytical methods

In general, suspended sediment concentrations are influenced by numerous environmental forces (see Lawson et al., 2007; Murphy and Voulgaris, 2006; Settlemyre and Gardner, 1977; Voulgaris and Meyers, 2004a). We analyzed the influence of four environmental drivers: river discharge (waterdata.usgs.gov/nwis/uv?site_no=01101000), wind speed (Giblin, 2017;

Giblin, 2018), precipitation (Giblin, 2017; Giblin, 2018), and tidal range (this study). The purpose of our analysis was to determine if the environmental drivers influenced the channel and the marsh differently. As such, we compared the daily average SSC at each sensor location in each year to daily average values for all of the environmental drivers through linear regressions.

We quantified the dispersion of the distribution of SSC of the entire available record for each sensor to quantify how temporal variability in SSC changes with distance into the marsh. We calculated the quartile coefficient of dispersion, which is a non-dimensional measure of how spread out a distribution is. Values closer to zero indicate a tighter or more uniform distribution and values closer to one indicate a more dispersed distribution. Additionally for each sensor, we calculated the difference between the mean concentration and the median concentration normalized by dividing by the mean. Relative mean-median difference values that are closer to zero would indicate a more uniform or linear normal distribution whereas values approaching positive one would indicate a more measurements in the right tail of the distribution. We determined how both of these non-dimensional measures of dispersion changed with distance via a linear regression.

To identify how coupling between channel and marsh sediment supply varies with time, we compared SSC under various temporal averaging windows from three geomorphic locations: channel, marsh edge, and marsh interior. We defined the marsh edge in 2017 as the average of the sensors located at 1.25m and 2.7m and the marsh interior as the average of the sensors located at 9.3m

and 24m. For each 15 minute increment within a tidal cycle, we averaged data from both years by location. From this, we also created heat density maps to visualize concentration within a tidal cycle by determining the number of data points that were within bins defined by 0.5 mg/L x 15 minutes. We compared the average concentration per stage in the tidal cycle for the three different geomorphic zones with linear regressions. For larger temporal windows (i.e. each tidal cycle, day, week, spring-neap cycle, and month) we used all data from both years when all sensors were flooded. For example, to calculate daily average SSC for the channel to compare to daily average SSC for the marsh edge, we remove all points from the channel SSC record when the marsh edge is not flooded. We conducted a linear regression between the three geomorphic zones for all time averaging windows. This was repeated including only flooding tides and only ebbing tides.

In 2016, we harvested plant biomass in replicate plots (n=3) of $0.0625m^2$ within 1 m of each marsh sensor location at equipment deployment, retrieval, and two additional times in between. There was no significant difference in biomass between sampling locations on the marsh platform (ANOVA, p=0.58), so we compared marsh average biomass to the percent decrease in SSC from the channel to the marsh edge, the marsh edge to the marsh interior, and the channel to the marsh interior. We targeted sampling windows for SSC that were centered on the biomass sampling dates. The analysis consisted of three linear regressions between 1. biomass and average percent decrease in SSC from the channel to the marsh edge, 2. biomass and percent decrease in SSC from the

channel to the marsh interior, and 3. biomass and percent decrease in SSC from the marsh edge to the marsh interior. We also conducted a two dimensional correlation test between the biomass vs. time curve and each percent decrease in SSC vs. time curves. To account for biomass sampling at the beginning and end of the monitoring, we performed our analysis for numerous different sampling schemes, given in Supplementary Table 1. All of the sampling schemes produced similar results, suggesting the results are not the artifact of a particular sampling window.

Results

Broad-scale Patterns

Suspended sediment concentrations decreased from the channel towards the marsh interior (Figure 4). Channel average SSC was 13.6mg/L ±9.19 (mean ±σ) compared to an average marsh concentration of 5.24mg/L ±4.12. The spatial pattern of SSC appeared to be an exponential decay to a non-zero background concentration in both 2016 and 2017 (Figure 4a). We utilize a natural logarithmic transformation of the data so that we can statistically test the fit of an exponential function with a non-zero background value. The log transformation of the average concentration for all sensors was significantly correlated with distance from the channel (R^2=0.52, p<0.05; Figure 4b).

Records of SSC from the channel tended to correlate with more environmental drivers than records on the marsh surface (Table 1). Channel SSC was positively correlated with tidal range (2016 p<0.05, 2017 p<0.05),

48

precipitation ($p<0.05$, $p<0.05$), and wind speed in both years ($p<0.05$, $p<0.05$). Channel SSC was positively correlated with river discharge in 2017 ($p<0.05$) but negatively correlated with discharge in 2016 ($p<0.05$). Correlations between environmental drivers and marsh SSC were inconsistent, with only 4 significant correlations out of 28 comparisons.

The non-dimensional measures of dispersion were largest in the channel and decreased with distance into the marsh. (Figure 5). In other words, with distance inland a greater number of measurements are closer in value to the mean. Both the quartile coefficient of dispersion and the relative mean-median difference had a significant linear relationship with distance ($R^2=0.54$, $p<0.05$; $R^2=0.61$, $p<0.05$, respectively)

The difference between average concentrations on flood tides versus that on ebb tides is a predictor of net sediment supply to the marsh complex (French et al., 2009; Ganju et al., 2017). We therefore divided the SSC records into flooding and ebbing tidal components using measured water level to determine the average flood-ebb differential. Overall, the flood-ebb differential is positive and relatively small for each sensor (Figure 6). The differential in the channel is just over 1mg/L and decreases exponentially with distance into the marsh to approximately 0.1mg/L (log-transformed, $R^2=0.85$, $p<0.05$; Figure 6).

Correlations between Channel and Marsh

The average of all tidal cycles indicates that the channel and the marsh SSC are generally coupled at this time scale, e.g. sediment concentrations on the marsh reflect concentrations in the channel (Figure 7). Values at all three

locations tend to decrease on the rising tide, reaching a minimum at slack high tide for the channel and marsh edge (Figure 7). The concentrations increase on the falling tide except for in the marsh interior. SSC concentrations are significantly correlated between the channel and marsh edge (R^2=0.58, $p<0.05$), and between the marsh edge and marsh interior (R^2=0.52, $p<0.05$), but not between the channel and marsh interior ($p=0.9$). This indicates general coupling of SSC between channel and marsh over individual tidal cycles.

At larger temporal scales (full tidal cycle to monthly), the channel and the marsh demonstrate decoupling, where marsh sediment concentrations do not reflect concentrations in the channel (Figure 8). Linear regressions between channel SSC and marsh edge or marsh interior SSC are either insignificant or significantly negatively correlated for all time averaging windows of interest (Figure 8; Supplementary Figure 5). Negative significant correlations mean that as channel SSC increases, marsh SSC decreases. In contrast, average SSC at the marsh edge is positively correlated to the marsh interior over tidal cycles ($p<0.05$), daily ($p<0.05$), weekly ($p<0.1$), spring-neap cycles ($p<0.05$) and monthly timescales ($p<0.1$, Supplementary Figure 5). This pattern is also consistent for either only rising tides or only falling tides (Supplementary Table 2).

Biomass varied seasonally and was strongly correlated with the proportional decrease in SSC from the channel to the marsh interior (all sampling schemes: $p<0.05$) and marsh edge to marsh interior (three sampling schemes: $p<0.05$, one sampling scheme: $p<0.1$; Figure 9a). Biomass did not significantly

correlate with the percent decrease of SSC from the channel to the marsh edge in three of the four sampling schemes (p>0.1), and was marginally correlated in one sampling scheme (p<0.1).

Discussion

Spatial patterns of suspended sediment transport

Our general findings are consistent with previous work in the system suggesting Plum Island Estuary marshes have a limited sediment supply. The average SSC in the tidal channel at our site (13.6 ±0.07 mg L^{-1}, mean ±SE) is similar to previous measurements in the system, especially those from similar distances upstream (~15mg/L, Cavatorta et al., 2003; 15.6mg/L ±3.6, median ±SE, Hopkinson et al., 2018). Sediment budgets indicate that seaward sediment sources, i.e. the ocean and eroding tidal flats in Plum Island Sound, are a more important source of sediment than rivers (Hopkinson et al., 2018). This seaward sediment source is consistent with our observations of a positive flood-ebb differential in the tidal channel, where flood tides would bring the oceanic and tidal flat sediment into the marsh and therefore have higher SSC than river-influenced ebb tides (Figure 6).

Our high resolution measurements support previous studies but also lead to new insight that cannot be captured with more conventional sampling methods. For example, our study is consistent with the paradigm that SSC is higher in tidal channels and decreases with distance into the marsh (Christiansen et al., 2000; Leonard and Reed, 2002; Poirier et al., 2017). However, continuous

sampling allows us to identify that concentrations in the channel have a more disperse distribution than concentrations on the marsh platform (Figure 5). Like many other studies, we find vegetation has an important control on SSC (Coleman and Kirwan 2019; Leonard and Reed 2002; Li and Yang, 2009; Temmerman et al., 2005), particularly in controlling the decrease in SSC into the marsh interior (Figure 9a). However, we find that changes in SSC from the channel to the marsh edge do not vary as strongly with plant biomass, suggesting vegetation is less important near channel edges (Figure 9a). This is perhaps because the hydrodynamic effect of the vegetation is overwhelmed by the effect of channelized flow overtopping the high escarpment.

Our measurements also suggests flux convergence across the marsh platform (Figure 6). Previous work has shown sediment flux is proportional to the flood-ebb SSC differential, even in the absence of flow velocity measurements (French et al., 2008; Ganju et al., 2017; Nowacki and Ganju 2019). Sediment flux is said to converge when there is a greater flux into a region than out of the region (Dickhudt et al., 2009; Harris et al., 2008). For example, the site at 2.7m has a flood-ebb SSC differential of +0.7 mg/L, while the site at 9.3m has a differential of +0.3 mg/L in 2017 (Figure 6). This indicates that the site has a greater influx of sediment at 2.7m than at 9.3 m, thus suggesting convergence and net sediment deposition in that region. Overall, the observed sediment flux is small and rapidly declines with distance inland (flood-ebb differential <0.2mg/L after the first 10m, Figure 2). The gradient is much greater along the marsh edge than in the interior, suggesting more sediment is being trapped close to the

channel and the marsh interior is largely—but not completely—deprived of

mineral sediment. This demonstrates that limited sediment supply to the marsh

interior is not exclusively a result of infrequent inundation. Our results are

therefore consistent with previous work in the system that found a small net

positive inorganic accretion rate (Wilson et al., 2014).

The flux convergence may be complicated by the location of our

measurements. For example, we measured SSC over the marsh but the

proportionality of flood-ebb differentials and sediment flux has only been explored

in tidal channels (French et al., 2008; Ganju et al., 2017; Nowacki and Ganju

2019). Our analysis therefore is based on the assumption that the proportionality

applies to both channel and over-marsh measurements. Although initial marsh

flooding occurs parallel to our transect, the proximity to a bifurcation in the

channel may mean there is lateral flow influencing the sensors at higher water

levels (Figure 1c). However, our results still suggest flux convergence. The SSC

in the bifurcation is likely similar to that of the main channel and the sensors

which we consider interior to the main channel are still interior to the secondary

channel (e.g. the sensor 24 m from the main channel is >20 m from the

secondary channel). We would expect similar flux convergence with distance

along all flow paths. In other words, lateral flow would experience the same

conditions as flow parallel to the transect so we expect similar decreases in

flood-ebb differential with distance, indicating flux convergence. Additionally, we

do not find evidence for strong resuspension, as there is only a minor increase in

marsh SSC at higher ebb velocities and only on the marsh edge. This is

consistent with the limited role resuspension plays in vegetated environments (Friedrichs and Perry, 2001).

Decoupling between channel and marsh sediment supply

Long-term, continuous measurements also allowed us to discover that marsh sediment supply is largely decoupled from channel sediment supply. Our measurements indicate that the tidal channel is the source of sediment, as evidenced by higher SSC in the channel than on the marsh and correlated fluctuations between marsh and platform SSC within tidal cycles (Figure 7). However, this coupling breaks down at timescales greater than a tidal cycle. This decoupling is present when only considering flooding tides, ebbing tides, or when considering all stages of the tidal cycle (Supplementary Table 2). At larger timescales, concentrations on the marsh are often lowest when concentrations in the channel are highest (Figure 8). For example, this negative relationship between channel and marsh SSC is evident in differences from 2016 to 2017, where mean annual SSC decreased in the channel (14.9mg/L ± 0.08 to 10.7mg/L ± 0.09) but increased on the marsh (4.21mg/L ± 0.05 to 6.20mg/L ± 0.06; mean ± s.e., Figure 4a). This decoupling likely arises because as concentration increases in the channel, a greater proportion of sediment settles before reaching the marsh edge sensor (Figure 9b).

We consider two possible mechanisms to explain the greater proportional reduction in concentration when channel sediment concentrations are high (Figure 9b). The first mechanism relates to changes in sediment stratification within the channel water column, whereby the center of mass of SSC shifts

downward. This could be caused by sediment in the channel beginning to settle

and therefore moving downward in the water column. The lower portion of the

water column, i.e. where our sensor was installed, could experience an increase

in concentration while the surface water SSC decreases. The mass of total

suspended sediment does not necessarily change, but it is distributed differently.

The marsh platform is directly interacting with surface waters and so would

receive reduced sediment transport. In this case the decoupling applies

specifically to near-bed channel measurements and could be mitigated by

measuring water surface concentrations. A second mechanism is that settling

velocity increases with increasing channel concentration. Increased settling

velocity with increased concentration is likely driven by flocculation and has been

well documented over a similar range of concentrations (Manning et al., 2010;

Ross, 1988; Wolanski et al., 1992). In this scenario, the larger volume of

sediment settles out more quickly within the channel, marsh bank, or first meter

of the marsh. One recent study in the Bay of Fundy, Canada, found that

increasing SSC led to increased flocculation and preferential deposition in the

channel and marsh bank so that sediment deposition on the marsh actually

declined with increasing channel SSC (Poirier et al., 2017). These two

mechanisms are likely connected as particle settling can cause increasing

concentrations at depth and decreasing concentrations at the surface

(Winterwerp, 2002).

The decoupling between channel and marsh SSC is also evident in the

correlation of SSC to environmental drivers. Channel SSC varies with all of the

analyzed environmental drivers (i.e. average daily wind speed, total daily precipitation, average daily Parker River discharge and tidal range), whereas our measurements of marsh platform SSC generally do not (Table 1). One of the only environmental drivers relevant to marsh SSC was wind speed, and it correlated in 2016 but not 2017. Daily average wind speed was significantly higher in 2016 (1.13 m/s) than 2017 (0.86 m/s; t=5.5, d.f.=273, p<0.05) due to interannual variability and seasonal differences captured by the different monitoring lengths. This suggests there is a threshold wind speed necessary to influence marsh SSC, but we did not observe a threshold effect in the channel. Our simplistic analysis of daily-averaged environmental drivers was aimed at discovering how these drivers impact SSC between the marsh and channel differently. To quantify the role of each environmental driver in controlling SSC would require a much more in depth analysis including wind direction, water level, and synergistic relationships between drivers. However, the current analysis further highlights the decoupling between the marsh and channel.

Datasets that are as robust as the one presented here are exceedingly rare for other tidal marshes, making it challenging to determine how our findings apply to other systems. Recent work in the Bay of Fundy illustrates decoupling between the channel and marsh platform in a very high sediment, hypertidal environment (Poirier et al., 2017), but direct observations of decoupling and flux convergence elsewhere are generally limited by a lack of high resolution SSC data on the marsh platform. We were unable to monitor the site in the winter so it is unclear if this time period differs significantly from our conclusions.

Nevertheless, the ultimate implication of flux convergence and source decoupling is that predicting marsh vulnerability on the basis of source-water sediment supply alone is difficult. This difficulty has been observed in a variety of environments, including microtidal salt marshes (Ganju et al., 2015), microtidal freshwater marshes (Palinkas and Engelhardt, 2018), mesotidal back-barrier marshes (Murphy and Voulgaris, 2006), hypertidal marshes (Poirier et al., 2017), and others (D'Alpaos and Marani, 2016; Duvall et al., 2017). Although more work is needed to determine the role of source decoupling and flux convergence in other environments, our work offers a mechanistic explanation for this phenomenon, and contributes to the growing body of literature that suggests marsh vulnerability is difficult to predict based on measurements of channel SSC alone.

Conclusion

Through high resolution, long term monitoring of SSC from a tidal channel and adjacent salt marsh, we show that channel and marsh interior SSC are largely decoupled at time scales longer than individual tidal cycles. This ultimately leads to large sections of the marsh platform that are insensitive to fluctuations in channel sediment supply. Specifically, the interior of the marsh, where marsh loss often begins (Schepers et al., 2016; Zhang et al., 2019), has a minimal sediment flux and is largely decoupled from broad scale environmental drivers and changes in channel SSC. Therefore, the vulnerability of interior marshes is not due to infrequent flooding alone and cannot be easily mitigated

through increased sediment concentration in the channel. Numerical and conceptual models of marsh vulnerability typically rely on channel-centric measures of sediment availability (Fagherazzi et al., 2012; Kirwan et al., 2010; Raposa et al., 2016; Ratliff et al., 2015). While it is unclear how the results apply to other systems, our work suggests that direct SSC measurements on the marsh platform may be required to adequately characterize mineral sediment availability and predict marsh vulnerability to sea level rise.

Acknowledgements

References

Argow, B. A., Hughes, Z. J., FitzGerald, D. M. (2011). Ice raft formation, sediment load, and theoretical potential for ice-rafted sediment influx on northern coastal wetlands. *Continental Shelf Research 31*(12): 1294-1305 https://doi.org/10.1016/j.csr.2011.05.004

Blum, M. D., & Roberts, H. H., (2009). Drowning of the Mississippi Delta due to insufficient sediment supply and global sea-level rise. *Nature Geoscience 2* 488-491, https://doi.org/10.1038/ngeo553

Cavatorta, J.R., Johnston, M., Hopkinson, C. & Valentine, V., (2003). Patterns of sedimentation in a salt marsh-dominated estuary. *The Biological Bulletin, 205*(2), 239-241.

Chen M. S., Wartel S., & Temmerman, S., (2005) Seasonal variation of floc characteristics on tidal flats, the Scheldt estuary. *Hydrobiologia 540*(1-3) 181-195 https://doi.org/10.1007/s10750-004-7143-6

Christiansen, T., Wiberg, P. L., & Milligan, T. G., (2000). Flow and sediment transport on a tidal salt marsh surface. *Estuarine, Coastal and Shelf Science 50*(3), 315-331, https://doi.org/10.1006/ecss.2000.0548

Coleman, D.J., & Kirwan, M.L., (2019). The effect of a small vegetation dieback event on salt marsh sediment transport. *Earth Surface Processes and Landforms 44*(4), 944-952, https://doi.org/10.1002/esp.4547

D'Alpaos, A., & Marani, M., (2016). Reading the signatures of biologic–geomorphic feedbacks in salt-marsh landscapes. *Advances in Water Resources 93b* 265-275. https://doi.org/10.1016/j.advwatres.2015.09.004

Day, J. W., Boesch, D. F., Clairain, E. J., Kemp, G. P., Laska, S. B., Mitsch, W.
J., et al. (2007). Restoration of the Mississippi Delta: Lessons from
Hurricane Katrina and Rita. *Science 315*(5819) 1679-1684.
doi/10.1126/science.1137030

Dickhudt, P.J., Friedrichs, C.T., Schaffner, L.C., Sanford, L.P., (2009) Spatial and
temporal variation in cohesive sediment erodibility in the York River
estuary, eastern USA: A biologically influenced equilibrium modified by
seasonal deposition. *Marine Geology 267*(3-4), 128-140,
https://doi.org/10.1016/j.margeo.2009.09.009

Duvall, M. S., Wiberg, P. L., & Kirwan M. L., (2019). Controls on sediment
suspension, flux, and marsh deposition near a bay-marsh boundary.
Estuaries and Coasts 42(2) 403-424, https://doi.org/10.1007/s12237-018-
0478-4

Ellison, J. C., & Stoddart, D. R., (1991). Mangrove ecosystem collapse during
predicted sea-level rise: Holocene analogues and implications. *Journal of
Coastal Research 7*(1) 151-165 https://www.jstor.org/stable/4297812

Fagherazzi, S., Kirwan, M.L., Mudd, S.M., Guntenspergen, G.R., Temmerman,
S., D'Alpaos, A., et al. (2012). Numerical models of salt marsh evolution:
Ecological, geomorphic, and climatic factors. *Review of Geophysics 50*(1),
doi/10.1029/2011RG000359

French, J. R., Burningham, H., & Benson, T., (2008) Tidal and meteorlogical
forcings of suspended sediment flux in a muddy, mesotidal estuary.
Estuaries and Coasts 31(843) https://doi.org/10.1007/s12237-008-9072-5

Fitzgerald, D. M., Buynevich I., & Argow, B., (2006). Model of tidal inlet and

barrier island dynamics in a regime of accelerated sea level rise. *Journal
of Coastal Research S.I.39*(II) 789-795,

https://www.jstor.org/stable/25741684

Friedrichs, C. T., & Perry, J. E., (2001). Tidal salt marsh morphodynamics: A

synthesis *Journal of Coastal Research 27*, 7-37.

https://www.jstor.org/stable/25736162

Ganju, N.K., Schoellhamer, D.H. & Bergamaschi, B.A., (2005). Suspended

sediment fluxes in a tidal wetland: Measurement, controlling factors, and

error analysis. *Estuaries 28*(6), 812-822.

Ganju N. K., Kirwan M. L., Dickhudt P. J., Guntenspergen G. R., Cahoon D. R., &

Kroeger K. D., (2015). Sediment transport-based metrics of wetland

stability. *Geophysical Research Letters 42*(19), 7992-8000.

Ganju N. K., Defne, Z., Kirwan, M. L., Fagherazzi, S., D'Alpaos, A., & Carniello

L., (2017). Spatially integrative metrics reveal hidden vulnerability of

microtidal salt marshes. *Nature Communications 8*

https://doi.org/10.1038/ncomms14156

Giblin, A., (2017). Year 2016, meteorological data, 15 minute intervals, from the

PIE LTER Marshview Farm weather station located in Newbury, MA

Environmental Data Initiative.

http://dx.doi.org/10.6073/pasta/d5bfbfc6de185cff9b7302884c78e0fe

Giblin, A., (2018). Year 2017, meteorological data, 15 minute intervals, from the

PIE LTER Marshview Farm weather station located in Newbury, MA

Environmental Data Initiative.

http://dx.doi.org/10.6073/pasta/80e0962b53d2549002fcc53eaf7394c6

Gunnell J. R., Rodriguez, A. B., & McKee, B. A., (2013). How a marsh is built

from the bottom up. *Geology 41*(8), 859-862,

https://doi.org/10.1130/G34582.1

Harris, C.K., Sherwood, C.R., Signell, R.P., Bever, A.J., & Warner, J.C., (2008)

Sediment dispersal in the northwestern Adriatic Sea. *Journal of*

Geophysical Research 113(C11S03) doi:10.1029/2006JC003868

Hopkinson, C.S., Morris, J.T., Fagherazzi, S., Wollheim, W.M., & Raymond, P.A.,

(2018). Lateral marsh edge erosion as a source of sediments for vertical

marsh accretion. *Journal of Geophysical Research: Biogeosciences*

123(8), 2444-2465

Jankowski, K. L., Tornqvist, T. E., & Fernandes, A. M., (2017). Vulnerability of

Louisiana's coastal wetlands to present-day rates of relative sea-level rise.

Nature Communications 8. https://doi.org/10.1038/ncomms14792

Kirwan, M. L., Guntenspergen, G. R., D'Alpaos, A., Morris, J. T., Mudd, S. M., &

Temmerman, S., (2010). Limits on the adaptability of coastal marshes to

rising sea level. *Geophysical Research Letters 37*(23),

https://doi.org/10.1029/2010GL045489

Kirwan, M. L., Murray, A. B., Donnelly, J. P., & Corbett, D. R. (2011). Rapid

wetland expansion during European settlement and its implication for

marsh survival under modern sediment delivery rates. *Geology 39*(5) 507-

510. https://doi.org/10.1130/G31789.1

Leonard, L. A., & Reed D. J. (2002). Hydrodynamics and sediment transport
through tidal marsh canopies. *Journal of Coastal Research S.I.36*, 459 –
469. https://doi.org/10.2112/1551-5036-36.sp1.459

Li H., & S. L. Yang (2009) Trapping effect of tidal marsh vegetation on
suspended sediment, Yangtze Delta. *Journal of Coastal Research 25*(4)
915 – 924, https://doi.org/10.2112/08-1010.1

Manning, A. J., Langston, W. J., & Jonas P. J. C., (2010). A review of sediment
dynamics in the Severn Estuary: Influence of flocculation. *Marine Pollution
Bulletin 61*(1-3) 37-51. https://doi.org/10.1016/j.marpolbul.2009.12.012

Millette, T. L., Argow, B. A., Marcano, E., Hayward, C., Hopkinson, C. S., &
Valentine, V., (2010). Salt marsh geomorphical analyses via integration of
multitemporal multispectral remote sensing with LIDAR and GIS. *Journal
of Coastal Research 2010*(265), 809-816.
https://doi.org/10.2112/JCOASTRES-D-09-00101.1

Morris, J. T., Barber, D. C., Callaway, J. C., Chambers, R., Hagen, S. C.,
Hopkinson C. S., et al. (2016). Contributions of organic and inorganic
matter to sediment volume and accretion in tidal wetlands at steady state.
Earth's Future 4(4) https://doi.org/10.1002/2015EF000334

Moskalski, S. M. & Sommerfield, C. K. (2012). Suspended sediment deposition
and trapping efficiency in a Delaware salt Marsh. *Geomorphology 139-
140,* 195-204. https://doi.org/10.1016/j.geomorph.2011.10.018

Murphy, S., & Voulgaris G., (2006). Identifying the role of tides, rainfall and
seasonality in marsh sedimentation using long-term suspended sediment

concentration data. *Marine Geology 227*(1-2) 31-50,

https://doi.org/10.1016/j.margeo.2005.10.006

Nowacki, D.J. & Ganju, N.K., (2019). Simple metrics predict salt-marsh sediment

fluxes. *Geophysical Research Letters.*

http://dx.doi.org/10.1029/2019GL083819

Palinkas, C. M. & Engelhardt, K. A. M., (2018). Influence of inundation and

suspended-sediment concentrations on spatiotemporal sedimentation

patterns in a tidal freshwater marsh. *Wetlands*

https://doi.org/10.1007/s13157-018-1097-3

Poirier, E., van Proosdij, D., & Milligan, T.G., (2017). The effect of source

suspended sediment concentration on the sediment dynamics of a

macrotidal creek and salt marsh. *Continental Shelf Research 148* 130-

138. https://doi.org/10.1016/j.csr.2017.08.017

Raposa K. B., Wasson, K., Smith, E., Crooks, J. A., Delgado, P., Fernald, S. H.,

et al. (2016). Assessing tidal marsh resilience to sea-level rise at broad

geographic scales with multi-metric indices. *Biological Conservation 204b*

263-275. https://doi.org/10.1016/j.biocon.2016.10.015

Ratliff K. M., Braswell A. E., & Marani, M., (2015). Spatial response of coastal

marshes to increased atmospheric CO2. *Proceedings of the National*

Academy of Sciences 112(51) 15580-15584.

https://doi.org/10.1073/pnas.1516286112

Reed D. J., Spencer, T., Murray, A. L., French, J. R., & Leonard, L., (1999).

Marsh surface sediment deposition and the role of tidal creeks:

Implications for created and managed coastal marshes. *Journal of Coastal Conservation 5*(1) 81-90, https://doi.org/10.1007/BF02802742

Ross, M. A., (1988). Vertical structure of estuarine fine sediment suspensions. PhD. Dissertation University of Florida. 206p.

Schepers, L., Kirwan, M. L., Guntenspergen, G., & Temmerman, S., (2016). Spatio-temporal development of vegetation die-off in a submerging coastal marsh. *Limnology and Oceanography 62*(1) https://doi.org/10.1002/lno.10381

Settlemyre, J. L., & Gardner, L. R. (1977). Suspended sediment flux through a salt marsh drainage basin. *Estuarine and Coastal Marine Science 5* 653-663.

Syvitski, J. P. M., Kettner, A. J., Hutton, E. W. H., Hannon, M. T., Brakenridge, G. R., Day, J., et al. (2009) Sinking deltas due to human activities. *Nature Geoscience 2* 681-686, https://doi.org/10.1038/ngeo629

Temmerman S., Bouma T. J., Govers G., Wang Z. B., De Vries M. B., & Herman P. M. J. (2005). Impact of vegetation on flow routing and sedimentation patterns: Three-dimensional modeling for a tidal marsh. *Journal of Geophysical Research 110*(F4), doi: 10.1029/2005JF000301

Tommasini, L., Carniello, L., Ghinassi, M., Roner, M., & D'Alpaos, A., (2019). Changes in the wind-wave field and related saltmarsh lateral erosion: inferences from the evolution of the Venice Lagoon in the last four centuries. *Earth Surface Processes and Landforms* https://doi.org/10.1002/esp.4599

Tweel A. W., & Turner, R. E., (2012) Landscape-scale analysis of wetland

sediment deposition from four tropical cyclone events. *PLOS One*

https://doi.org/10.1371/journal.pone.0050528

Voulgaris, G., & Meyers, S. T., (2004a). Temporal variability of hydrodynamics,

sediment concentration and sediment settling velocity in a tidal creek.

Continental Shelf Research 24(15) 1659-1683,

https://doi.org/10.1016/j.csr.2004.05.006

Wang, F. C., Lu, T., & Sikora, W. B., (1993). Intertidal marsh suspended

sediment transport processes, Terrebonne Bay, Louisiana, U.S.A. *Journal

of Coastal Research 9*(1) 209-220, https://www.jstor.org/stable/4298078

Weston, N. B., (2014). Declining sediments and rising seas: An unfortunate

convergence for tidal wetlands. *Estuaries and Coasts 37*(1) 1-23,

https://doi.org/10.1007/s12237-013-9654-8

Wilson C. A., Hughes, Z. J., Fitzgerald, D. M., Hopkinson C. S., Valentine, V., &

Kolker A. S., (2014). Saltmarsh pool and tidal creek morphodynamics:

Dynamic equilibrium of northern latitude saltmarshes? *Geomorphology

213*, 99-115, https://doi.org/10.1016/j.geomorph.2014.01.002

Winterwerp J. C., (2002) On the flocculation and settling velocity of estuarine

mud. *Continental Shelf Research 22*(9) 1339-1360

https://doi.org/10.1016/S0278-4343(02)00010-9

Wolanski, E., Gibbs, R. J., Mazda, Y., Mehta, A., & King, B., (1992). The role of

turbulence in the settling of mud flocs. *Journal of Coastal Research 8*(1)

35-46, https://www.jstor.org/stable/4297950

Zhang, X., Leonardi, N., Donatelli, C., & Fagherazzi, S., (2019) Fate of cohesive

sediments in a marsh-dominated estuary. *Advances in Water Resources*

125 32-40, https://doi.org/10.1016/j.advwatres.2019.01.003
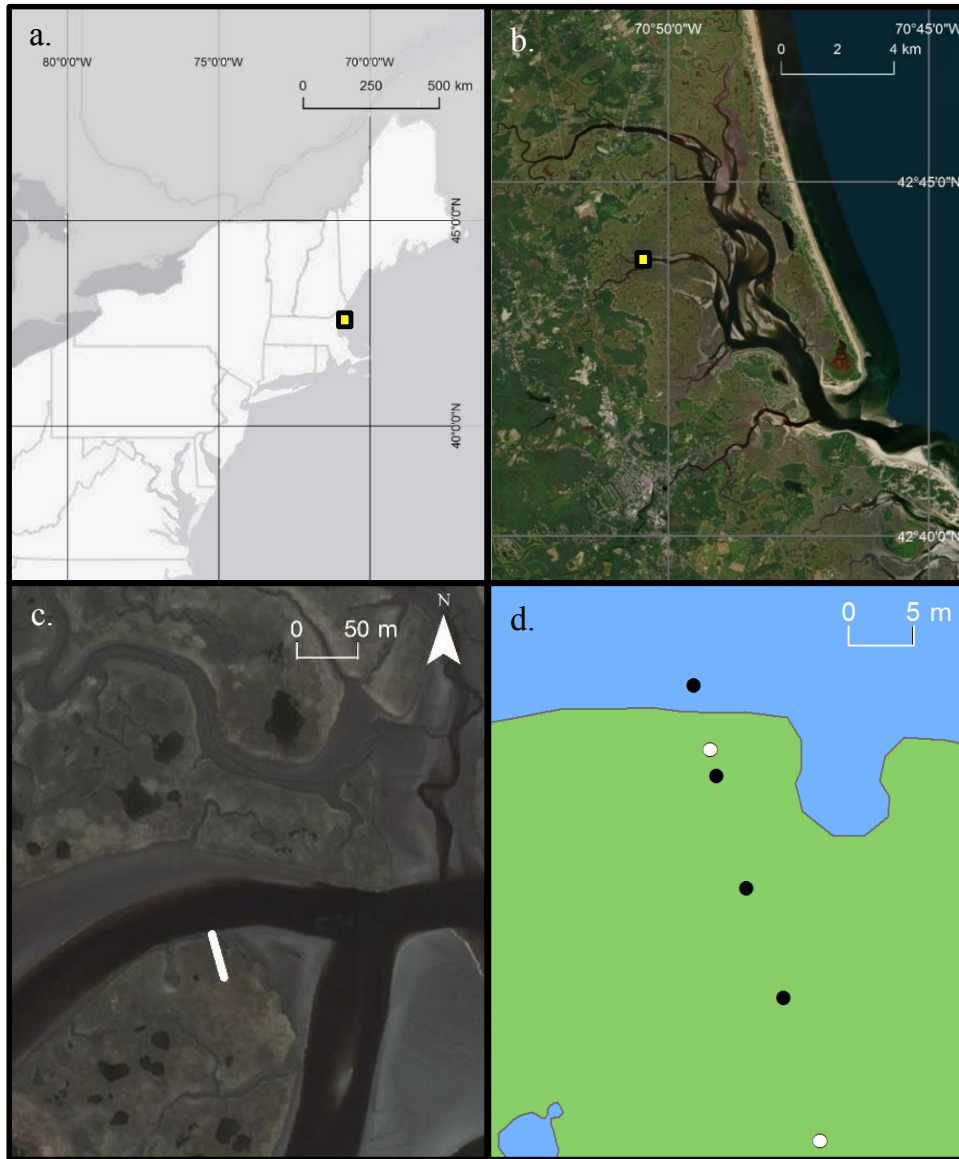
Figure 1: A. Map of the northeast of the US, showing location of Plum Island Estuary in the yellow square. B. Map of the Plum Island Estuary showing the study site in the yellow square. Extensive sand flats downstream of the study site are visible. C. Regional scale map of the Laws Point study site with sensor transect (white line). D. Detailed site map showing transect from West Creek into the marsh interior, where black circles represent turbidity sensors with pressure transducers and white circles represent turbidity sensors without pressure transducers. The turbidity sensor located at 17m inland malfunctioned in 2017 and did not record data. All turbidity sensors on the marsh platform were positioned 7 cm above the bed.
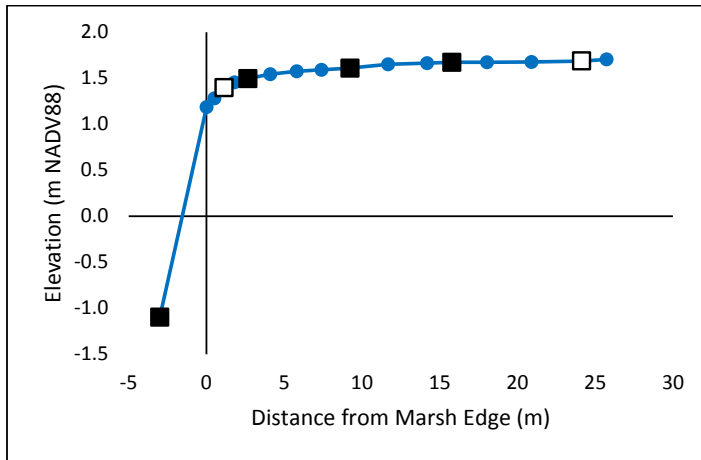
Figure 2: The elevation of the marsh platform via RTK GPS measurements. The squares indicate the location of sensors, with black filled squares indicating sensors also equipped with a pressure sensor. The blue points are additional RTK survey points that did not correspond to a sensor location. The steep slope between the channel sensor and the marsh edge is indicative of the large marsh escarpment common in the system.
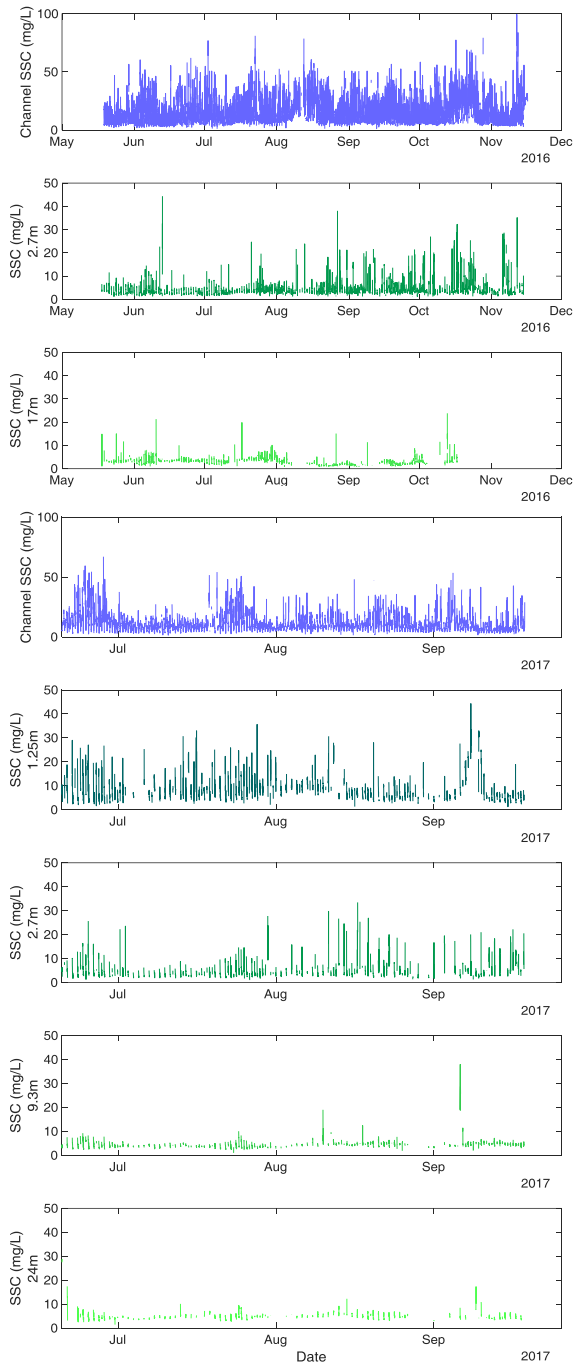
Figure 3: SSC through time for all channel and marsh sensor locations in 2016 and 2017. Blue lines represent the channel and progressively lighter green lines represents progressively more inland marsh. Note vertical scale is different between the channel and marsh locations due to larger magnitude of SSC in the channel. Distances on y-axis represent distance from the marsh-channel edge.
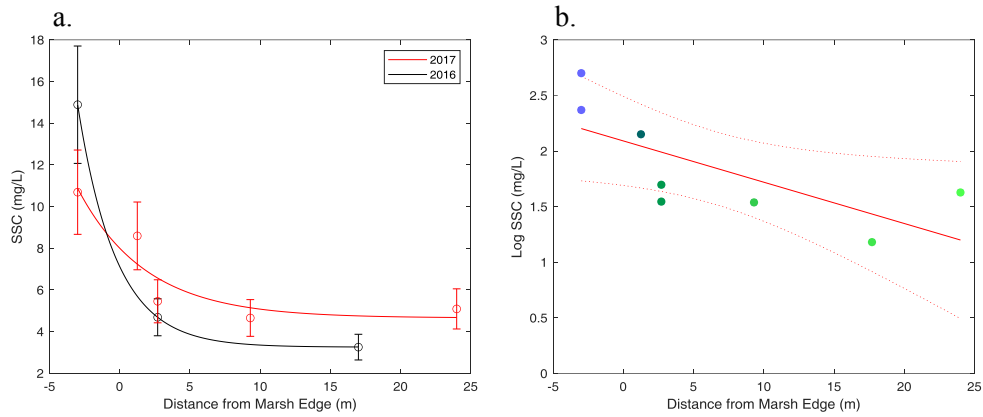
Figure 4: A. Mean suspended sediment concentration at each sensor location for the entire record of a given year. Error bars represent 95% confidence interval of SSC calibration and the lines indicate best fit exponential decay curves. B. Log of the average SSC decreases significantly with distance into the marsh edge, with dashed lines representing 95% confidence interval (R^2=0.52, p<0.05).
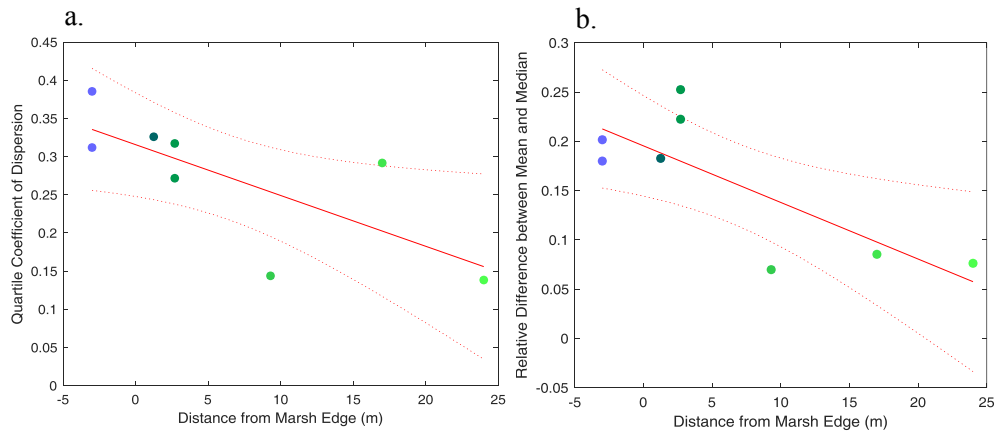
Figure 5: A. Quartile coefficient of dispersion decreases significantly with distance (R^2=0.54, p<0.05) B. The relative mean-median difference for each sensor decreases significantly with distance into the marsh (R^2=0.61, p<0.05). Dashed lines represented the 95% confidence intervals

71
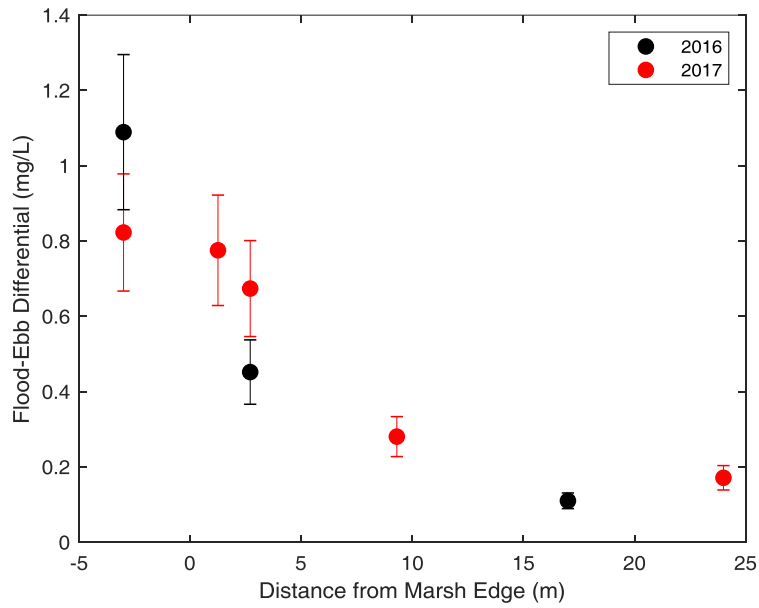
Figure 6: The difference between flood and ebb SSC decreases with distance into the marsh for both 2016 (black) and 2017 (red). Concentrations represent averages of the entire record available for each sensor. Error bars represent 95% confidence interval of SSC calibration. The sediment flux converges (indicating deposition) when the flood-ebb differential at one sensor location is larger than that of the next, more interior, sensor location.
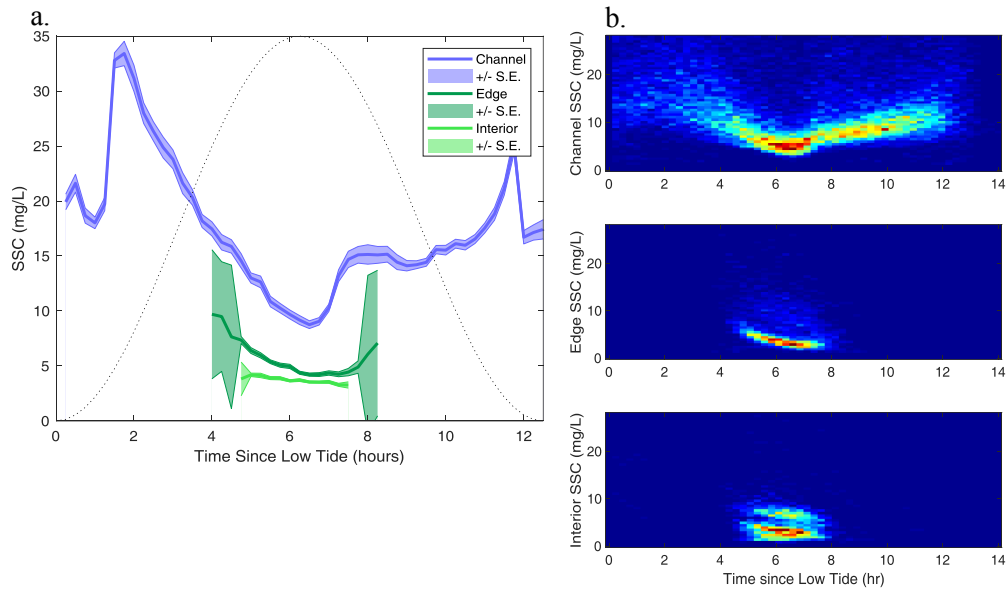
Figure 7: Relationship between SSC and tidal stage for different portions of the marsh-channel system. Data represents the average of all measurements over 2 growing seasons for a given tidal stage. A. Average SSC for each 15 minute increment in the tidal cycle for the channel (blue), marsh edge (dark green), and marsh interior (light green) with envelopes representing one standard error. Superimposed is a hypothetical water level curve (dotted line). Only tidal stages with available data from at least 50 tidal cycles are included. The SSC is statistically significantly related via linear regressions between the channel to the marsh edge (R^2=0.58), and the marsh edge to the marsh interior (R^2=0.52), but not the channel to the marsh interior. B. Heat density map of concentrations over a tidal cycle, where warmer colors represent a higher number of data points that fall within a given 0.5 mg/L by 15 minute bin.
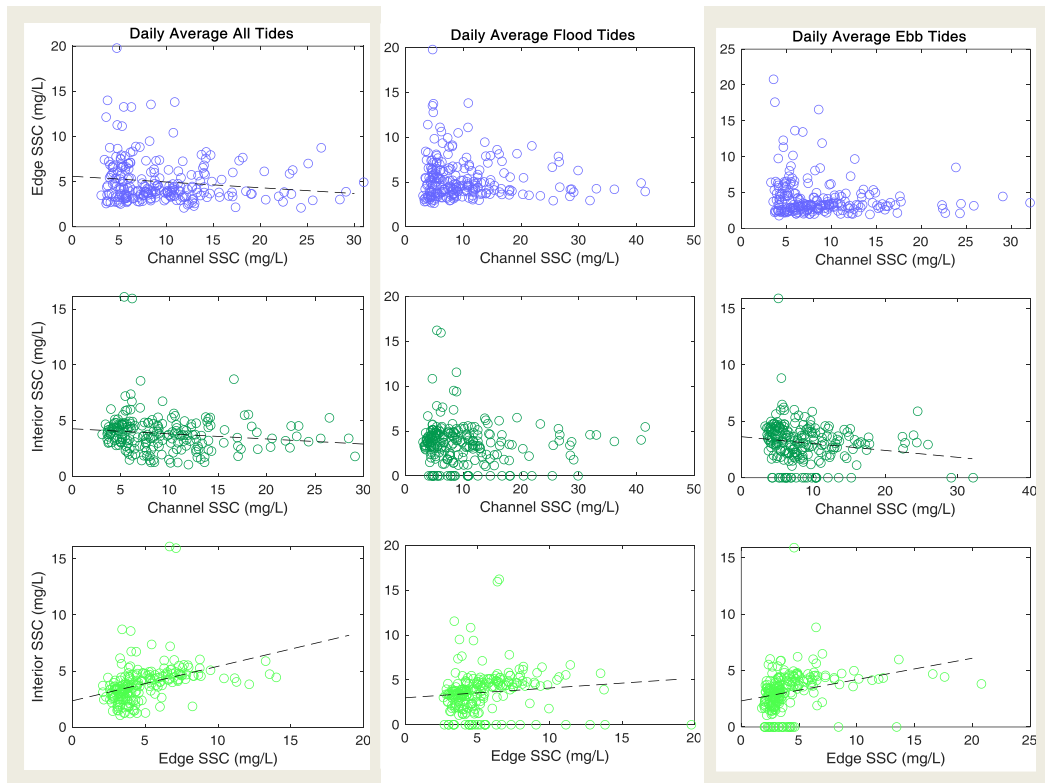
Figure 8: Correlations of daily average SSC between channel, marsh edge, and marsh interior locations. Each point represents a daily averaged concentration only including time points when both sensors being compared were inundated. For example, to calculate the daily average SSC for the channel to compare to the daily average SSC of the marsh edge, we first remove all points when the channel is flooded but the marsh edge is not. Dashed lines represent the best fit linear regression when significant. The first column of graphs includes data for both flooding and ebbing tides, while the second and third column only include data collected during flooding tides and ebbing tides, respectively. The daily average SSC in the channel does not have a significant positive correlation with the daily average SSC in the marsh regardless of which tides are analyzed. In contrast, daily average marsh edge SSC is significantly positively related to the daily average marsh interior SSC for all tides.
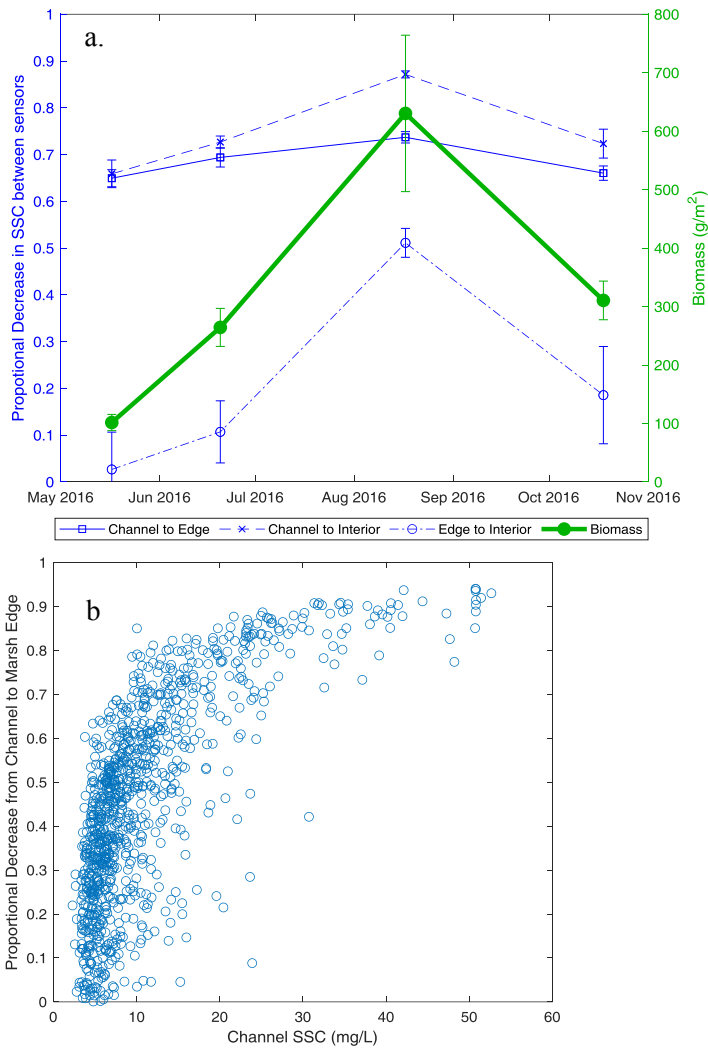
Figure 9: Potential mechanisms for observed spatial patterns in sediment transport. A. Proportional decrease in SSC was calculated over 2 week periods before and after biomass sampling dates (where possible). Platform-average biomass (green line, right axis) is significantly related to the proportional decrease in SSC from the channel to the marsh interior (R^2=0.99, x dashed line, left axis) and from the marsh edge to the marsh interior (R^2=0.98, circle dash-dotted line, left axis). The change in SSC from the channel to the edge (R^2=0.90, square solid blue line, left axis) is at most marginally correlated with biomass. Error bars represent standard error. B. Each point represents the channel concentration and proportional decrease from the channel to the marsh edge at a single measurement point during a flooding tide. At higher channel concentrations, there is a larger decrease in SSC between the channel and marsh, indicating that a smaller proportion of channel sediment is transported to the marsh.

Table 1: Correlation between SSC at each sensor location to 4 environmental drivers. The – or + indicates the direction of correlation between significantly related variables and n.s. indicates no significance at α=0.1. The source of the environmental driver data is given at the bottom followed by an interpretation of how each driver relates to the channel and the marsh.

		Wind Speed	Precip- itation	River Discharge	Tidal Range
2016	Channel	+	+	--	+
	2.7 m	+	n.s.	n.s.	+
	17.0 m	+	n.s.	+	n.s.
2017	Channel	+	+	+	+
	1.25 m	n.s.	n.s.	n.s.	n.s.
	2.7 m	n.s.	n.s.	n.s.	n.s.
	9.3 m	n.s.	n.s.	n.s.	n.s.
	24 m	n.s.	n.s.	n.s.	n.s.
Data source		PIE LTER	PIE LTER	USGS	This Study
Relationship Summary	Channel	Positive	Positive	Interannual Variability	Positive
	Marsh	Thres- hold	None	Predominately none	Predominately none

Supplementary Figure 1: An example photo of an RBR sensor deployed on the marsh surface
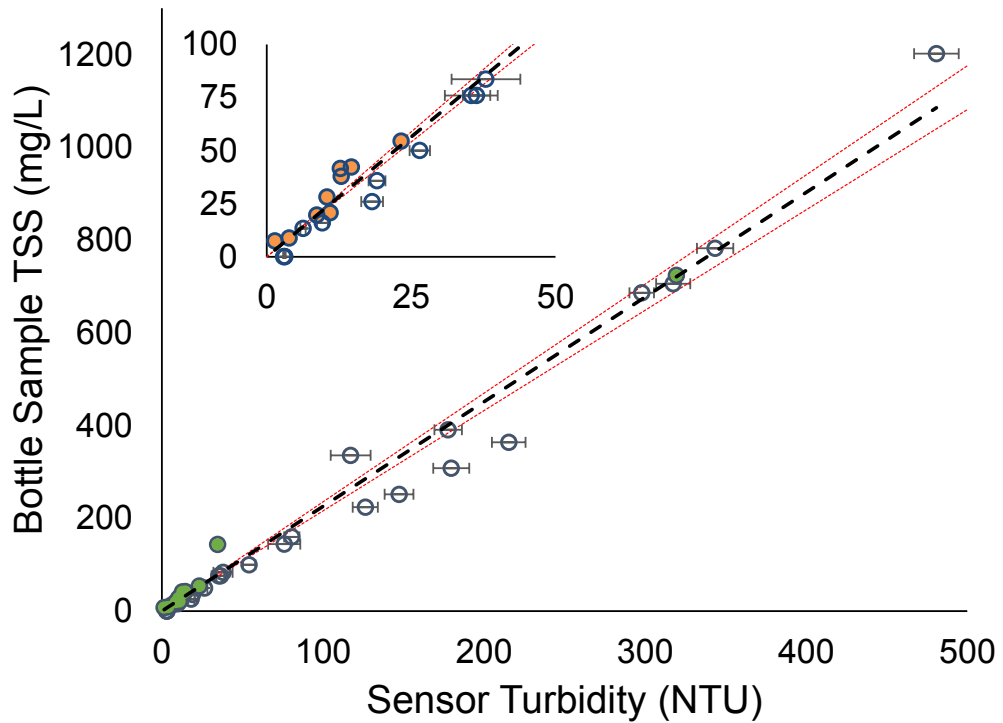
Supplementary Figure 2: Calibration curve used to convert from turbidity (NTU) to suspended sediment concentration (mg/L) is based off of a lab calibration (open circles) and in situ measurements (green filled circles). For lab measurements, we created sediment-water slurries with a range of SSC and measured them with an additional turbidity sensor. For in situ measurements, we measured turbidity with an additional sensor at various locations around the site and at different tidal stages. We collected a water sample in conjunction with each turbidity measurement. Then, we compared sensor turbidity measurements to total suspended solid measurements obtained via vacuum filtration of water samples and sediment-water slurries. The dashed black line represent the linear calibration curve: SSC (mg/L) =2.26*Sensor Turbidity (NTU) (R^2=0.98, n=35, p<<0.001) and the red dotted lines represent the 95% confidence interval. Inset (top left) provides close up of points at lower turbidities.

Supplementary Table 1: A description of the 4 different time window schemes and the correlation coefficient (R) and significance (p-value) of the proportional decrease in SSC from one geomorphic region to another compared to biomass. The number of weeks refers to the data frame which was included in calculating the average proportional decrease in SSC between geomorphic regions. Scheme 1 was designed to be symmetric with two weeks on either side of the intermediate sampling dates and either two weeks after or before the first and last dates, respectively. Scheme 2 was designed so that all data windows were 4 weeks in length. This includes an overlap in the first and last window, meaning some data is included twice. In scheme 3, we shortened the first and second data window so that there was no overlap. Finally, in scheme 4 we included four weeks of data for all points except for the first point, again to avoid overlapping data.

	Deployment	Inter-mediate Visit 1	Inter-mediate Visit 2	Take-down	Channel to Edge	Edge to Interior	Channel to Interior
Dates	May 17, 2016	June 20, 2016	August 17, 2016	October 18, 2016			
Scheme 1	2 weeks after	2 weeks before and after	2 weeks before and after	2 weeks before	$p<0.1$ R=0.9	$p<0.05$ R=0.99	$p<0.05$ R=0.99
Scheme 2	4 weeks after	2 weeks before and after	2 weeks before and after	4 weeks before	$p=0.16$	$p<0.05$ R=0.95	$p<0.05$ R=0.99
Scheme 3	3 weeks after	1.5 weeks before and after	2 weeks before and after	4 weeks before	$p=0.16$	$p<0.1$ R=0.91	$p<0.05$ R=0.99
Scheme 4	2 weeks after	2 weeks before and after	2 weeks before and after	4 weeks before	$p=0.13$	$p<0.05$ R=0.96	$p<0.05$ R=0.99
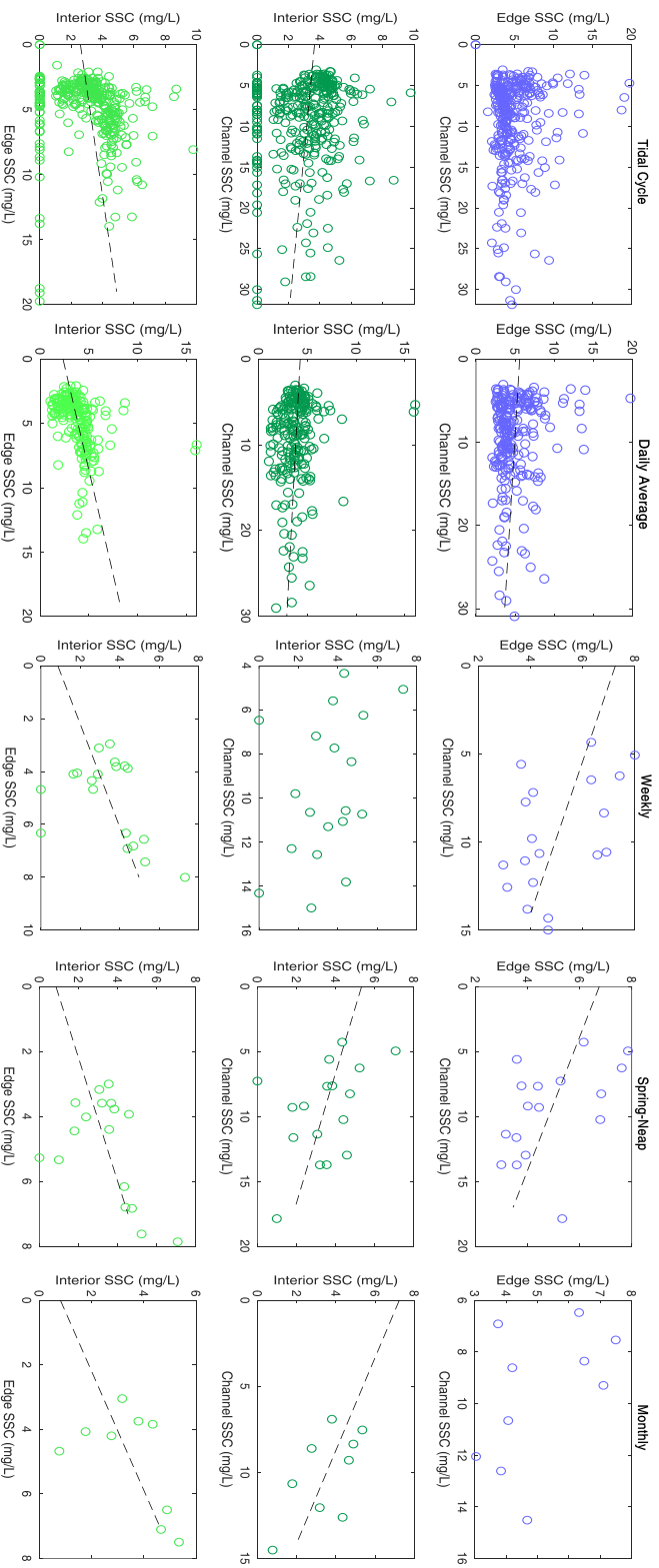
Supplementary Figure 3: A comparison of the channel, marsh edge, and marsh interior concentrations averaged over the window listed at the top of each column of graphs. Only points when both sensors being compared are flooded are included. Dashed lines represent the best fit linear regression if the regression is significant (p<0.1). The channel is never positively correlated with either marsh location and the marsh edge is always positively correlated with the marsh interior.

Supplementary Table 2: Correlation between the locations for different averaging windows. The – or + indicates the direction of correlation between significantly related variables (without asterisk $p<0.05$, with asterisk $0.05<p<0.1$). The R^2 value for significant correlations and the p-value for insignificant correlations is given. Highlighted in yellow are all significant positive correlations

	Channel vs. Marsh Edge			Channel vs. Marsh Interior			Marsh Edge vs. Interior		
	All Tides	Flood	Ebb	All Tides	Flood	Ebb	All Tides	Flood	Ebb
Tidal Cycle	p=0.18	p=0.52	p=0.18	-- R^2=0.02	p=0.18	-- R^2=0.02	+ R^2=0.13	+ R^2=0.02	+ R^2=0.10
Day	-- R^2=0.02	p=0.15	p=0.13	-- R^2=0.02	p=0.14	-- R^2=0.03	+ R^2=0.03	+* R^2=0.01	+ R^2=0.12
Week	-- R^2=0.22	-- R^2=0.23	-- R^2=0.17	p=0.11	p=0.25	-- R^2=0.23	+* R^2=0.20	+* R^2=0.21	+ R^2=0.23
Spring-Neap	--* R^2=0.20	--* R^2=0.20	p=0.11	--* R^2=0.19	p=0.16	--* R^2=0.22	+ R^2=0.25	+ R^2=0.23	+ R^2=0.30
Month	p=0.16	p=0.13	p=0.40	--* R^2=0.39	p=0.14	p=0.11	+* R^2=0.34	p=0.13	+ R^2=0.44

Supplementary Table 3: Correlation between SSC at each sensor location to 4 environmental drivers. The – or + indicates the direction of correlation between significantly related variables (without asterisk p<0.05, with asterisk 0.05<p<0.1). The source of the environmental driver data is given at the bottom followed by an interpretation of how each driver relates to the channel and the marsh. The R^2 value for significant correlations and the p-value for insignificant correlations is given.

		Wind Speed	Precipitation	River Discharge	Tidal Range
2016	Channel	+ R^2=0.04	+ R^2=0.05	-- R^2=0.04	+ R^2=0.04
	2.7 m	+ R^2=0.09	p=0.75	p=0.38	+ R^2=0.05
	17.0 m	+ R^2=0.04	p=0.37	+ R^2=0.06	p=0.24
2017	Channel	+ R^2=0.11	+ R^2=0.06	+ R^2=0.09	+ R^2=0.25
	1.25 m	p=0.42	p=0.61	p=0.56	p=0.78
	2.7 m	p=0.30	p=0.76	p=0.13	p=0.41
	9.3 m	p=0.50	p=0.37	p=0.31	p=0.91
	24 m	p=0.14	p=0.46	p=0.15	p=0.84
Data source		PIE LTER	PIE LTER	USGS	This Study
Relation-ship Summary	Channel	Positive	Positive	Interannual Variability	Positive
	Marsh	Threshold	None	Predominately none	Predominately none

CHAPTER III

The Geomorphic Impact of Mangrove Encroachment in an Australian Salt Marsh

Abstract

Mangroves are encroaching into salt marshes throughout the world as a result of environmental change, including sea level rise. Previous studies suggest that mangroves survive sea level rise through sediment trapping better than salt marshes. The presence of creek-adjacent mangroves may therefore decrease sediment supply to interior salt marsh, leading to greater mangrove encroachment. Despite a poor understanding of sediment transport in mixed marsh-mangrove systems, mangrove removal has been proposed to preserve ecologically-threatened salt marshes. Here we directly test the hypothesis that mangroves reduce the ability of interior marsh to keep pace with sea level rise by measuring sediment transport across salt marsh platforms, with and without a 6-meter fringing band of mangroves at the tidal creek edge. We find that salt marsh and mangroves have equivalent sediment trapping efficiencies along the wetland edge. Suspended sediment concentrations, mass accumulation rates, and long term accretion rates are not lower in salt marshes than mangroves at corresponding distances from the creek edge. Therefore, our work suggests that a relatively narrow band of mangroves does not impact salt marsh accretion, and that mangrove removal is unlikely to help preserve salt marshes in the face of sea level rise.

Introduction

Mangrove swamps and salt marshes are valuable and vulnerable ecosystems that occupy intertidal environments around the world. They offer similar ecosystem services such as storm surge protection, carbon sequestration, and nursery habitat (Kelleway et al., 2017; Himes-Cornell et al., 2018; Lefcheck et al., 2019). Both wetland communities are threatened by human impacts, especially reduced sediment supply and sea level rise. One key difference between these wetland communities is the latitudinal ranges they occupy, with mangroves dominating in the tropics and marshes in temperate zones. Where these communities overlap around the world, marshes tend to be out-competed by mangroves, which themselves are range-limited by physical factors (Kangas and Lugo, 1990; Guo et al., 2013; Saintilan et al., 2014).

Climate change tends to promote mangrove encroachment into salt marsh (Saintilan and Wilton, 2001; Krauss et al., 2011; Osland et al., 2012; Saintilan et al., 2014; Rogers and Krauss, 2019), but the drivers of mangrove encroachment are regionally dependent. For example, the predominant poleward expansion of mangroves in the USA has been attributed to a reduction in the number of winter freeze events (Osland et al., 2012; Cavanaugh et al., 2104). However, Australia has a more cold-tolerant mangrove species that occupies the entire mainland coast (Duke 2006; Rogers and Krauss, 2019). Additionally, Australian mangroves typically occupy more seaward locations and lower elevations than marshes (Clarke and Hannon, 1967; Rogers and Krauss, 2019). As a result, the primary direction of encroachment is landward rather than poleward (Saintilan and

Williams, 1999; Rogers and Krauss, 2019). Rising sea level can convert land ideal for salt marsh vegetation into prime habitat for mangroves (Rogers et al., 2005; Rogers and Krauss, 2019).

The direct effects of mangroves on the encroachment process remains unclear, although sediment trapping could play a role. In other systems, certain species are known to facilitate the displacement of competitors. This conspecific or self-facilitation can occur through many different mechanisms such as allelopathy (Rice 2012), shading (Kangas and Lugo, 1990), and altering fire regimes (Brooks et al., 2004). In the mangrove-salt marsh system of Australia, a mechanism of self-facilitation could be sediment dynamics. If creek-adjacent mangroves trap sediment such that interior marshes are less capable of maintaining elevation relative to rising sea level, the marsh may lose elevation with respect to the tidal frame, which could promote landward mangrove expansion. The expansion of the mangrove band into salt marsh habitat could then trap more sediment in a positive feedback that results in runaway mangrove encroachment. Mangrove expansion has been shown to be more rapid in areas with lower marsh accretion, which is consistent with this proposed mechanism (Saintilan and Rogers, 2006).

Removal of mangroves has been proposed to protect salt marsh, as well as improve recreation and property value (Harty 2009). Temperate zone salt marsh is identified as an ecologically threatened community by the Australian and NSW governments (Federal EPBC Act 1999, NSW Threatened Species Conservation Act 1995), and sea-level rise identified as a key threatening

86

process. The geomorphic and ecological impact of mangrove removal on salt marshes has yet to be established. Previous work suggests that mangroves are more efficient at capturing sediment than marshes, but this finding is inconsistent and confounded by differences in elevation across sites (Rogers et al., 2005; Perry et al., 2009; Lovelock et al. 2014; Kelleway et al., 2017). If superior sediment trapping of mangroves is attributable to vegetation structure, then removing mangroves may allow for increased sediment supply to the landward salt marshes. However, if observed differences in sediment trapping are purely a result of relative position in the landscape, then removing mangroves would not be expected to affect salt marsh sediment supply.

In this study, we aim to determine how mangroves influence sediment transport to a landward salt marsh by comparing two locations within a wetland system, one with creek-side mangroves and landward salt marsh and one with salt marsh abutting the creek edge. We hypothesize that mangroves will decrease suspended sediment concentration (SSC) more than salt marsh plants, leading to reduced short and long-term vertical accretion of landward salt marsh.

Methods

Two contrasting transects were established in Currambene Creek, which empties into Jervis Bay in New South Wales, Australia (Figure 1). The estuary has a semi-diurnal tidal range of approximately 2 meters and supports a temperate saline wetland ecosystem characteristic of the broader region (Owers et al. 2016). The transects were shore-normal and ran from the tidal creek to the

marsh interior, with and without a fringing mangrove band. The mixed-vegetation transect had a narrow band of *Aegiceras corniculatum* mangroves approximately 6 m in width along the creek with extensive *Sporobolus virginicus* salt marsh inland. The marsh transect lacked this band of mangroves and featured *S. virginicus* adjacent to the tidal creek. We conducted a topographic survey with a real-time kinematic GPS (8 mm horizontal precision and 15 mm vertical precision) to ensure each site had a similar elevation range (Figure 2). The mixed transect elevations decreased gradually to the creek whereas the marsh transect had a scarp. The elevation range on the wetland surface itself was similar between the two transects.

Optical back scatter turbidity sensors (RBR) were deployed along the two transects to quantify sediment transport in the presence and absence of a fringing mangrove band. On each transect, one sensor was located 30 cm above the bed in the tidal creek, and four sensors were located 7cm above the bed on the marsh or mangrove surface (Figure 1). Sensors were deployed on the mixed transect so that two were located within the mangrove zone and two were in the saltmarsh zone. Sensors along the marsh transect were located at distances from the creek that correspond to the distances along the mixed transect. All sensors recorded turbidity every 15 minutes from the end of July/beginning of August to mid-September 2018. This record was divided into flooding and ebbing tides based on atmospheric-corrected pressure data from the creek sensors (atmospheric data from Australian Bureau of Meteorology). The pressure record was also used to remove any data points in which a given sensor was not

flooded. We also removed data points in which a sensor was fouled or obstructed following Ganju et al. (2005). Turbidity was calibrated to SSC via *in situ* sampling and laboratory calibration following Coleman and Kirwan (2019), resulting in the equation SSC (mg/L) = 0.6421 * Sensor Turbidity (NTU) (n=20, R^2=0.9146, p<0.01).

To quantify plant biomass of both marsh and mangrove species, we utilized non-destructive measurement techniques. Marsh biomass was measured via terrestrial laser scanning (Owers et al. 2018a) in a 1m^2 plot at each sensor location and at one additional plot located 13m farther inland. The calculation of biomass from the terrestrial laser scans depends on statistical relationships previously determined for this site (Owers et al., 2018a). We measured height, crown area, and stem circumference for all branches greater than 5 cm circumference for all mangrove individuals within a 25m^2 plot centered on the transect. These measurements were used to calculate biomass using allometric equations created for *A. corniculatum* at this study site (Owers et al., 2018b). We then calculated the average mangrove biomass per square meter. This approach produces a single spatially-averaged value of mangrove biomass without a standard deviation.

We deployed filter paper sediment traps to measure short-term mass accumulation rates. The sediment traps consisted of pre-combusted, pre-weighed 90 mm glass microfiber filter paper fixed to square ceramic tiles that were staked to the marsh surface. Five replicate traps were deployed at each sensor on the wetland surface at the end of July/beginning of August and

collected in mid-September (Figure 1). We then calculated the mass of the accumulated sediment divided by the deployment length normalized to the filter paper area to determine a mass accumulation rate ($mg/cm^2/day$). Additionally, we calculated sediment trapping efficiency ((g/cm^2)/(mg/L)) as the mass accumulation per unit area divided by the average SSC at that corresponding sensor. For both mass accumulation rate and trapping efficiency, we constructed linear mixed effect models with fixed effect variables of transect type (mixed or marsh-only) and distance from the shoreline and random variables of vegetation biomass and sediment trap replicate. Elevation was collinear with distance and therefore not included as a separate variable within the model. This model allows us to test our hypothesis that more sediment is retained within the mangrove band and less penetrates into the inland marsh compared to the marsh-only transect. We would expect the mangrove band of the mixed transect to have the highest mass accumulation rate and trapping efficiency while the inland salt marsh of the mixed transect to have the lowest mass accumulation rate.

To measure long-term accretion rates and sediment properties, we collected two sediment cores from each site. One core was located 1 m from the shoreline and the other 7 m from the shoreline, corresponding with sensor locations (Figure 1). Cores were sectioned into 1 cm increments over the first 20 cm. We calculated bulk density for each section by determining the mass of a 1 cm diameter x 1 cm height cylindrical subsample dried at 100°C until a constant mass was achieved. Dry subsamples were then ground and combusted at 500°C for 8 hours to determine loss on ignition, a measure of organic matter content.

We calculated percent sand, silt, and clay of each increment in the top 20 cm using a Malvern Mastersizer 2000. Finally, we calculated accretion rates using radioisotope geochronology. Dating recent sediments usually relies on the determination of the vertical distribution of unsupported or 'excess' ^{210}Pb (half-life 22.3 years), a naturally occurring fallout radionuclide, which then allows ages to be ascribed to sedimentary layers based on the known decay rate of ^{210}Pb (Appleby and Oldfield, 1992). Briefly, total ^{210}Pb was measured by alpha spectroscopy following Nittrouer et al. (1979) where ca. 1.5 g of sediment was spiked with ^{209}Po followed by partial digestion with 8 N nitric acid (HNO3) by microwave heating. We electroplated ^{209}Po and ^{210}Po onto nickel planchets in a dilute acid solution. The supported ^{210}Pb activity for this core was assumed to be equal to the uniform background activity found at depth (Nittrouer et al., 1979). The ^{210}Pb-derived accretion rates are based on the constant rate of supply (CRS) model (Appleby and Oldfield, 1992; Corbett and Walsh, 2015).

Results

The spatial pattern of average SSC for the entire record and when flood or ebb tides were isolated was similar between the two transects (Figure 3). The concentrations were low with an average of 1.1 mg/L along the mixed transect and 0.9 mg/L along the marsh transect. Concentrations were generally highest in the creek and decreased rapidly with distance into the wetland (Figure 3). The notable exception to this pattern was a substantial spike in SSC at the inland sensor of the mangrove band of the mixed site. This spike did not appear to

affect the amount of sediment reaching the marsh, however. On the flooding tide, the first marsh sensor of the mixed transect had an average SSC that was 43% less than the creek sensor, which translates to a 43% decrease in the SSC of water passing through the mangrove band. Over the corresponding distance along the marsh transect, there was a 74% decrease in SSC. Spatial patterns are similar on flood tides (b) and ebb tides (c).

Vegetation biomass was similar between transects. The average biomass for the mixed transect (4.84 kg/m^2 ± 2.40) was not significantly different than the average biomass of the marsh-only transect (4.70 kg/m^2 ± 2.00; Student's t-test, p=0.92). Similarly, the average biomass of the marsh portion of the mixed transect (4.31 kg/m^2 ± 2.9) was not significantly different than the average biomass at the corresponding locations in the marsh-only transect (5.34 kg/m^2 ± 1.35; Student's t-test, p=0.60). The mangrove biomass was 5.91 kg/m^2 while the marsh edge biomass was 3.96 ± 2.39 kg/m^2, but these values cannot be compared statistically due to the approach of calculating mangrove biomass.

Mass accumulation rate and sediment trapping efficiency increased with distance from the shore at both the mixed and marsh-only transects (Figure 4). Mass accumulation rate ranged from 0.07 to 0.21 (mg/cm^2/day) and sediment trapping efficiency ranged from 2.24 to 12.3 (g/cm^2)/(mg/L). Based on the model-quality estimator Akaike information criterion (AIC) and parsimony analysis, the best linear mixed effect model for mass accumulation was Mass Accumulation~ Distance + (1|Trap Replicate) and for trapping efficiency was Trapping Efficiency~ Distance + (1|Trap Replicate). Distance from the shore was a

significant predictor for both mass accumulation rate and sediment trapping efficiency (regression coefficient $\beta=0.0085 \pm 0.0034$, p<0.05; $\beta=0.72 \pm 0.19$, p<0.001), whereas transect was not (Figure 4). In other words, for a given distance from the shoreline, mass accumulation rate and sediment trapping efficiency are not different between the mixed transect and the marsh transect ($\beta=-0.021 \pm 0.024$, p=0.39; $\beta=1.61 \pm 1.50$, p=0.29, Figure 4).

Sediment properties were generally consistent between the top 20 cm of cores from all locations. The site with the lowest average bulk density of the top 20 cm was located in the mangrove band of the mixed transect (1.11 g/cm^3, range of 0.55 g/cm^3) and the site with the highest average bulk density was 7 m from the shore at the marsh-only transect (1.28 g/cm^3, range of 0.65 g/cm^3). Inter-site variability of average bulk density was less than the variability in bulk density with depth in a given core. Average organic matter content of the top 20 cm was very low in all cores, with no core having greater than 5% by mass. The mangrove band had the coarsest grain size (54% sand, range of 24%) and the corresponding location in the marsh site was the finest (34% sand, range of 31%). The interior marshes had an average sand content of 46% (range of 18%) and 40% (range of 32%) for the mixed and marsh-only transects, respectively.

Long term accretion rates were higher along the mixed transect compared to the marsh-only transect and in the interior compared to the edge. The accretion rates averaged over the last 50 years for all cores were significantly different from one another (ANOVA, $F(3,29)=5.59$, p<0.05). The mangrove portion of the mixed transect accreted significantly faster than the marsh edge at

the marsh-only transect (2.1 mm/yr compared to 1.1 mm/yr, Student's t-test, p<0.05). Similarly, the marsh portion of the mixed transect accreted significantly faster than the marsh interior at the marsh-only transect (2.6 mm/yr compared to 1.6 mm/yr, Student's t-test, p<0.05). Within a single transect, the edge and the interior did not have statistically different accretion rates (Student's t-test, p>0.2 for the mixed and marsh-only transects). Accretion rates generally increased through time; rates in the most recent 20 years are faster than any other time in the past 100 at all sites except the marsh interior of the marsh-only transect (Figure 6).

Discussion

The presence of mangroves does not appear to alter sediment supply to the landward marshes. The percentage of sediment passing through the mangrove band and into the marsh (57%) was actually greater than the percentage that passed through the corresponding location at the marsh-only transect (26%; Figure 3). Similarly, the mass accumulation rate and long-term accretion rate of the marsh at the mixed transect was not significantly lower than the corresponding location at the marsh-only transect (Figure 4). There is a noticeable increase in SSC in the landward portion of the mangroves. However, this increase was present in both flood and ebb tides and the mass accumulation rate at that sensor was not elevated. This suggests the increase is not indicative of significant sediment flux and may be caused by a more dynamic sedimentary environment (Figure 3 and 4). The sediment concentrations, accumulation, and

accretion rates are extremely low in this system. It is possible that our inability to

detect a difference between the marsh components between the two transects

may be partially attributable to these low values. However, all three of these

sediment-based metrics were actually higher in the marsh component of the

mixed transect than the corresponding location at the marsh-only transect.

Together these results suggest that mangroves do not promote further

encroachment into salt marshes via limiting sediment transport to interior

marshes.

While previous work suggests that mangroves have higher accretion rates

than salt marshes and may be more resilient to sea level rise, this remains

unclear (Rogers et al., 2005; Lovelock et al. 2014; Kelleway et al., 2017). Some

of the accretion difference may be attributable to the position of mangroves lower

in the tidal frame than salt marsh, particularly in Australia (Kelleway et al., 2017).

Wetlands lower in the tidal frame tend to have greater sediment accumulation

rates because they are inundated for longer durations (Mudd et al., 2010; Kirwan

and Guntenspergen, 2012; Cadol et al., 2014; Kirwan et al., 2016). In North

America, however, mangroves are not consistently lower in elevation than

marshes and do not have consistently higher accretion rates (Perry et al., 2009;

Bianchi et al., 2013). In our study, mangroves occurred at an elevation range that

encompassed the elevation range of the salt marsh, and mass accumulation

rates were not different between mangroves and salt marshes at similar

distances from the creek edge. This suggests that previously inferred differences

in accumulation rates between vegetation types may instead depend on relative

elevation rather than vegetation type. However, long term accretion rates were higher in the mangroves than marshes at corresponding locations (Figure 6a). The greater long-term accretion rate in the mangroves may be caused by greater belowground contributions to the soil by mangrove roots than salt marsh plants (Rogers et al., 2005; Kelleway et al., 2017) and not reflected in short-term measurements of surface deposition. Mangroves may therefore be more capable than salt marsh at building elevation to keep pace with rising sea level due to belowground rather than aboveground processes.

Mangrove vegetation may also attenuate waves to a greater extent than salt marsh vegetation, however this remains uncertain (Gedan et al., 2011; Kelleway et al., 2017). Direct comparisons of wave attenuation between salt marsh and mangroves are limited and often do not account for other environmental factors (Kelleway et al., 2017). However, previous work has shown vegetation size is a crucial factor in the efficiency of dissipating energy from incoming flows (Montgomery et al. 2018). The greater aboveground biomass, structural complexity, and rigidity of mangroves could make them more capable of wave attenuation than salt marsh plants (Kelleway et al., 2017). Mangroves may therefore protect the landward marshes and aid the stability of the entire mixed marsh-mangrove system.

Our work does not support mangrove removal as an effective salt marsh management strategy. Such plans for the removal of mangroves have been considered by local government bodies in Australia due to concerns that sea-level driven mangrove encroachment will displace ecologically vulnerable salt

marshes (Harty 2009). In our study, the presence of mangroves did not reduce the ability of inland salt marsh to survive SLR. Furthermore, our work is consistent with previous studies that suggest mangroves may be more capable of surviving SLR in the long term than marshes (Rogers et al. 2005). Given the higher rates of long-term accretion (Figure 6a) and the potential of mangroves to attenuate waves better than marshes (Kelleway et al., 2017), the removal of mangroves may therefore have a net negative impact on the ability of the wetland system to survive SLR. Mangrove encroachment has been described as a symptom of other environmental change processes and mangrove removal as an ineffective management strategy that does not address the underlying cause of vegetation shifts (Harty 2009). There is an effective hierarchy of salt marsh management over mangrove management (Harty 2009), but both vegetation communities offer valuable ecosystem services on their own (Kelleway et al., 2017; Himes-Cornell et al., 2018; Lefcheck et al., 2019) and synergistically (Saintilan et al. 2007). Other management strategies, such as limiting development into coastal wetlands or allowing for upland migration, will likely be more effective at protecting both salt marsh and mangroves (Evans and Williams, 2001; Kirwan et al., 2016; Schieder et al., 2018).

Conclusion

We found that a fringing mangrove band had no negative effects on sediment supply, mass accumulation rate, or long-term accretion rates of a landward salt marsh. These results suggest that removing mangroves would not

help salt marshes survive sea level rise. Previous work suggests mangroves may be more capable than marshes of surviving sea level and resisting erosion from waves and storms. Thus, our work suggests that the removal of mangroves to protect ecologically threatened marshes may have a negative impact on the marsh and wetland system as a whole.

Acknowledgement

References

Appleby, P.G., Oldfield, F., 1992. Application of 210Pb to sedimentation studies. In: Ivanovich, M., Harmon, R.S. (Eds.), Uranium Series Disequilibrium. Oxford University Press, Oxford, pp. 731-778.

Bianchi, T. S., Allison, M. A., Zhao, J., Li, X., Comeaux, R. S., Feagin, R. A., & Kulawardhana, R. W. (2013). Historical reconstruction of mangrove expansion in the Gulf of Mexico: linking climate change with carbon sequestration in coastal wetlands. *Estuarine, Coastal and Shelf Science*, *119*, 7-16.

Brooks, M. L., D'antonio, C. M., Richardson, D. M., Grace, J. B., Keeley, J. E., DiTomaso, J. M., ... & Pyke, D. (2004). Effects of invasive alien plants on fire regimes. *BioScience*, *54*(7), 677-688.

Cadol, D., Engelhardt, K., Elmore, A., & Sanders, G. (2014). Elevation-dependent surface elevation gain in a tidal freshwater marsh and implications for marsh persistence. *Limnology and Oceanography*, *59*(3), 1065-1080.

Cavanaugh, K. C., Kellner, J. R., Forde, A. J., Gruner, D. S., Parker, J. D., Rodriguez, W., & Feller, I. C. (2014). Poleward expansion of mangroves is a threshold response to decreased frequency of extreme cold events. Proceedings of the National Academy of Sciences, 111(2), 723-727.

Clarke, L. D., & Hannon, N. J. (1967). The mangrove swamp and salt marsh communities of the Sydney district: I. Vegetation, soils and climate. *The Journal of Ecology*, 753-771.

Coleman, D.J., & Kirwan, M.L., (2019). The effect of a small vegetation dieback

event on salt marsh sediment transport. *Earth Surface Processes and*

Landforms 44(4), 944-952, https://doi.org/10.1002/esp.4547

Corbett, D. R., and J. P. Walsh. 2015. [210]Lead and [137]Cesium Establishing a

chronology for the last century. In I. Shennan, A. J. Long, and B. P. Horton

(Ed.) Handbook of sea-level research. John Wiley & Sons, Inc. Pp. 361-

372.

Duke, N. C. (2006). *Australia's mangroves: the authoritative guide to Australia's*

mangrove plants. MER.

Evans M. J., and R. J. Williams. (2001). Historical distribution of estuarine

wetlands at Kurnell Peninsula, Botany Bay. *Wetlands (Australia)* 19(2):61–

71.

Ganju, N.K., Schoellhamer, D.H. & Bergamaschi, B.A., (2005). Suspended

sediment fluxes in a tidal wetland: Measurement, controlling factors, and

error analysis. *Estuaries 28*(6), 812-822.

Gedan, K. B., Kirwan, M. L., Wolanski, E., Barbier, E. B., & Silliman, B. R. (2011).

The present and future role of coastal wetland vegetation in protecting

shorelines: answering recent challenges to the paradigm. *Climatic*

change, *106*(1), 7-29.

Guo, H., Zhang, Y., Lan, Z., & Pennings, S. C. (2013). Biotic interactions mediate

the expansion of black mangrove (A vicennia germinans) into salt

marshes under climate change. *Global Change Biology*, *19*(9), 2765-2774.

Harty, C. (2004). Planning strategies for mangrove and saltmarsh changes in

Southeast Australia. *Coastal Management*, *32*(4), 405-415.

Himes-Cornell, A., Grose, S. O., & Pendleton, L. (2018). Mangrove ecosystem

service values and methodological approaches to valuation: Where do we

stand?. *Frontiers in Marine Science*, *5*, 376.

Kangas, P. C., & Lugo, A. E. (1990). The distribution of mangroves and

saltmarsh in Florida. *Tropical Ecology*, *31*(1), 32-39.

Kelleway, J. J., Cavanaugh, K., Rogers, K., Feller, I. C., Ens, E., Doughty, C., &

Saintilan, N. (2017). Review of the ecosystem service implications of

mangrove encroachment into salt marshes. *Global Change

Biology*, *23*(10), 3967-3983.

Kirwan, M. L., & Guntenspergen, G. R. (2010). Influence of tidal range on the

stability of coastal marshland. *Journal of Geophysical Research: Earth

Surface*, *115*(F2).

Kirwan, M. L., Temmerman, S., Skeehan, E. E., Guntenspergen, G. R., &

Fagherazzi, S. (2016). Overestimation of marsh vulnerability to sea level

rise. *Nature Climate Change*, *6*(3), 253-260.

Krauss, K. W., From, A. S., Doyle, T. W., Doyle, T. J., & Barry, M. J. (2011). Sea-

level rise and landscape change influence mangrove encroachment onto

marsh in the Ten Thousand Islands region of Florida, USA. *Journal of

Coastal Conservation*, *15*(4), 629-638.

Lefcheck, J. S., Hughes, B. B., Johnson, A. J., Pfirrmann, B. W., Rasher, D. B.,

Smyth, A. R., Williams, B. L., Beck, M. W., & Orth, R. J. (2019). Are

coastal habitats important nurseries? A meta-analysis. *Conservation Letters*, *12*(4), e12645.

Lovelock, C. E., Adame, M. F., Bennion, V., Hayes, M., O'Mara, J., Reef, R., & Santini, N. S. (2014). Contemporary rates of carbon sequestration through vertical accretion of sediments in mangrove forests and saltmarshes of South East Queensland, Australia. *Estuaries and coasts*, *37*(3), 763-771.

McIvor, A. L., Möller, I., Spencer, T., & Spalding, M. (2012). Reduction of wind and swell waves by mangroves. *Natural Coastal Protection Series: Report 1. Cambridge Coastal Research Unit Working Paper 40. ISSN 2050-7941.*

Montgomery, J. M., Bryan, K. R., Horstman, E. M., & Mullarney, J. C. (2018). Attenuation of tides and surges by mangroves: contrasting case studies from New Zealand. *Water*, *10*(9), 1119.

Mudd, S. M., Fagherazzi, S., Morris, J. T., & Furbish, D. J. (2004). Flow, sedimentation, and biomass production on a vegetated salt marsh in South Carolina: toward a predictive model of marsh morphologic and ecologic evolution. *The Ecogeomorphology of Tidal Marshes, Coastal Estuarine Stud*, *59*, 165-187.

Nittrouer, C.A., Sternberg, R.W., Carpenter, R. and Bennett, J.T., 1979. The use of 210Pb geochronology as a sedimentological tool: application to the Washington Continental Shelf. Marine Geology 31, 297–316.

Osland, M. J., Enwright, N., Day, R. H., & Doyle, T. W. (2013). Winter climate change and coastal wetland foundation species: salt marshes vs.

mangrove forests in the southeastern United States. *Global change biology*, *19*(5), 1482-1494.

Owers, C. J., Rogers, K., Mazumder, D., & Woodroffe, C. D. (2016). Spatial variation in carbon storage: A case study for Currambene Creek, NSW, Australia. *Journal of Coastal Research*, *75*(sp1), 1297-1301.

Owers, C. J., Rogers, K., & Woodroffe, C. D. (2018a). Terrestrial laser scanning to quantify above-ground biomass of structurally complex coastal wetland vegetation. *Estuarine, Coastal and Shelf Science*, *204*, 164-176.

Owers, C. J., Rogers, K., & Woodroffe, C. D. (2018b). Spatial variation of above-ground carbon storage in temperate coastal wetlands. *Estuarine, Coastal and Shelf Science*, *210*, 55-67.

Perry, C. L., & Mendelssohn, I. A. (2009). Ecosystem effects of expanding populations of *Avicennia germinans* in a Louisiana salt marsh. *Wetlands*, *29*(1), 396-406.

Rice, E. L. (2012). *Allelopathy*. Academic press.

Rogers, K., & Krauss, K. W. (2019). Moving from generalisations to specificity about mangrove–saltmarsh dynamics. *Wetlands*, *39*(6), 1155-1178.

Rogers, K., Saintilan, N., & Heijnis, H. (2005). Mangrove encroachment of salt marsh in Western Port Bay, Victoria: the role of sedimentation, subsidence, and sea level rise. *Estuaries*, *28*(4), 551-559.

Saintilan, N., Hossain, K., & Mazumder, D. (2007). Linkages between seagrass, mangrove and saltmarsh as fish habitat in the Botany Bay estuary, New South Wales. *Wetlands Ecology and Management*, *15*(4), 277-286.

Saintilan, N., & Rogers, K. (2006). Coastal wetland elevation trends in southeast
Australia. In *Catchments to Coast. Society of Wetland Scientists 27th
International Conference* (pp. 42-54).

Saintilan, N., & Williams, R. J. (1999). Mangrove transgression into saltmarsh
environments in south-east Australia. *Global Ecology and
Biogeography*, *8*(2), 117-124.

Saintilan, N., Wilson, N. C., Rogers, K., Rajkaran, A., & Krauss, K. W. (2014).
Mangrove expansion and salt marsh decline at mangrove poleward
limits. *Global change biology*, *20*(1), 147-157.

Saintilan, N., & Wilton, K. (2001). Changes in the distribution of mangroves and
saltmarshes in Jervis Bay, Australia. *Wetlands Ecology and
Management*, *9*(5), 409-420.

Schieder, N. W., Walters, D. C., & Kirwan, M. L. (2018). Massive upland to
wetland conversion compensated for historical marsh loss in Chesapeake
Bay, USA. *Estuaries and Coasts*, *41*(4), 940-951.

Shepard, C. C., Crain, C. M., & Beck, M. W. (2011). The protective role of coastal
marshes: a systematic review and meta-analysis. *PloS one*, *6*(11).
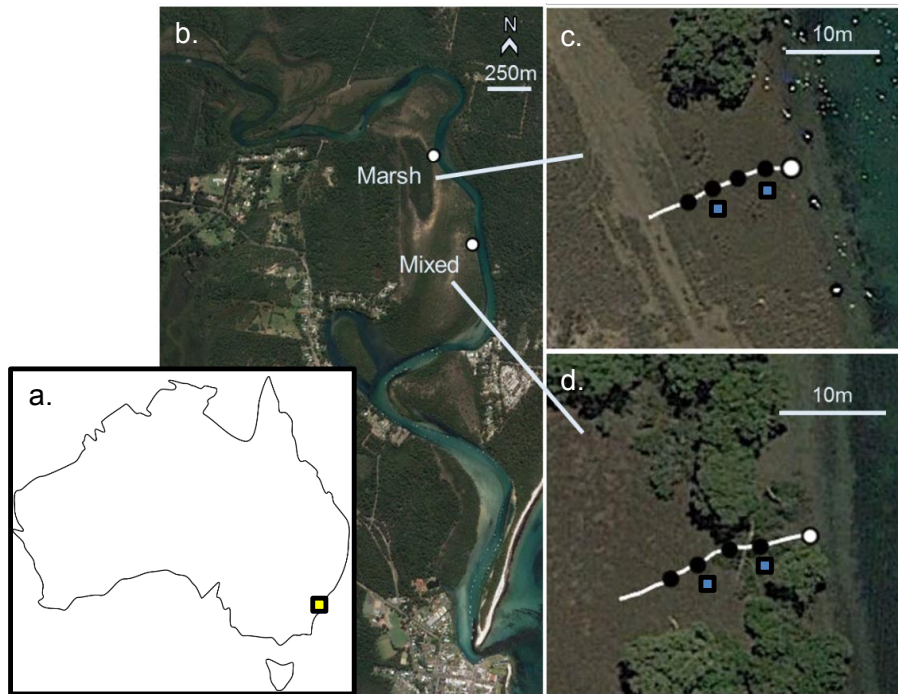
Figure 1. Site maps showing the location of Currambene Creek (yellow box) on the map of Australia (a.) and each transect with respect to Currambene Creek (b.). At the marsh-only transect (c.), and the mixed transect (d.), black circles represent locations of sediment tiles and the sensors on the wetland surface. The white point represents the sensor in the creek and blue squares represent the core locations. The white line indicates the GPS transects.
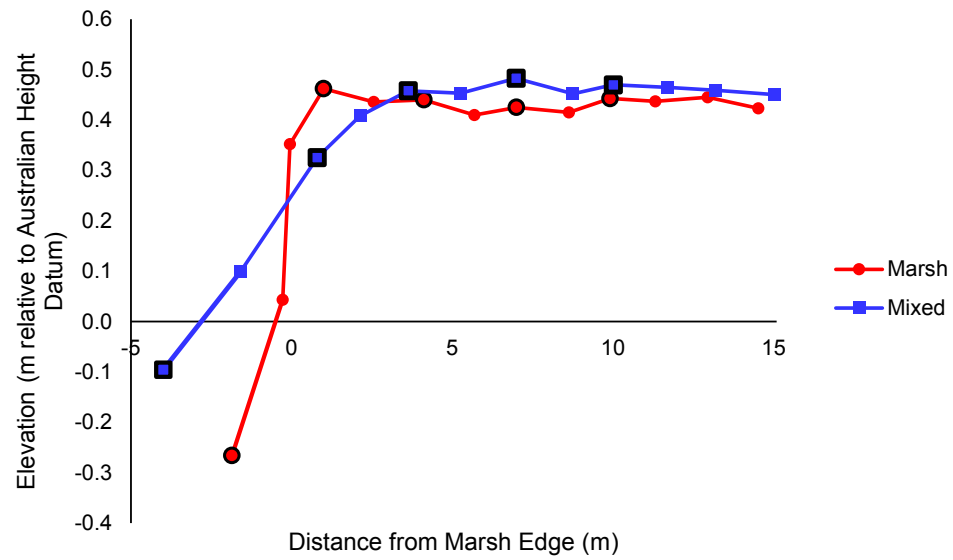
Figure 2. Elevation profiles for the mixed site (blue) and marsh-only site (red), where points outlined in black indicate sensor locations.
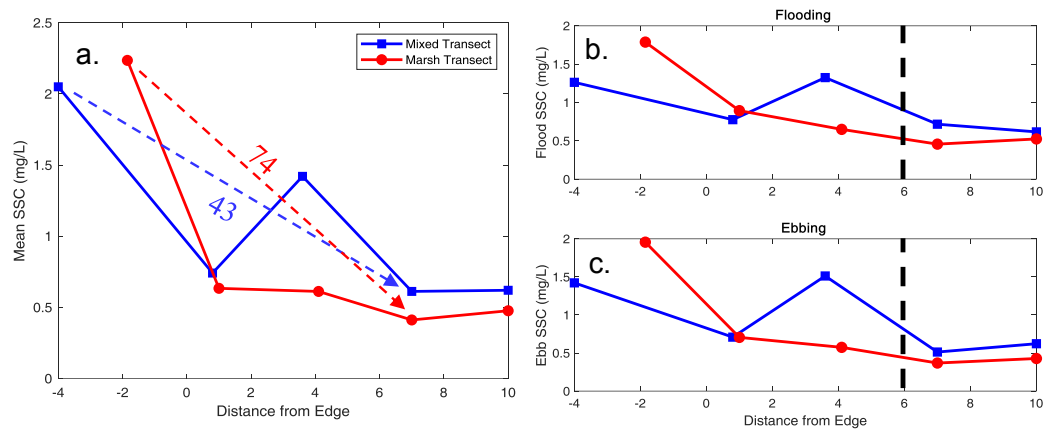
Figure 3. Spatial patterns of SSC across the wetland platform, where distance from edge refers to the distance from a tidal creek. (a) SSC averaged over the entire period of record declines with distance except for localized high concentrations within the mangrove band. The colored dashed line indicates the percent decrease in creek SSC over the width of the mangrove band.
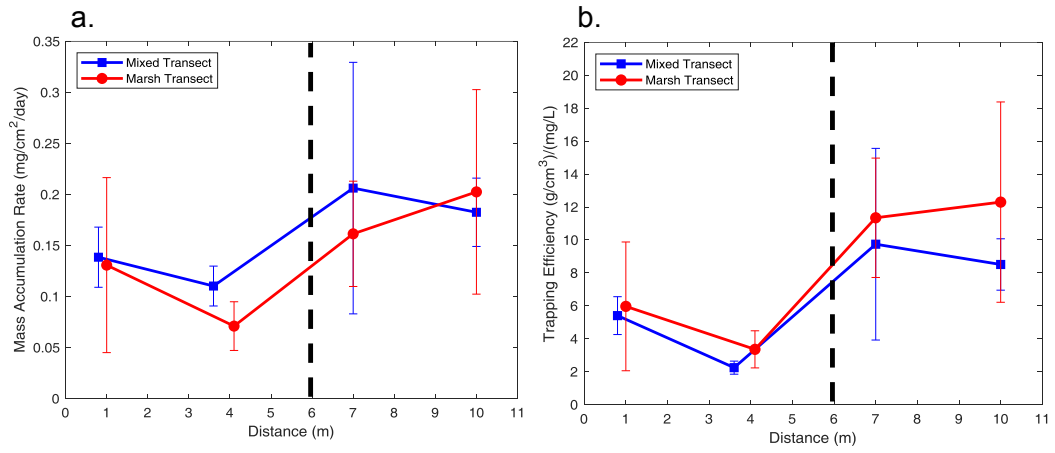
Figure 4. Mass accumulation rate (a) and trapping efficiency (b) with distance from the wetland edge for the mixed transect (blue) and the marsh-only transect (red). Error bars represent one standard deviation of replicate plots. The dashed line indicates the boundary between mangroves and marsh at the mixed transect.
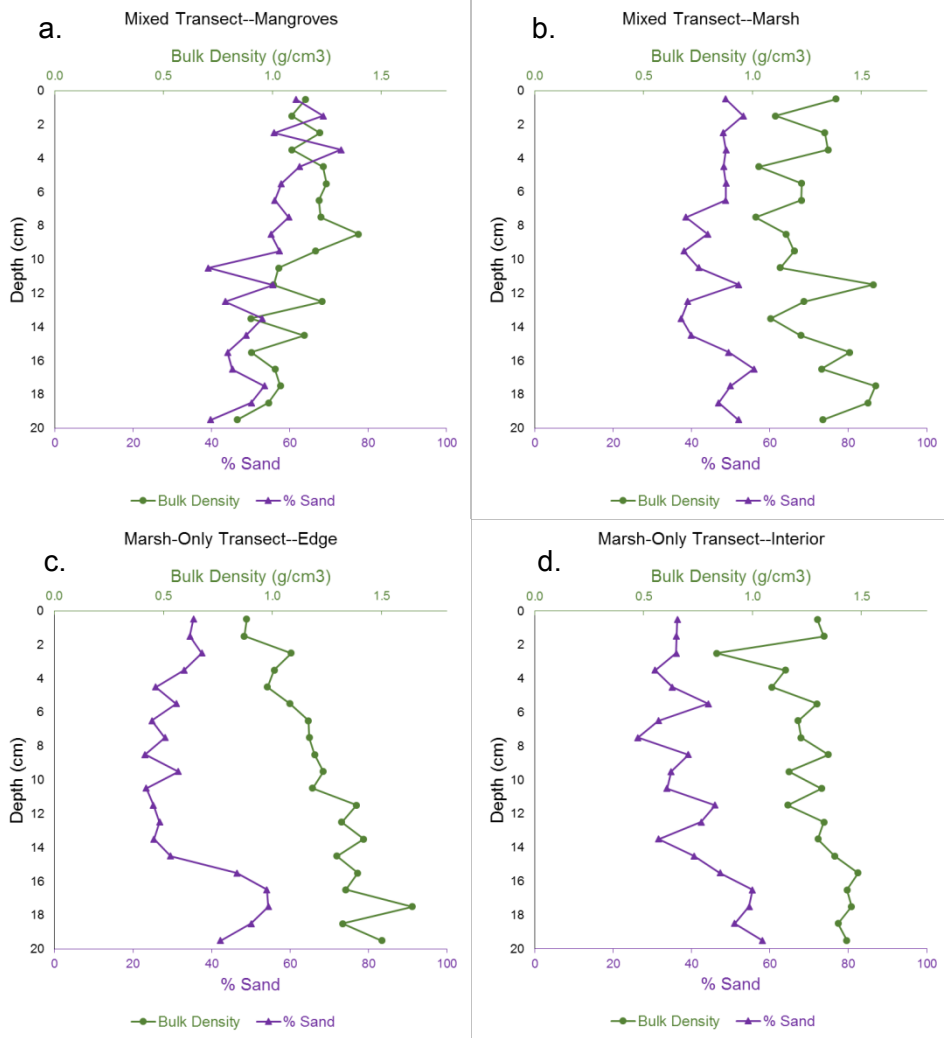
Figure 5: Bulk density and percent sand content for sediment cores at (a.) the mangrove band of the mixed transect, (b.) the adjacent marsh at the mixed transect, (c.) the edge site of the marsh-only transect, and (d.) the interior marsh of the marsh-only transect.
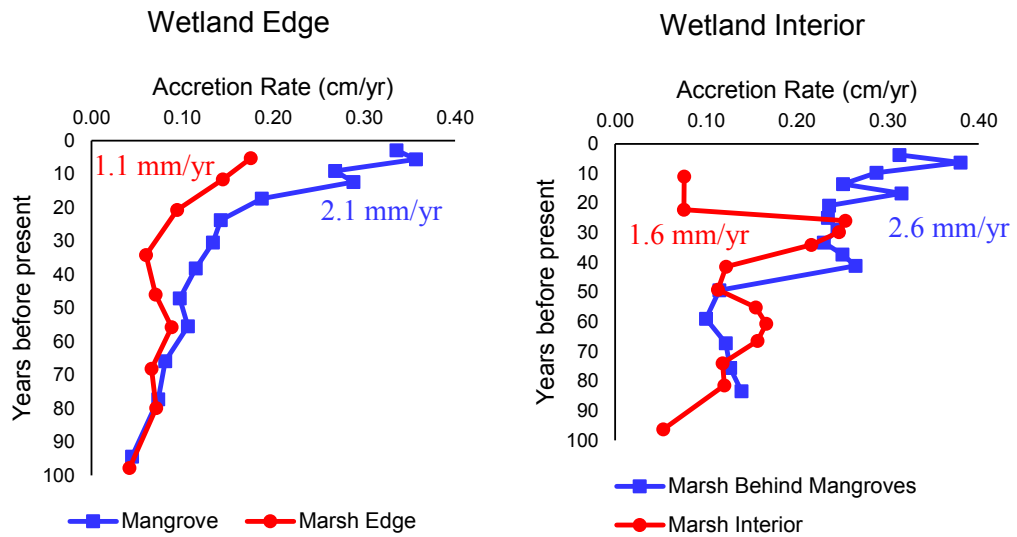
Figure 6: Accretion rate through time based on CRS Pb-210 radiochronology. Accretion rates accelerate through time for all sites except at the marsh interior site of the marsh-only transect. Labels indicate accretion rate averaged over the past 50 years in mm/yr.

CHAPTER IV

The Role of Suspended Sediment Concentration in Determining Marsh

Vulnerability to Sea Level Rise

.

Abstract

Tidal marsh survival in the face of sea level rise and declining sediment supply depends largely on the ability of marshes to build soil vertically. Numerical models emphasize the role of mineral sediment in determining marsh vulnerability, but predict threshold rates of sea level rise that exceed most field-based measurements of vertical accretion. Here, we measure suspended sediment concentration (SSC), tidal range (TR) and vertical accretion in seven marshes, compile data from 70 additional marshes from around the world, and show that over 70% of the variability in marsh accretion rates can be explained by physical characteristics, such as SSC and TR. Accretion rates for a given SSC and TR are highest in frequently flooded, low elevation marshes, and are consistent with threshold sea level rise rates predicted by numerical models. We explain apparent discrepancies between models and field measurements by showing that marshes around the world require less sediment to survive SLR than to maintain their existing elevation and vegetation species composition. Together these results help bridge the gap between numerical models and field measurements of wetland vulnerability, and reinforce the paradigm that mineral sediment supply is the key determinant of vertical marsh accretion at regional to global scales.

Introduction

Accelerating rates of sea level rise and declining sediment supplies threaten coastal wetlands. In places where marshes are unable to migrate landward, marshes must build soils vertically to survive. The global sea level rise (SLR) rate of 3.5 mm yr^{-1} is expected to increase to as high as 16 mm yr^{-1} by the end of the century (Dieng et al., 2017; Church et al., 2013). In addition to enhanced stress from SLR, sediment delivery to the coast has significantly declined in many locations (Wang et al., 2011; Weston 2014). Coastal wetlands therefore require faster rates of elevation change to keep pace with sea level but are receiving less inorganic material to do so. This combination of forces limits the ability of coastal wetlands to persist into the future and may ultimately lead to wetland loss (Weston 2014; Crosby et al., 2016; Watson et al., 2017; and others)

Estimates for the rates of SLR which will cause marsh loss differ drastically, especially between numerical models and empirical measurements. Numerical models often predict stability under relatively high rates of sea level rise in the future (Kirwan et al., 2016), whereas field measurements suggest vulnerability at lower rates observed today (Jankowski et al., 2017; Morris et al., 2016; Crosby et al. 2016). For example, a meta-analysis of vertical accretion rates suggests widespread drowning at current rates of sea level rise (Crosby et al., 2016), despite numerical models that predict marsh survival at SLR rates of up to 10–50 mm yr^{-1} (Kirwan et al. 2016). Threshold rates are thought to depend on sediment supply and tidal range (Kirwan et al. 2010). Nevertheless, under conditions generally representative of U.S. Atlantic Coast estuaries (TR= 1 m; SSC= 30mg

L^{-1}), measurements of organic content and bulk density suggest drowning under SLR rates greater than 5 mm yr^{-1} (Morris et al., 2016) while an ensemble of numerical models predicts a threshold SLR rate twice as high (Kirwan et al., 2010).

There are inherent advantages and disadvantages to using both numerical models and empirical measurements to predict the maximum rate of SLR that existing marshes can survive without migrating landward. Numerical models typically focus on basic feedbacks between inundation and sediment transport that allow projections of elevation building through time in response to changing environmental conditions (Fagherazzi et al., 2012; Kirwan et al., 2016). Yet, models are inherent simplifications of real world process that often rely on simplistic treatment of vegetation, lack of spatial resolution, and sensitivity to poorly constrained parameters such as particle settling velocity (Marani et al., 2007; Wiberg et al., 2020). Field measurements, on the other hand, directly measure current and historical rates of vertical accretion influenced by a more complete suite of processes (DeLaune et al., 1978; Parkinson et al., 2017; Jankowski et al. 2017). Yet, accretion rates tend to increase with flooding depth and duration (Friedrichs and Perry, 2001), making it difficult to project measurements based on current or historical conditions into a future characterized by faster sea level rise rates (Kirwan et al., 2016).

Here, we attempt to bridge the gap between numerical models and field measurements by developing an empirical model of salt marsh vulnerability based on novel field measurements and a global meta-analysis of accretion and

suspended sediment concentration (SSC). Our work finds that vertical accretion and marsh vulnerability are fundamentally tied to suspended sediment concentration and tidal range, and suggests that perceived differences between models and measurements can be explained by the difference between elevation loss relative to sea level and marsh drowning.

Drivers of Vertical Accretion

We directly measured SSC and vertical accretion in seven tidal marshes spanning the eastern coast of the US and one on the eastern coast of Australia (Figure 1). In contrast to the traditional approach of quantifying SSC using bottle sampling and vacuum filtration (e.g. Christiansen et al., 2000; Leonard and Reed, 2002; Moskalski and Sommerfield, 2012; Poirier et al., 2017; Wang et al., 1993; Ensign et al. 2017a), we measured SSC every 15 minutes over seasonal to annual time scales and across the marsh platform rather than discontinuous measurements in tidal channels. Four of these sites were located within extremely low, youthful marshes where marshes are expanding or recovering from disturbance. Low marshes are thought to have local maximum rates of vertical accretion because high vegetation biomass and frequent inundation leads to rapid sediment deposition (Morris et al., 2002; Mudd et al., 2010; Kirwan and Guntenspergen, 2012; Cadol et al., 2014; Kirwan et al., 2016). We then compiled vertical accretion and SSC data from the literature for 70 coastal marshes around the world, with the greatest concentration of sites in Europe and North America (Figure 1). In contrast to our direct field measurements, these

sites varied widely in marsh elevation, tidal range, vegetation type, and the

methodology used to measure accretion and SSC (Supplementary Table 1).

Therefore, our analyses include marshes across a wide range of environmental

gradients; SSC ranged from approximately 5-30 mg L^{-1} and TR from 1.1 to 3.6 m

in low marsh monitored sites, whereas the meta-analysis sites encompassed a

wider variety of SSC from 0.5-358 mg L^{-1} and TR from 0.3-12 m.

We found that accretion rate is significantly related to SSC*TR (robust

linear regression, R^2=0.73, p<0.001; Figure 2a). We determined a simple

empirical model to describe this relationship, defined as,

$$Accretion = C_1 * SSC * TR \qquad\qquad (1)$$

This equation is analogous to accretion rate having a fixed proportional

relationship (C_1) to the sediment suspended in flooding waters. We calculated

C_1=0.2212 ± 0.008 (± s.e.) for all sites excluding 5 outliers and C_1=0.3535 ±

0.059 for the four low marsh monitored sites monitored in this study. The higher

value of C_1 for the low marsh monitored sites is consistent with observations that

frequently flooded, youthful marshes have higher rates of accretion, and our

assumption that these types of marshes would have local maximum accretion

rates (Morris et al., 2002; Mudd et al., 2010; Kirwan and Guntenspergen, 2012;

Cadol et al., 2014; Kirwan et al., 2016). Interestingly, we found no significant

difference between modern sedimentation measurements (C_1=0.2452 ± 0.009)

and modern elevation change measurements (C_1=0.1980 ± 0.019), suggesting

that shallow subsidence did not play a major consistent role in the relationship

between SSC*TR and accretion over regional-continental gradients (Cahoon et

al., 2006). Radiochronological methods that measure accretion over multi-decade to century timescales produced a significantly lower slope between measured accretion and SSC*TR (C_1=0.1014 ± 0.008) than short-term measurements of sediment deposition (Figure 2b). This difference could be attributed to either accretion rates that are accelerating in parallel with sea level rise (Kolker et al., 2010; Kirwan and Temmerman, 2009) or the long-term effect of compaction and organic matter decomposition that are not fully expressed in short-term measurements (Kearney et al., 2004; Bartholdy et al., 2010; Tornqvist et al., 2008; Breithaupt et al., 2018).

Conceptual and numerical models often emphasize the role of mineral sediment supply in determining marsh vulnerability (Reed, 1995; Mudd et al., 2004; FitzGerald et al., 2008; Kirwan et al., 2010; Fagherazzi et al., 2015; Kirwan and Megonigal, 2013), though attempts to demonstrate the connection in the field have been inconsistent. For example, many field studies do not find a relationship between SSC and accretion within a single study site (see Ganju et al., 2015; Palinkas and Engelhardt, 2018; Murphy and Voulgaris, 2006; Poirier et al., 2017; D'Alpaos and Marani, 2016; Duvall et al., 2017). Similarly, the relationship between TR and accretion has been shown to be inconsistent (Kirwan and Guntenspergen, 2010), with some studies finding a positive relationship (Harrison and Bloom, 1977; Stevenson et al., 1986), some suggesting a negative relationship (Chmura and Hung, 2004) and some finding no relationship at all (Cahoon et al., 2006; French, 2006). In contrast, robust linear regression with all 77 of our marsh sites indicates that over 70% of the

variability in accretion is explained by terms that directly relate to inorganic

accretion, SSC and TR (R^2=0.73, p<0.001; Figure 2a). We suggest that the

definitive role of physical processes becomes apparent only by considering SSC

and TR together, and at regional to global spatial scales. Together, our results

demonstrate the primary importance of inorganic accretion and support

assumptions of numerical models that aim to predict accretion rates based

largely on physical processes (see Mudd et al., 2004; Kirwan et al. 2016;

Temmerman et al., 2003; Marani et al., 2007).

Nevertheless, our work also illustrates substantial variability in accretion

rates that cannot be explained by physical factors such as SSC and TR alone.

The empirical model predicts accretion rates that are more than twice as high as

measured rates in many locations. For example, the empirical model predicts

that marshes in the German Wadden Sea (SSC=34 mg L^{-1}, TR=2 m; Scheurch et

al., 2013) should have accretion rates of ~15 mm yr^{-1}, whereas measured rates

are 3.5 mm yr^{-1} (Scheurch et al., 2012). As discussed in the next section, we

attribute this type of discrepancy to variability in the sampling locations on the

marsh platform, where low marshes close to channels have higher accretion

rates than high elevation marshes far from channels (this study; Stoddart et al.,

1989; Bricker-Urso et al., 1989; Friedrichs and Perry, 2001; Temmerman et al.,

2003). Variability in predicted accretion rates may also be attributed to organic

accretion, which is not explicitly included in our empirical model. Belowground

organic matter accumulation is more important for vertical accretion than

inorganic sedimentation in many marshes (Turner et al. 2002, Morris et al. 2016)

and could explain measured rates that exceed predicted rates, especially in low

SSC and TR environments (Figure 2a) Therefore, our work provides empirical

support to the paradigm that mineral sediment availability drives wetland

vulnerability at the regional-global scale, while emphasizing that accretion rates

at any particular location will be influenced by a number of other factors that

cannot be predicted with simple numerical models.

Comparison with Numerical Models

To understand potential differences between field measurement and

numerical models, we used an ensemble of 5 numerical models (Kirwan et al.

2010) to predict the threshold rate of SLR that each marsh in our dataset could

survive given its site-specific SSC and TR. Following Schuerch et al., (2018), the

ensemble model results can be summarized as,

$$Threshold\ SLR = a * SSC * TR^b + c \qquad (4)$$

where the constants a, b, and c equal 0.292, 0.915, and 1.5, respectively. The

ensemble model indicates threshold SLR rates increase linearly with SSC for a

given tidal range (Kirwan et al., 2010), which is consistent with our empirical

model. However, linear regression demonstrates that the ensemble model

predicts threshold SLR rates that are higher than measured accretion rates when

all marshes are included (i.e., slope m= 0.6, R^2=0.60, p<0.001 where m = 1

would indicate modeled threshold rates equivalent to measured accretion rates)

(Figure 3a). We then repeated the comparison using only marshes reported as

low elevation (n=41), including the four low marsh sites which we monitored. In

this case, linear regression reveals that measured accretion rates in low elevation marshes are nearly identical to modeled threshold rates of sea level rise for a given SSC and TR (Figure 3b; m=0.92, R^2=0.89, p<0.001).

These results illustrate a fundamental link between marsh elevation and vulnerability that may help reconcile field-based measurements of marsh accretion with numerical models of marsh survival. For example, a previous meta-analysis found that approximately 75% of marsh locations were accreting at rates less than the 7.4 mm yr^{-1} rate of sea level rise projected under the IPCC RCP6.0 scenario and concluded that those marshes would not survive (Crosby et al., 2016). These types of observations inspire concern that numerical models predict accretion rates that will be far more rapid than what has been measured, and therefore underestimate marsh vulnerability (Parkinson et al., 2017; Jankowski et al., 2017). Indeed, we find that across our global network of sites, 40% (31 of 77) of accretion measurements are less than 7.4 mm yr^{-1}. Yet measured accretion rates are not themselves an indicator of the threshold rate a marsh can survive because accretion rates tend to increase with flooding depth and duration (Friedrichs and Perry, 2001; Fitzgerald et al. 2008; Kirwan et al., 2016).

While a low marsh plant community that loses elevation relative to sea level is at risk of drowning (i.e. conversion to open water), a high marsh plant community that loses elevation is at risk of first converting into a low marsh community, assuming this ecological transition is possible in the given system. When we restrict our analysis to low marsh sites, we find that less than 15% (6 of

41) of locations have accretion rates less than 7.4 mm yr^{-1}, and that measured

low marsh accretion rates are similar to threshold rates of sea level rise predicted

by numerical models for a given SSC and TR (Figure 3b). These results are

consistent with observations of increased marsh inundation under current SLR

rates, evidenced by accretion deficits and shifts towards more flood tolerant

vegetation (Donnelly and Bertness, 2001; Raposa et al., 2017), despite relatively

few locations with extensive marsh drowning (Kirwan et al., 2016). Thus, our

empirical analysis is consistent with numerical models that predict accelerated

accretion rates may enable survival of many marshes, albeit with significant

geomorphic and ecological changes.

Global Analysis of Critical SSC

We applied the Dynamic Interactive Vulnerability Assessment Wetland

Change Model (DIVA) to assess global tidal marsh vulnerability using our

empirical model coefficients for marsh accretion, and DIVA's database of TR,

SSC, and local relative SLR rates for coastal segments that contain marshes

around the world (Spencer et al., 2016; Schuerch et al., 2018). Our initial goal

was to use the empirical model to calculate the spatial extent of marsh drowning

under different sea level rise rates. However, we found that the GlobColour

satellite-derived SSC data used by DIVA was considerably lower than and

inconsistently related to the SSC in our meta-analysis (Supplementary Figure 1).

We suggest that this discrepancy is due to the resolution of the satellite data

(4.6km; GlobColour, 2020), which presumably includes low-SSC waters further

offshore. This suggests limitations in predicting global threshold rates of SLR and that previous estimates of marsh vulnerability (e.g. Schurech et al., 2018) may be conservative.

We instead consider the critical SSC needed for marsh accretion, based on DIVA TR and relative SLR data, and our empirical model coefficients that predict marsh accretion under these physical parameters. We calculated the SSC that would be required to produce accretion rates equal to the current RSLR rate using both empirical model coefficients, C_1=0.2212 (calculated from all marshes) and C_1=0.3535 (calculated from low marsh monitored sites). In these projections, we assume that the lower empirical model coefficient (C_1=0.2212) results in a critical SSC required for the marsh to maintain its current elevation relative to sea level, below which marshes become more inundated and subject to vegetation shifts (i.e. increase in flood tolerant species). In contrast, we assume that projections based on the higher coefficient (C_1=0.3535), represent the critical SSC required to survive SLR, below which marshes convert to open water.

Mapping of critical SSC reveals three distinct behaviors related to the maintenance of current marsh elevation and the long-term survival of marshes (Figure 4). First, there are locations where SSC exceeds both the critical SSC required to maintain relative elevation and the critical SSC to survive relative SLR. This behavior is illustrated by marshes in Great Britain, where high tidal ranges and low relative sea level rise rates lead to critical SSC of less than 10 mg L^{-1}. Estimated SSC in this region are at least four times greater than the

critical concentrations, and many locations have actually experienced substantial

marsh expansion (Ladd et al. 2019). Second, sediment supply in other locations

is insufficient to maintain elevation or to survive. For example, the low tidal range

of western Mediterranean marshes results in critical SSC greater than 100 mg L^{-1}

under both empirical model conditions. Previous work indicates low SSC in the

region and large scale wetland loss that is consistent with our empirical model

predictions (Ibáñez et al., 2010; Day et al., 2011). Finally, the vulnerability

mapping reveals a number of locations where SSC are likely lower than the

critical SSC to maintain relative elevation, but higher than the critical SSC

required to survive. This behavior is consistent with marshes in the Northeastern

United States, where accretion deficits are leading to increasing dominance of

flood tolerant vegetation (Donnelly and Bertness, 2001; Raposa et al., 2017), but

marshes are surviving sea level rise because accretion rates accelerate with

inundation duration (Kolker et al. 2010; Wilson et al., 2014).

To explore the effect of sea level rise on marsh vulnerability, we calculated

the percentage of global marsh area that would require SSC greater than a

reference value under different scenarios of accelerated sea level rise. Like our

previous analyses, we consider both the critical SSC needed to maintain

marshes at their current elevation, and the critical SSC needed for marshes to

survive. We use 30 mg L^{-1} as a reference value as the median SSC of our

dataset is 33 mg L^{-1} and the average SSC for U.S. coastal rivers is 30.3 mg L^{-1}

(Weston 2014). Suspended sediment concentration is declining in rivers

throughout the world (Wang et al., 2011; Weston 2014), meaning this reference

value may not be representative of average SSC in the future. We find that approximately 13% of global marsh area requires SSC > 30 mg L^{-1} to maintain elevation under the current rate of eustatic SLR (3 mm yr^{-1}), and that the percentage increases with SLR (i.e. 50% at 10 mm yr^{-1}) (Figure 4a). However, to survive current SLR (3 mm yr^{-1}) only 5% of global marsh area requires SSC > 30 mg L^{-1} to, increasing to 23% at high rates of SLR (10 mm yr^{-1}) (Figure 4b). This global analysis suggests that the conditions necessary for maintaining marsh elevation are much more restrictive than the conditions necessary for marsh survival, assuming high marshes are capable of the ecological transition to low marshes. While many other factors (e.g. organic accretion, compaction) influence local marsh survival, measured accretion rates in low marshes are consistent with modeled threshold rates of sea level rise for a given TR and SSC (Figure 3b). Together, these results help bridge the gap between numerical models and field measurements, and suggest that threshold rates of SLR can be predicted primarily by physical factors at the regional to global scale.

Supplementary Material

Direct measurements of SSC and vertical accretion

We measured SSC and vertical accretion at seven sites spanning the eastern coast of the US and one on the eastern coast of Australia. Four of these sites were located within low, youthful marshes, located at Plum Island Ecosystems Long Term Ecological Research station (PIE LTER), Virginia Coastal Reserve LTER (VCR LTER), Chesapeake Bay National Estuarine Research Reserve (CB

NERR), and Georgia Coastal Ecosystems LTER (GCE LTER), respectively

(Figure 1). We conducted long term turbidity measurements on the marsh

platform, site-specific SSC calibrations, and direct accretion measurements at

these four low marsh sites. The three additional sites were monitored for shorter

durations (maximum=2 months) and either relied on measurements from other

studies or were at higher elevations. All monitored sites were included within the

meta-analysis.

Optical backscatter turbidity probes were deployed on the marsh platform and

in the adjacent tidal creek to determine the average SSC for each site. Our basic

approach to measuring SSC follows methods described in previous work at the

GCE and PIE (Coleman and Kirwan, 2019; Coleman et al., *In Review*), where 3-6

sensors were deployed across a transect from tidal channel to marsh interior,

measuring turbidity every 15 minutes for the length of the deployment (1-15

months). Pressure transducers were used to calculate water depth, which was

used to estimate tidal range and to remove data points corresponding to time

periods when the marsh was not flooded. Turbidity was converted to SSC via *in

situ* field calibrations and lab calibrations with native sediment from each site

(Coleman and Kirwan, 2019). All calibration equations are in the form of

SSC=Turbidity*Calibration Coefficient. The calibration coefficients for the PIE

LTER, VCR LTER, CB NERR, and GCE LTER are 2.26 (R^2=0.98), 1.31

(R^2=0.99), 1.04 (R^2=0.98), and 1.33 (R^2=0.93), respectively. Suspect data points

were removed from the SSC time series following Ganju et al. (2005). These

points represent times when the sensor may have been obstructed by

vegetation, or subject to fouling. The SSC time series demonstrate distinct tidal patterns and changes in concentration with distance into the marsh (see Coleman and Kirwan, 2019; Coleman et al., *In Review*; Supplementary Figure 2). Nevertheless, here we define the SSC of each site simply as the average over-marsh concentration calculated from the entire record of all marsh sensors at a given site.

We measured short-term accretion using sediment tiles made of 14.5cm x 14.5cm plastic grids with $1.5cm^2$ openings cut from fluorescent tube lighting covers installed flush to the marsh surface (Coleman et al., 2019). These grids allow plants to grow through them and represent a more natural surface for sediment accumulation. On subsequent visits to the sites, we measured the thickness of sediment that had accumulated on the grid to calculate an accretion rate. Sediment tile deployments varied in length, from 9-24 months.

Long-term accretion rates were calculated from the vertical distribution of excess Pb-210 ($^{210}Pb_{xs}$) in sediment cores (15 cm diameter x 100 cm length) collected from each study sites. Each core was sectioned at 1-cm interval with a subset of intervals (every other sample for top 20 cm and every fourth sample beyond 20 cm) prepared for radiometric analysis. Briefly, each interval was dried, pulverized, quantitatively spiked with 6.0 dpm (100 mBq) of polonium-209 (^{209}Po), and reacted with hot (nitric and hydrochloric) acids to leach ^{210}Po (granddaughter of ^{210}Pb) from sediments. Leachate was conditioned following a modified procedure of Flynn (1968) (also reviewed by Sethy et al. 2015) to promote the spontaneously deposition of Po-isotopes on silver (Ag) planchets.

The planchets were measured on alpha spectrometry to quantify both ^{209}Po (4.86 MeV) and ^{210}Po (5.41 MeV) isotopes. Leachable ^{210}Po (and ^{210}Pb) was quantified by multiplying the ^{209}Po activity-to-count rate-ratio by the ^{210}Po count rate. Excess ^{210}Pb was assumed to be in secular equilibrium and thus equivalent to acid-leached polonium-210 (^{210}Po). Accretion rates were estimate using log-linear relationships between ^{210}Pb$_{xs}$ and depth in the core following Robbins et al. (1975). Mid-depth samples (four to five samples between approximately 15 and 45 cm in select cores) were also analyzed for cesium-137 (^{137}Cs) to corroborate and/or supplement ^{210}Pb$_{xs}$-based accretion rates. Dry and pulverized samples were sealed in a container and measured on a Canberra (now Mirion Technologies, Inc.) Low-Energy, Germanium (LeGe) detector using the 661.7 keV photopeak. Self-absorption correction for samples followed Cutshall et al. (1983).

The four low marsh monitored sites ranged in over-marsh SSC from approximately 5-30 mg L^{-1}, TR from 1.1-3.6 m, and accretion rate from approximately 7-27 mm yr^{-1} (Supplementary Table 2). Spatially, SSC was highest in the tidal channel at all sites, except for the CB NERR site which has a sandy berm proximal to the marsh interior sensor. Temporally, SSC tended to be the highest at mid-tide, presumably coincident with the fastest flow velocities. The sites at the PIE LTER and the CB NERR had the lowest SSC (5.2 and 13.4 mg L^{-1}, respectively) and lower accretion rates, which were successfully determined with Pb-210 (6.6 and 7.3 mm yr^{-1}, respectively; Supplementary Figure 3). SSC was higher at the VCR LTER (27.7 mg L^{-1}) and GCE LTER (31 mg L^{-1}), but

accretion rates could not be determined with radiochronology methods because the sites were accreting too rapidly or experienced erosion. Instead, we calculated accretion rates at these sites from sediment grids (27 and 24 mm yr^{-1}, respectively; Supplementary Figure 4). These short-term accretion rates were verified by comparing them to other studies in the system and estimates of accretion based on the timing of vegetation colonization in aerial photographs and changes in organic content, bulk density, and water content observed in sediment cores (Supplementary Table 2). The accretion rate of all four sites were greater than the local relative SLR rate and similar to numerical model-predicted threshold SLR rates.

Meta-analysis and Empirical Model Formulation

Data from the literature was compiled to include a wider range of salinities, vegetation types, elevations, SSC, TR, and accretion. We included data from an additional 70 tidal marshes (for a total of 77 sites) where there were direct measurements of SSC and accretion from around the world in addition to the sites we directly measured (Supplementary Table 1). The greatest concentration of sites were in Europe and North America. The sites had a range of SSC of 0.5-358 mg L^{-1}, TR of 0.3-12 m, and accretion rates of 1-400 mm yr^{-1}. In situations where SSC and accretion data came from different sources, sites were only included if measurements were conducted within 2 km and approximately 15 years from one another.

We removed outliers from the significant linear relationship between SSC*TR and accretion to determine the empirical model coefficient most useful for making predictions. First all points were used in creating a linear model between SSC*TR and accretion. We then identified the data point with the largest residual and calculated a new linear model excluding this data point. Data points were removed in sequence until the removal of an additional outlier had a negligible effect on the slope of the relationship between SSC*TR and accretion based on an analysis of the derivative of the change in slope with number of outliers removed. Removing 5 of the 77 marsh sites was deemed most appropriate. This approach removes variability from the linear regression so that the resulting slope (C_1) is representative of the majority of the data but not overly-influenced by extreme data points.

We analyzed several potential equations to determine the best empirical relationship between SSC, TR, and vertical accretion (Supplementary Table 3). The simplest empirical equation is analogous to a fixed proportion of the sediment suspended in the flooding waters being converted to vertical marsh accretion (equation 1). We then binned marsh sites into 6 groups based on spring tidal range. A plot of the slope of linear regressions between measured accretion and SSC*TR for each tidal range group appeared as a logistic curve, which was then used to define a second model (Supplementary Table 3). For a third empirical model, we determined the best fit linear model (Supplementary Table 3). This simplistic equation predicted accretion as well as the two more complex equations (Supplementary Table 3).

Influence of Different Methodology

Accretion rates and SSC measurements vary with timescale and location of sampling (Christiansen et al., 2000; Parkinson et al. 2016; Breithaupt et al., 2018; Coleman et al., *In Review*) so we analyzed the relationship between SSC and vertical accretion separately for different methods of measuring accretion and SSC. Accretion methods were classified as radiochronology (Pb210, Cs137), modern sediment deposition (sediment tiles and marker horizons), or modern elevation change (surface elevation tables). We distinguished between measurements of SSC made with bottle sampling and automated sensors, and between measurements made in the channel and over the flooded marsh. For each methodological approach, we calculated the slope between measured accretion and SSC*TR (C_1 in equation 1).

The slope calculated using modern accretion rates was slightly greater but not significantly different than the slope calculated using elevation change rates (modern accretion C_1=0.2452 ± 0.009; elevation change C_1=0.1980 ± 0.019; Figure 2b). The main difference between these approaches is that shallow subsidence is incorporated into elevation change measurements but not accretion measurements (Cahoon et al., 1995; Cahoon et al. 2006; Jankowski et al. 2017). Our results therefore suggest that shallow subsidence is not a significant contributor to short-term elevation change for a given TR and SSC at the spatial scales and levels of observational uncertainty considered in our study. The slope calculated using only radiochronological measurements was

significantly lower than the other approaches (C_1=0.1014 ± 0.008), indicating that

accretion rates measured over long timescales are lower than rates measured

over short timescales for a given SSC and TR. Our work therefore adds to the

growing body of literature identifying a "timescale bias" in which apparent

accretion rates decrease with increasing timescale (Breithaupt et al., 2018).

Lower apparent accretion rates could be explained by accretion rates that decline

as youthful marshes approach an equilibrium elevation (Redfield, 1972), a longer

period of time for compaction and organic matter decomposition (Bartholdy et al.,

2010), and/or accretion rates averaged over periods of time with slower SLR

(Kirwan et al., 2016). The impacts of shallow subsidence are likely being masked

by the variability in accretion rates between sites, whereas the impact of long-

term subsidence may be too large to be masked by inter-marsh variability. In any

case, our finding that accretion rates are lower when measured over longer

timescales is consistent with previous work that highlights the influence of long-

term subsurface elevation loss in long-term accretion rates (Kearney et al., 2004;

Bartholdy et al., 2010; Tornqvist et al., 2008), as well as the observation that

accretion rates have increased in response to the recent acceleration in the rate

of SLR (Kolker et al., 2010; Hill and Anisfeld 2015). Short-term accretion rates

potentially underestimate marsh vulnerability because they do not fully account

for subsurface processes that manifest over longer time periods (Parkinson et al.,

2017), whereas long-term accretion rates overestimate marsh vulnerability

because accretion rates increase in response to accelerating rates of sea level

rise (Kirwan et al., 2017). Since the best approach for assessing wetland

vulnerability is unclear (Breithaupt et al., 2018), we incorporate both long-term and short-term measurements of accretion in our empirical modeling (Figures 2 and 3). This approach allows us to quantify the impact of different methods over a broad range of environmental conditions, and shows that methodological differences increase with greater sediment availability and more rapid rates of accretion (Figure 2b).

We also explored how the relationship between accretion and SSC*TR depends on differences in the SSC measurement methodology. Sites were grouped based on whether SSC was measured via bottle sampling or automated sensors, and whether SSC measurements were made in the channel or over the flooded marsh. Although the different SSC measurement approaches had different values of C_1, it is difficult to determine how generalizable the results are (Supplementary Figure 5). Measurements made by sensors and measurements over the marsh (n=31; n=16) were less common and covered a narrower range of SSC values than measurements made with bottle sampling and in the channel (n=46; n=61). Although previous work suggests strong temporal variability in SSC that may only be captured with sensors or sampling over long durations (Coleman et al., *In Review*), and strong spatial gradients between SSC measured in channels and SSC across the marsh platform (Christiansen et al., 2000; Leonard and Reed, 2002; Poirier et al., 2017), there was insufficient information to sufficiently understand the effect of SSC methodology on the relationship between accretion and SSC. We consequently combined all SSC measurement methods in our meta-analysis and empirical modeling, and note

that significant trends between accretion and SSC emerge despite this potential variability.

Global Analysis Methodology

The global modelling of sediment balances is based on the Global Coastal Wetland Model by Schuerch et al. (2018). This relies on the global database from the DIVA including TR and areal coastal wetland data (McOwen et al., 2017), attributed to a total of 12,148 coastline segment of varying length (depending on bio-physical and socio-economic coastline characteristics; Spencer et al., 2016). Spring tidal range data was derived from a new global tidal range dataset (Pickering et al. 2017) using the global tide model OTISmpi (Egbert et al., 2004). Mean spring high water levels and mean spring low water levels were retrieved from a 15-day sea-level reconstruction based on the tidal constituents M2, S2, K1 and O1 (Schuerch et al. 2018).

Critical SSC for each coastline segment was calculated as a function of spring TR and global sea-level rise for current (3 mm/yr) and accelerated rates (5 and 10 mm/yr). Global sea-level rise rates were adjusted by regional vertical land movement due to glacial isostatic adjustment (Peltier et al., 2004) and accelerated land subsidence in delta regions (2 mm/yr for every delta in the database) to derive regional relative sea-level rise (RSLR) rates. Based on equation 1, and assuming that the maximum possible accretion rate equals RSLR, critical SSC was calculated as follows:

$$SSC_{crit} = RSLR/(C_1 * TR) \tag{5}$$

The resulting SSC$_{crit}$ values were binned into five categories for each of which total saltmarsh areas were calculated.

References

Bartholdy, J., Pedersen, J. B. T., & Bartholdy, A. T. (2010). Autocompaction of shallow silty salt marsh clay. *Sedimentary Geology*, *223*(3-4), 310-319.

Breithaupt, J. L., Smoak, J. M., Byrne, R. H., Waters, M. N., Moyer, R. P., & Sanders, C. J. (2018). Avoiding timescale bias in assessments of coastal wetland vertical change. *Limnology and oceanography*, *63*(S1), S477-S495.

Bricker-Urso, S., Nixon, S. W., Cochran, J. K., Hirschberg, D. J., & Hunt, C. (1989). Accretion rates and sediment accumulation in Rhode Island salt marshes. *Estuaries*, *12*(4), 300-317.

Cadol, D., Engelhardt, K., Elmore, A., & Sanders, G. (2014). Elevation-dependent surface elevation gain in a tidal freshwater marsh and implications for marsh persistence. *Limnology and Oceanography*, *59*(3), 1065-1080.

Cahoon, D. R., Hensel, P. F., Spencer, T., Reed, D. J., McKee, K. L., & Saintilan, N. (2006). Coastal wetland vulnerability to relative sea-level rise: wetland elevation trends and process controls. In *Wetlands and natural resource management* (pp. 271-292). Springer, Berlin, Heidelberg.

Cahoon, D. R., Reed, D. J., & Day Jr, J. W. (1995). Estimating shallow subsidence in microtidal salt marshes of the southeastern United States: Kaye and Barghoorn revisited. *Marine geology*, *128*(1-2), 1-9.

Christiansen, T., Wiberg, P. L., & Milligan, T. G., (2000). Flow and sediment transport on a tidal salt marsh surface. *Estuarine, Coastal and Shelf Science 50*(3), 315-331

Chmura, G. L., and G. A. Hung (2004), Controls on salt marsh accretion: A test in salt marshes of eastern Canada, Estuaries, 27, 70–81

Church, J.A., P.U. Clark, A. Cazenave, J.M. Gregory, S. Jevrejeva, A. Levermann, M.A. Merrifield, G.A. Milne, R.S. Nerem, P.D. Nunn, A.J. Payne, W.T. Pfeffer, D. Stammer and A.S. Unnikrishnan, (2013). Sea Level Change. In: Climate Change 2013: The Physical Science Basis. Contribution of Working Group I to the Fifth Assessment Report of the Intergovernmental Panel on Climate Change [Stocker, T.F., D. Qin, G.-K. Plattner, M. Tignor, S.K. Allen, J. Boschung, A. Nauels, Y. Xia, V. Bex and P.M. Midgley (eds.)]. Cambridge University Press, Cambridge, United Kingdom and New York, NY, USA.

Coleman, D.J., & Kirwan, M.L., (2019). The effect of a small vegetation dieback event on salt marsh sediment transport. *Earth Surface Processes and Landforms* 44(4), 944-952, https://doi.org/10.1002/esp.4547

Crosby, S. C., Sax, D. F., Palmer, M. E., Booth, H. S., Deegan, L. A., Bertness, M. D., & Leslie, H. M. (2016). Salt marsh persistence is threatened by predicted sea-level rise. *Estuarine, Coastal and Shelf Science*, *181*, 93-99.

Cutshall, N. H., I. L. Larsen, and C. R. Olsen (1983), Direct analysis of 210Pb in sediment samples: Self-absorption corrections, *Nuclear Instruments & Methods B*, *206*, 309-312.

D'Alpaos, A., & Marani, M., (2016). Reading the signatures of biologic–geomorphic feedbacks in salt-marsh landscapes. *Advances in Water Resources 93b* 265-275

Day, J., Ibáñez, C., Scarton, F., Pont, D., Hensel, P., Day, J., & Lane, R. (2011). Sustainability of Mediterranean deltaic and lagoon wetlands with sea-level rise: the importance of river input. *Estuaries and Coasts*, *34*(3), 483-493.

DeLaune, R. D., Patrick, W. H., & Buresh, R. J. (1978). Sedimentation rates determined by 137 Cs dating in a rapidly accreting salt marsh. *Nature*, *275*(5680), 532-533.

Dieng, H. B., Cazenave, A., Meyssignac, B., & Ablain, M. (2017). New estimate of the current rate of sea level rise from a sea level budget approach. *Geophysical Research Letters*, *44*(8), 3744-3751.

Donnelly, J. P., & Bertness, M. D. (2001). Rapid shoreward encroachment of salt marsh cordgrass in response to accelerated sea-level rise. *Proceedings of the National Academy of Sciences*, *98*(25), 14218-14223.

Duvall, M. S., Wiberg, P. L., & Kirwan M. L., (2019). Controls on sediment suspension, flux, and marsh deposition near a bay-marsh boundary. *Estuaries and Coasts 42*(2) 403-424, https://doi.org/10.1007/s12237-018-0478-4

Egbert, G. D., Ray, R. D. & Bills, B. G. Numerical modeling of the global semidiurnal tide in the present day and in the last glacial maximum. J. Geophys. Res. Oceans 109, C03003 (2004).

Ensign, S., Currin, C., Piehler, M., & Tobias, C. (2017). A method for using shoreline morphology to predict suspended sediment concentration in tidal creeks. *Geomorphology*, *276*, 280-288.

Fagherazzi, S., Kirwan, M. L., Mudd, S. M., Guntenspergen, G. R., Temmerman, S., D'Alpaos, A., ... & Clough, J. (2012). Numerical models of salt marsh evolution: Ecological, geomorphic, and climatic factors. Reviews of Geophysics, 50(1).FitzGerald, D. M., Fenster, M. S., Argow, B. A., & Buynevich, I. V. (2008). Coastal impacts due to sea-level rise. *Annual Review of Earth and Planetary Sciences*, *36*.

Flynn, W. W. (1968), The determination of low levels of polonium-210 in environmental materials, *Analytica Chimica Acta*, *43*, 221-227.

French, J. (2006), Tidal marsh sedimentation and resilience to environmental change: Exploratory modeling of tidal, sea-level, and sediment supply forcing in predominantly allochthonous systems, Mar. Geol., 235, 119–136

Friedrichs, C. T., & Perry, J. E. (2001). Tidal salt marsh morphodynamics: a synthesis. *Journal of Coastal Research*, 7-37.

Ganju N. K., Kirwan M. L., Dickhudt P. J., Guntenspergen G. R., Cahoon D. R., & Kroeger K. D., (2015). Sediment transport-based metrics of wetland stability. *Geophysical Research Letters 42*(19), 7992-8000.

Ganju, N.K., Schoellhamer, D.H. & Bergamaschi, B.A., (2005). Suspended sediment fluxes in a tidal wetland: Measurement, controlling factors, and error analysis. *Estuaries 28*(6), 812-822.

GlobColour (2020). Product User's Guide. Version 4.2, Reference GC-UM-ACR-
     PUG-01

Harrison, E. Z., and A. L. Bloom (1977), Sedimentation rates on tidal salt
     marshes in Connecticut, J. Sediment. Petrol., 47, 1484–1490

Hill, T. D., & Anisfeld, S. C. (2015). Coastal wetland response to sea level rise in
     Connecticut and New York. *Estuarine, Coastal and Shelf Science*, *163*,
     185-193.

Ibáñez, C., Sharpe, P. J., Day, J. W., Day, J. N., & Prat, N. (2010). Vertical
     accretion and relative sea level rise in the Ebro Delta wetlands (Catalonia,
     Spain). *Wetlands*, *30*(5), 979-988.

Jankowski, K. L., Törnqvist, T. E., & Fernandes, A. M. (2017). Vulnerability of
     Louisiana's coastal wetlands to present-day rates of relative sea-level
     rise. *Nature Communications*, *8*(1), 1-7.

Kearney, M. S., Stevenson, J. C., & Ward, L. G. (1994). Spatial and temporal
     changes in marsh vertical accretion rates at Monie Bay: Implications for
     sea-level rise. *Journal of Coastal Research*, 1010-1020.

Kirwan, M. L., & Guntenspergen, G. R. (2010). Influence of tidal range on the
     stability of coastal marshland. *Journal of Geophysical Research: Earth
     Surface*, *115*(F2).

Kirwan, M. L., & Megonigal, J. P. (2013). Tidal wetland stability in the face of
     human impacts and sea-level rise. *Nature*, *504*(7478), 53-60.

Kirwan, M., & Temmerman, S. (2009). Coastal marsh response to historical and

    future sea-level acceleration. *Quaternary Science Reviews*, *28*(17-18),

    1801-1808.

Kirwan, M. L., Temmerman, S., Guntenspergen, G. R., & Fagherazzi, S. (2017).

    Reply to'Marsh vulnerability to sea-level rise'. *Nature Climate*

    Change, *7*(11), 756-757.

Kirwan, M. L., Temmerman, S., Skeehan, E. E., Guntenspergen, G. R., &

    Fagherazzi, S. (2016). Overestimation of marsh vulnerability to sea level

    rise. *Nature Climate Change*, *6*(3), 253-260.

Kolker, A. S., Kirwan, M. L., Goodbred, S. L., & Cochran, J. K. (2010). Global

    climate changes recorded in coastal wetland sediments: empirical

    observations linked to theoretical predictions. *Geophysical Research*

    Letters, *37*(14).

Ladd, C. J., Duggan-Edwards, M. F., Bouma, T. J., Pagès, J. F., & Skov, M. W.

    (2019). Sediment supply explains long-term and large-scale patterns in

    salt marsh lateral expansion and erosion. *Geophysical Research*

    Letters, *46*(20), 11178-11187.

Leonard, L. A., & Reed D. J. (2002). Hydrodynamics and sediment transport

    through tidal marsh canopies. *Journal of Coastal Research S.I.36*, 459 –

    469.

Marani, M., D'Alpaos, A., Lanzoni, S., Carniello, L., & Rinaldo, A. (2007).

    Biologically-controlled multiple equilibria of tidal landforms and the fate of

    the Venice lagoon. *Geophysical Research Letters*, *34*(11).

McOwen, C. et al. A global map of saltmarshes. Biodivers. Data J. 5, e11764
(2017).

Morris, J. T., Barber, D. C., Callaway, J. C., Chambers, R., Hagen, S. C.,
Hopkinson, C. S., ... & Wigand, C. (2016). Contributions of organic and
inorganic matter to sediment volume and accretion in tidal wetlands at
steady state. *Earth's future*, *4*(4), 110-121.

Moskalski, S. M. & Sommerfield, C. K. (2012). Suspended sediment deposition
and trapping efficiency in a Delaware salt Marsh. Geomorphology 139-
140, 195-204.

Mudd, S. M., Fagherazzi, S., Morris, J. T., & Furbish, D. J. (2004). Flow,
sedimentation, and biomass production on a vegetated salt marsh in
South Carolina: toward a predictive model of marsh morphologic and
ecologic evolution. *The Ecogeomorphology of Tidal Marshes, Coastal
Estuarine Stud*, *59*, 165-187.

Murphy, S., & Voulgaris G., (2006). Identifying the role of tides, rainfall and
seasonality in marsh sedimentation using long-term suspended sediment
concentration data. *Marine Geology 227*(1-2) 31-50,

Palinkas, C. M. & Engelhardt, K. A. M., (2018). Influence of inundation and
suspended-sediment concentrations on spatiotemporal sedimentation
patterns in a tidal freshwater marsh. *Wetlands*

Parkinson, R. W., Craft, C., DeLaune, R. D., Donoghue, J. F., Kearney, M.,
Meeder, J. F., ... & Turner, R. E. (2017). Marsh vulnerability to sea-level
rise. *Nature Climate Change*, *7*(11), 756-756.

Peltier, W. Global glacial isostasy and the surface of the ice-age earth: the ice-5G (VM2) model and GRACE. Annu. Rev. Earth Planet. Sci. 32, 111–149 (2004).

Pickering, M. D. et al. The impact of future sea-level rise on the global tides. Cont. Shelf Res. 142, 50–68 (2017).

Poirier, E., van Proosdij, D., & Milligan, T.G., (2017). The effect of source suspended sediment concentration on the sediment dynamics of a macrotidal creek and salt marsh. *Continental Shelf Research 148* 130-138.

Raposa, K. B., Weber, R. L., Ekberg, M. C., & Ferguson, W. (2017). Vegetation dynamics in Rhode Island salt marshes during a period of accelerating sea level rise and extreme sea level events. *Estuaries and Coasts*, *40*(3), 640-650.

Redfield, A. C. (1972). Development of a New England salt marsh. Ecological monographs, 42(2), 201-237.

Reed, D. J. (1995). The response of coastal marshes to sea-level rise: Survival or submergence?. *Earth Surface Processes and Landforms*, *20*(1), 39-48.

Robbins, J. A., and D. N. Edgington (1975), Determination of recent sedimentation rates in Lake Michigan using Pb-210 and Cs-137, *Geochimica et Cosmochimica Acta*, *39*(3), 285-304.

Schuerch, M., Rapaglia, J., Liebetrau, V., Vafeidis, A., & Reise, K. (2012). Salt marsh accretion and storm tide variation: an example from a barrier island in the North Sea. *Estuaries and Coasts*, *35*(2), 486-500.

Schuerch, M., Spencer, T., Temmerman, S., Kirwan, M. L., Wolff, C., Lincke, D.,
    ... & Hinkel, J. (2018). Future response of global coastal wetlands to sea-
    level rise. *Nature*, *561*(7722), 231-234.

Schuerch, M., Vafeidis, A., Slawig, T., & Temmerman, S. (2013). Modeling the
    influence of changing storm patterns on the ability of a salt marsh to keep
    pace with sea level rise. *Journal of Geophysical Research: Earth
    Surface*, *118*(1), 84-96.

Sethy, N. K., A. K. Sutar, P. Rath, V. N. Jha, P. M. Ravi, and R. M. Tripathi
    (2015), A review of radio chemical analysis and estimation of 210Po in soil
    matrices, *Journal of Radiation Research and Applied Sciences*, *8*(4), 590-
    596.

Spencer, T., Schuerch, M., Nicholls, R. J., Hinkel, J., Lincke, D., Vafeidis, A. T.,
    ... & Brown, S. (2016). Global coastal wetland change under sea-level rise
    and related stresses: The DIVA Wetland Change Model. *Global and
    Planetary Change*, *139*, 15-30.

Stevenson, J. C., Ward, L. G., & Kearney, M. S. (1986). Vertical accretion in
    marshes with varying rates of sea level rise. In *Estuarine variability* (pp.
    241-259). Academic Press.

Stoddart, D. R., Reed, D. J., & French, J. R. (1989). Understanding salt-marsh
    accretion, Scolt Head Island, Norfolk, England. *Estuaries*, *12*(4), 228-236.

Temmerman, S., Govers, G., Meire, P., & Wartel, S. (2003). Modelling long-term
    tidal marsh growth under changing tidal conditions and suspended

sediment concentrations, Scheldt estuary, Belgium. *Marine Geology*, *193*(1-2), 151-169.

Törnqvist, T. E., Wallace, D. J., Storms, J. E., Wallinga, J., Van Dam, R. L., Blaauw, M., ... & Snijders, E. M. (2008). Mississippi Delta subsidence primarily caused by compaction of Holocene strata. *Nature Geoscience*, *1*(3), 173-176.

Turner, R. E., Swenson, E. M., & Milan, C. S. (2002). Organic and inorganic contributions to vertical accretion in salt marsh sediments. In *Concepts and controversies in tidal marsh ecology* (pp. 583-595). Springer, Dordrecht.

Wang, H., Saito, Y., Zhang, Y., Bi, N., Sun, X., & Yang, Z. (2011). Recent changes of sediment flux to the western Pacific Ocean from major rivers in East and Southeast Asia. *Earth-Science Reviews*, *108*(1-2), 80-100.

Watson, E. B., Raposa, K. B., Carey, J. C., Wigand, C., & Warren, R. S. (2017). Anthropocene survival of southern New England's salt marshes. *Estuaries and Coasts*, *40*(3), 617-625.

Weston, N. B. (2014). Declining sediments and rising seas: an unfortunate convergence for tidal wetlands. *Estuaries and Coasts*, *37*(1), 1-23.

Wiberg, P. L., Fagherazzi, S., & Kirwan, M. L. (2020). Improving predictions of salt marsh evolution through better integration of data and models. *Annual review of marine science*, *12*, 389-413.

Wilson, C. A., Hughes, Z. J., FitzGerald, D. M., Hopkinson, C. S., Valentine, V., & Kolker, A. S. (2014). Saltmarsh pool and tidal creek morphodynamics:

Dynamic equilibrium of northern latitude

saltmarshes?. *Geomorphology*, *213*, 99-115.
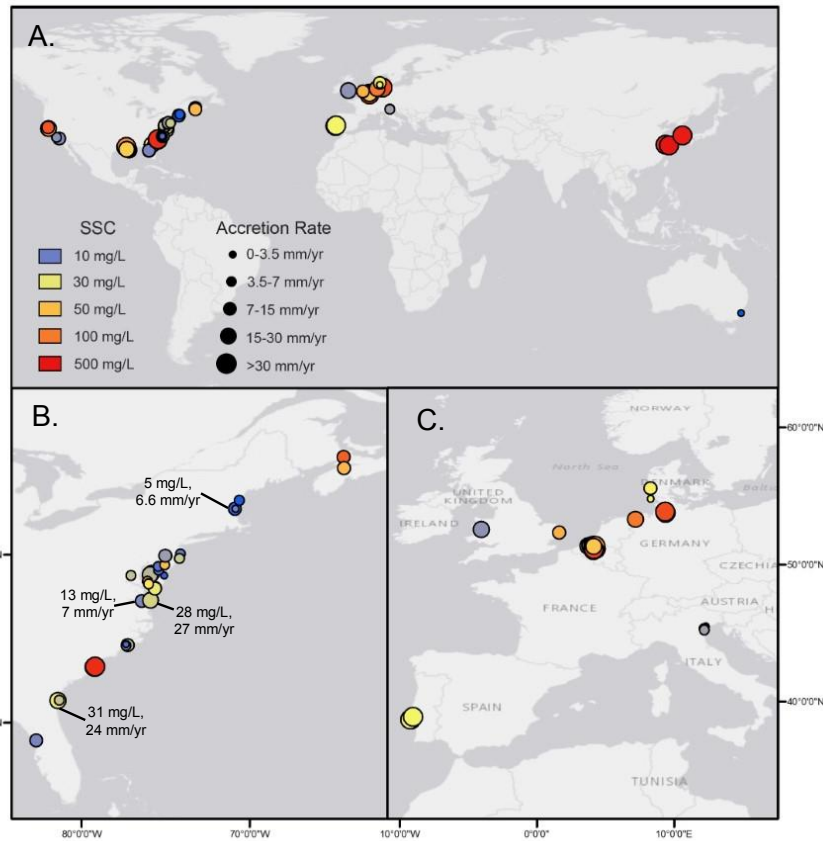
Figure 1: A. Site map showing SSC and accretion rate of sites used in the meta-analysis. Warmer colors indicate higher SSC and reference values are displayed in the legend. Size of the circle represents accretion rate, with larger circles indicating greater accretion rates. B. Magnified view of the east coast of North America and C. Western Europe, with labels indicating SSC and accretion of low marsh monitoring sites.
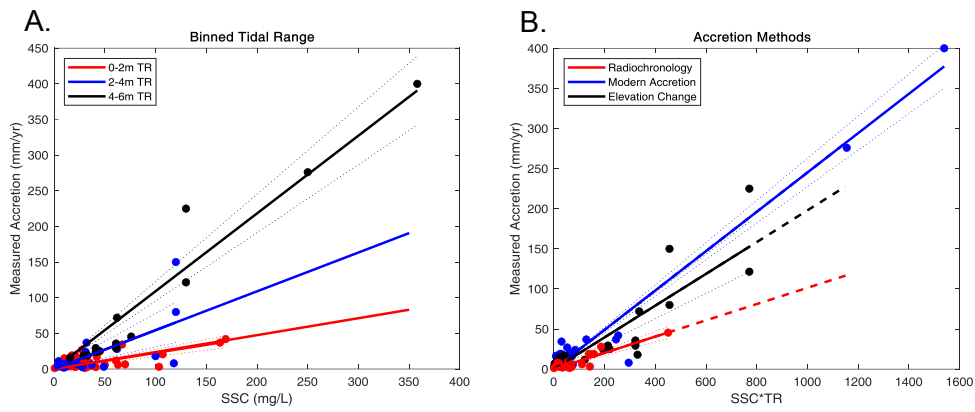
Figure 2: A. Measured accretion rate is linearly positively related to SSC for a given TR B. Relationship between accretion, SSC, and TR is dependent on methodology, with radiochronology (red) having a significantly lower slope than moder accretion (blue) or elevation change (black).
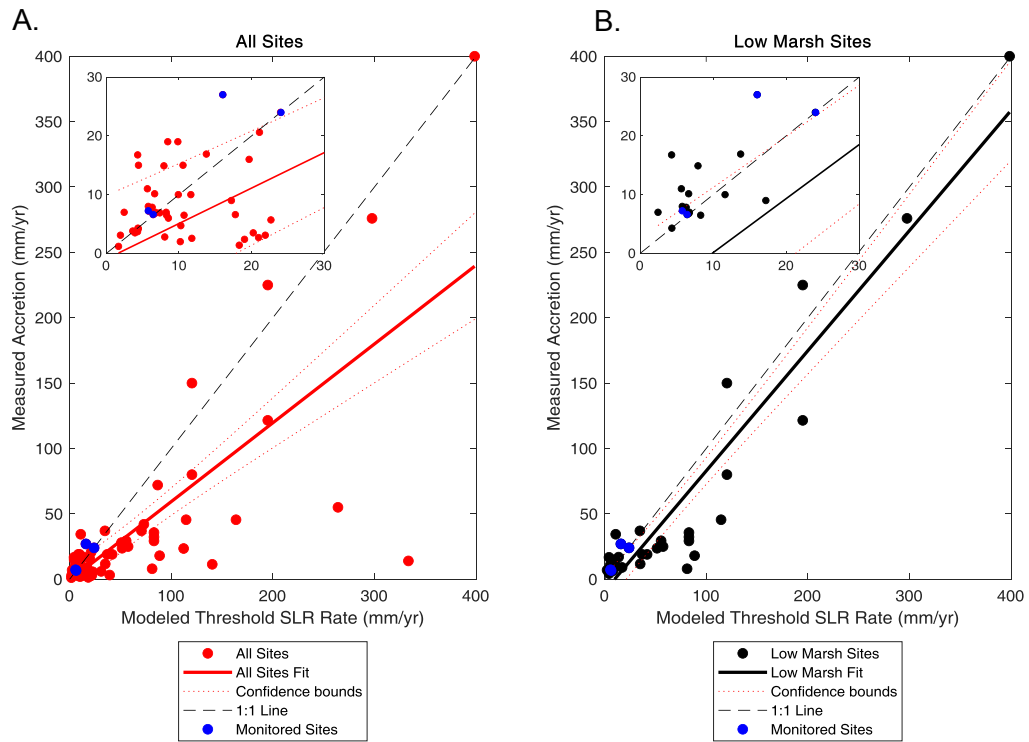
Figure 3: A. Comparison of observed accretion rate with threshold SLR determined from the ensemble model for all sites. B. Comparison of observed accretion rate with threshold SLR determined from the ensemble model for only sites that were reported as low marsh. Blue points represent the four low marsh monitoring sites, and the insets are a magnified view of 0-30 mm/yr.

A.

TSM [mg/l] needed for saltmarshes to accrete at rate of local RSLR

— No saltmarshes

Crit. TSM [mg/l] - 3 mm/yr
- —— <10
- —— 10 - 30
- —— 30 - 50
- —— 50 - 100
- —— >100

TSMcrit = RSLR / 0.3535 x Spring Tidal Range)

| Crit. TSM range [mg/l]		Global mean SLR 3 mm/yr		Global mean SLR 6 mm/yr		Global mean SLR 10 mm/yr	
		Global area [km2]	Fraction [%]	[km2]	Fraction [%]	[km2]	Fraction [%]
0	10	36,457	67	26,265	48	18,086	33
10	30	14,926	27	19,178	35	18,891	35
30	50	1,313	2	5,825	11	10,164	19
50	100	1,300	2	1,444	3	4,493	8
100	9250	665	1	1,950	4	3,028	6

B.

TSM [mg/l] needed for saltmarshes to accrete at rate of local RSLR (assuming no bio-physical feedbacks)

— No saltmarshes

Crit. TSM [mg/l] - 3 mm/yr
- —— <10
- —— 10 - 30
- —— 30 - 50
- —— 50 - 100
- —— >100

TSMcrit = RSLR / (0.2212 x Spring Tidal Range)

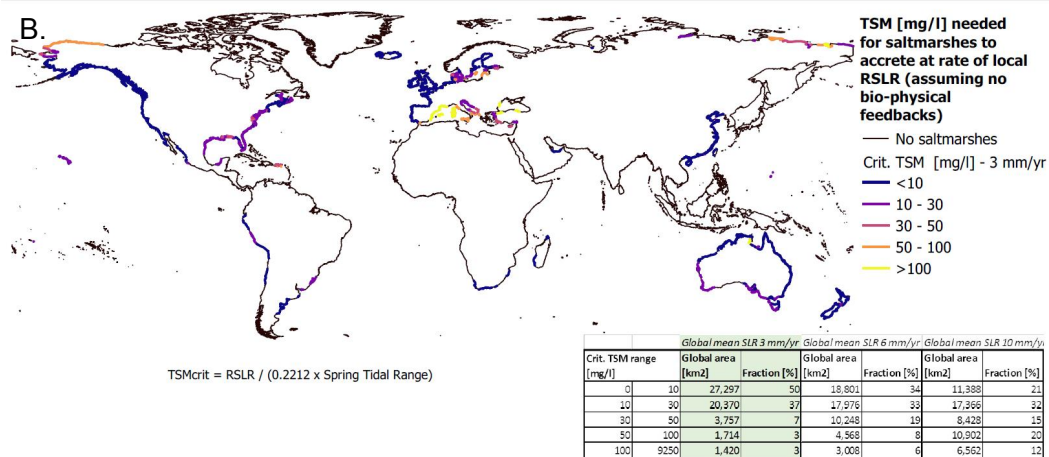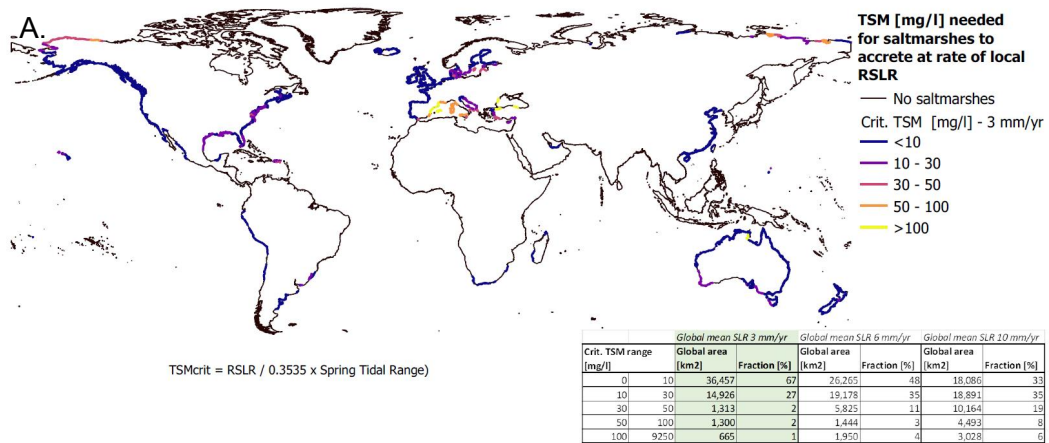| Crit. TSM range [mg/l]		Global mean SLR 3 mm/yr		Global mean SLR 6 mm/yr		Global mean SLR 10 mm/yr	
		Global area [km2]	Fraction [%]	[km2]	Fraction [%]	[km2]	Fraction [%]
0	10	27,297	50	18,801	34	11,388	21
10	30	20,370	37	17,976	33	17,366	32
30	50	3,757	7	10,248	19	8,428	15
50	100	1,714	3	4,568	8	10,902	20
100	9250	1,420	3	3,008	6	6,562	12

Figure 4: A. World map indicating critical SSC needed to survive current local rates of SLR. B. Conditions representative SSC required to maintain current elevation.
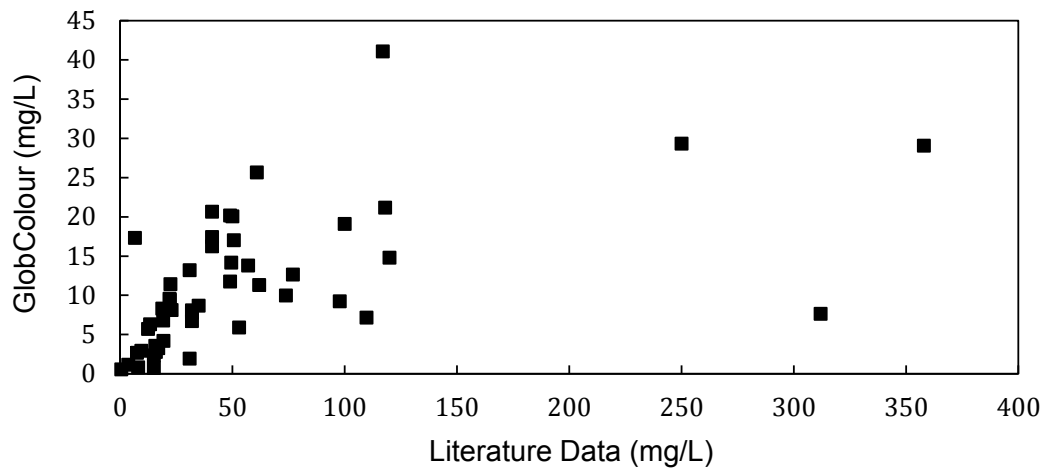
Supplementary Figure 1: Comparison of GlobColour satellite-derived SSC and literature-derived field measurements.

Supplementary Table 1: List of all sites included in the meta-analysis. Source refers to the original data source. All SSC are in mg L⁻¹. Accretion rates (Acc.) are in mm yr⁻¹, and TR are spring tidal ranges in meters. Marsh or Channel and Sensor or Bottle columns refer to how SSC was measured, with the letter corresponding to the first letter of the methodology. The Acc. Method column refers to how accretion rates were measured and are classified as either radiochronology (R), modern accretion (A), or elevation change (E). If the site was specifically described as a low elevation marsh, it is indicated with an X.

Location	SSC Source	SSC	Marsh or Channel	Sensor or Bottle	Accretion Source	Acc.	Acc. Method	Low Marsh	TR
Plum Island, MA	This Study	5.2	M	S	This Study	6.6	R	X	3.6
Upper Plum Island, MA	This Study	4.4	M	S	This Study	11.0	A	X	3.6
Goodwin Island, VA	This Study	13.4	M	S	This Study	7.2	R	X	1.1
Mockhorn Island, VA	This Study	27.6	M	S	This Study	27.0	A	X	1.9
South Altamaha, GA	This Study	31.0	M	S	This Study	24.0	A	X	2.7
North Altamaha, GA	This Study	22.4	C	S	Loomis and Craft 2010	6.6	R		2.7
Currambene Creek, Australia	This Study	0.5	M	S	This Study	1.2	R		1.1
Scheldt Estuary	Temmerman et al. 2004	130	C	B	Temmerman et al. 2004	225	E	X	5.9
Scheldt Estuary	Temmerman et al. 2004	109	C	B	Temmerman et al. 2004	45.5	R	X	5.9
Scheldt Estuary	Temmerman et al. 2004	76	M	B	Temmerman et al. 2004	45.5	R	X	5.9
Scheldt Estuary	Temmerman et al. 2004	41	C	B	Temmerman et al. 2004	29.4	E	X	5.2
Scheldt Estuary	Temmerman et al. 2004	33	C	B	Temmerman et al. 2004	19	R	X	4.8
Scheldt Estuary	Temmerman et al. 2004	29	M	B	Temmerman et al. 2004	19	R	X	4.8
Scheldt Estuary	Temmerman et al. 2004	41	C	B	Temmerman et al. 2004	23.7	E	X	4.8
Scheldt Estuary	Temmerman et al. 2004	61	C	B	Temmerman et al. 2004	35.7	E	X	5.3
Scheldt Estuary	Temmerman et al. 2004	61	C	B	Temmerman et al. 2004	29.3	E	X	5.3

Scheldt Estuary	Temmerman et al. 2004	61	C	B	Temmerman et al. 2004	32.3	E	X	5.3
Scheldt Estuary	Temmerman et al. 2004	104	C	B	Temmerman et al. 2004	23.5	R	X	4.1
Scheldt Estuary	Silinski et al. 2016	62	C	B	Silinski et al. 2016	72	E		5.4
Elbe Estuary	Kappenberg & Grabeman 2001	120	C	B	Schoutens et al. 2019	150	E	X	3.8
Elbe Estuary	Kappenberg & Grabeman 2001	120	C	B	Schoutens et al. 2019	80	E	X	3.8
Delaware Bay	Stumpf 1983	5	M	B	Kim et al. 1997	3.5	R	X	1.8
Cedar Creek, FL	Leonard et al. 1995	12.5	M	B	Leonard et al. 1995	7.2	A	X	1.2
Choptank River	Ensign et al. 2014	17.5	C	B	Ensign et al. 2014	19	A	X	1.4
Choptank River	Ensign et al. 2014	21	C	S	Ensign et al. 2014	19	A	X	1.4
Pocomoke River	Ensign et al. 2014	10	C	B	Ensign et al. 2014	15	A	X	1
Pocomoke River	Ensign et al. 2014	31	C	B	Ensign et al. 2014	15	A	X	1
Blackwater Wildlife Refuge, MD	Stevenson et al. 1985	103.5	C	B	Stevenson et al. 1985	3.1	R		0.7
Hengsha Island, Yangzte	Qing et al. 2003	250	C	B	Yang et al. 2000	276	A	X	4.6
Town Creek, SC	Murphy & Voulgaris 2006	28	C	B	Sharma et al. 1987	2.4	R	X	2.3
Oyster Landing, SC	Murphy & Voulgaris 2006	30.5	C	B	Sharma et al. 1987	1.4	R	X	2
Mud Bay, North Inlet, SC	Hutchinson et al. 1995	163.5	C	B	Hutchinson et al. 1995	37	A		1.5
Sixty Bass, North Inlet, SC	Hutchinson et al. 1995	169.1	C	B	Hutchinson et al. 1995	42	A		1.5
Scheld Estuary	Temmerman et al. 2004	130	C	B	Vandenbruwaene et al., 2011	122	E	X	5.9
Scheld Estuary	Wang & Temmerman, 2004	45	C	B	Wang & Temmerman, 2013	25	E	X	4.9
Venice Lagoon	Venier et al. 2014	20.7	C	S	Bellucci et al. 2007	2.8	R	X	1.1
Venice Lagoon	Venier et al. 2014	29.1	C	S	Day et al. 1999	6.5	A	X	1.1
Venice Lagoon	Carniello et al. 2012	16.6	C	S	D'Alpaos et al. 2017	7	R	X	1.1

Location	Reference				Reference				
Wadden Sea, Dollart, Germany	Ridderinkhof et al. 2000	100	C	S	Esselink et al. 1998	18	E	X	3.3
Blythe Estuary, UK	French et al. 2005	60.9	C	S	French et al. 2005	11.7	E	X	2
Freemans Creek, NC	Ensign & Currin, 2016	20.9	M	B	Currin et al. 2017	10.2	E	X	0.8
Traps Bay Creek, New River, NC	Ensign et al. 2017a	16	C	B	Currin et al. 2017	3.7	E		0.6
French Creek, New River, NC	Ensign et al. 2017a	8	C	B	Currin et al. 2017	3.1	E		0.2
Nelson Island, Plum Island, MA	LeMay 2007	9.3	C	B	Kirwan et al. 2011	2	R		3.6
Club Head Creek, Plum Island, MA	LeMay 2007	11	C	B	Kirwan et al. 2011	2.6	R		3.6
Blackwater Wildlife Refuge, MD	Ganju et al. 2017	63	C	S	Ganju et al. 2015	6	A		0.4
Fishing Bay, MD	Ganju et al. 2017	39	C	S	Ganju et al. 2015	4.7	A		0.8
Ogunquit, ME	Ganju et al. 2017	3.7	C	S	Neil Ganju	3.8	E		2.1
Seal Beach, CA	Ganju et al. 2017	15	C	S	Rosencranz et al. 2017	10	A	X	2.5
Point Mugu, CA	Ganju et al. 2017	15	C	S	Rosencranz et al. 2017	7	A		1.6
Reedy Creek, NJ	Ganju et al. 2017	9.5	C	S	Elsey-Quirk 2016	7	E	X	0.3
Potomac River	Palinkas & Engelhardt 2018	22.1	C	B	Palinkas & Engelhardt 2018	6.9	A		0.9
Bayou Chitigue, LA	Wang 1997	20	C	B	Cahoon et al. 2006	16.8	A	X	0.4
Bayou Chitigue, LA	Day et al. 2011	67	C	B	Day et al. 2011	34.4	A	X	0.4
Old Oyster Bayou, LA	Day et al. 2011	107	C	B	Day et al. 2011	20.6	A	X	0.6
St. Jones, DE	Moskalski & Sommerfield, 2012	6	M	B	Kraft et al. 1992	4.3	R	X	1.7
Bombay Hook, DE	Sommerfield & Wong, 2011	9	C	S	Kraft et al. 1992	6.8	R	X	2.1
Bayou Penchant, LA	Lane et al. 2002	26.2	C	B	DeLaune et al. 1987	7.8	R	X	0.6
Fourleague Bay, LA	Lane et al. 2002	70	C	B	DeLaune et al. 1987	6.5	R	X	0.3

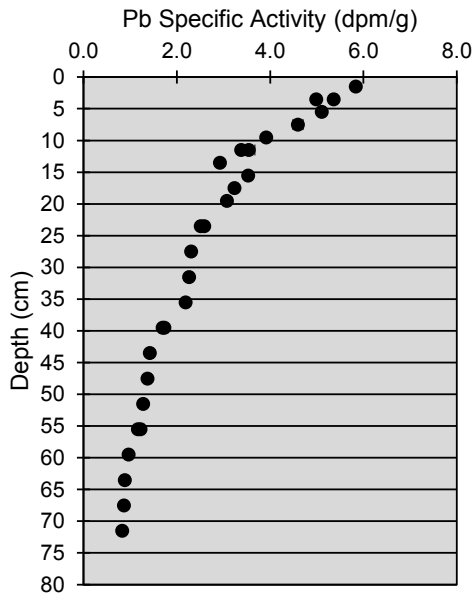| Location	Reference				Reference				
Napa River, CA	Buchanan & Ganju, 2003	49	C	S	Schile et al. 2014	3.2	R		2.9
Mallard Island, CA	Buchanan & Ganju, 2003	41	C	S	Schile et al. 2014	2.7	R		1.7
San Mateo Bridge, CA	Buchanan & Ganju, 2003	37	C	S	Patrick & Delaune, 1990	6	R		3
Far South SF Bay, CA	Buchanan & Ganju, 2003	62	C	S	Watson 2004	28	R		3
Tagus Estuary, Portual	Vale & Sundby, 1987	32	C	B	Salgueiro & Cacador 2007	37	A	X	4
Sylt, Wadden Sea, Germany	Scheurch et al. 2013	34	M	B	Scheurch et al. 2012	3.5	R		2
Skallingen, Denmark	Bartholdy & Anthony 1998	35	C	S	Bartholdy & Madsen 1985	9	R	X	1.6
Wax Lake Delta, LA	W. Wagner, unpublished	42	C	S	Wagner et al. 2017	16.9	E	X	1
Wax Lake Delta, LA	W. Wagner, unpublished	22	C	S	Wagner et al. 2017	14.9	E	X	1
Dyfi Estuary, Wales	S. Jackson, unpublished	15.7	C	B	Shi 1993	16.0	A		4.5
Delaware Bay Mouth	Haaf et al. 2019	50	C	B	Haaf et al. 2019	5.7	A		1.5
Delaware River	Haaf et al. 2019	16	C	B	Haaf et al. 2019	10.0	A		1.9
Barnegut Bay, NJ	Haaf et al. 2019	23	C	B	Haaf et al. 2019	4.2	A		0.4
San Pablo Bay, CA	Lacy et al. 2019	118	M	S	Lacy et al. 2019	8.0	A		2.5
Yinshuichuan, Yangtze, China	Chen et al. 2003	358	C	B	Yang et al. 2003	400	A	X	4.3
Suncheon Bay, South Korea	Lee et al. 2008	312	C	B	Lee et al. 2008	55	A	X	3.1
Allen Creek, Canada	Davidson-Arnott et al. 2002	117	M	S	van Proosdij et al., 2006	14	E		12
Kingsport, Canada	Proirier et al. 2017	53	M	S	Proirier et al. 2017	11.4	A		11

Supplementary Table 2: Additional details on the four low marsh monitoring sites.

Location	Site Affiliation	S. alterniflora form	Latitude	Longitude	Monitoring Duration	Accretion Verification
Plum Island, MA	PIE LTER	Short	42°43'55.43"N	70°50'30.78"W	9 months	Comparison to Wilson et al. 2014
Goodwin Island, VA	CB NERR	Tall	37°13'15.35"N	76°24'56.29"W	24 months	Aerial imagery and core properties
Mockhorn Island, VA	VCR LTER	Tall	37°16'51.35"N	75°52'44.83"W	18 months	Aerial imagery and core properties
South Altamaha, GA	GCE LTER	Tall	31°18'10.07"N	81°24'22.52"W	12 months	Aerial imagery and core properties
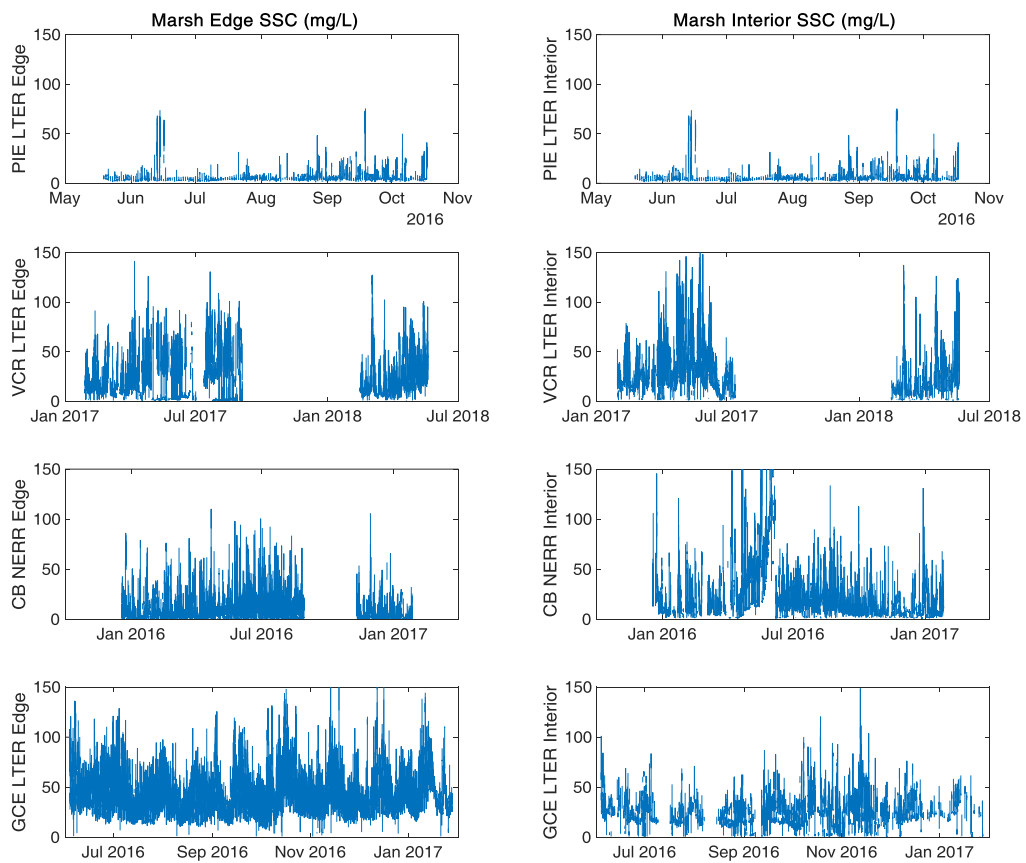
Supplementary Figure 2: SSC time series of the marsh edge and interior of the four low marsh sites. Note differences in the x-axis that correspond to different monitoring lengths. Gaps in the record represent times when the sensors were being repaired or field conditions prohibited site monitoring. Additional data for the PIE LTER can be found in Chapter 2.

PIE LTER Edge

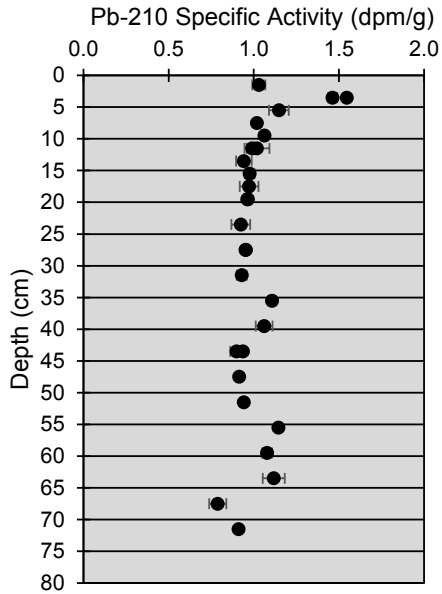Pb Specific Activity (dpm/g)
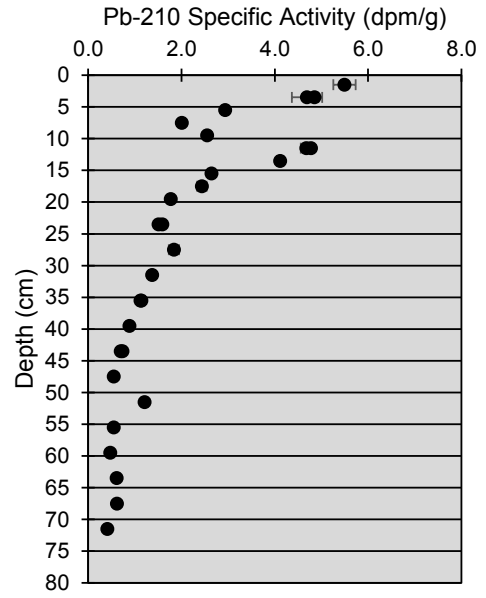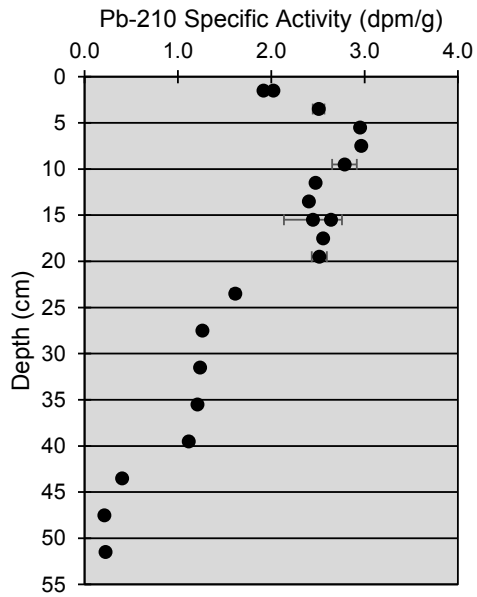
PIE LTER Interior

Pb-210 Specific Activity (dpm/g)

CB NERR Edge

Pb-210 Specific Activity (dpm/g)

CB NERR Interior

Pb-210 Specific Activity (dpm/g)
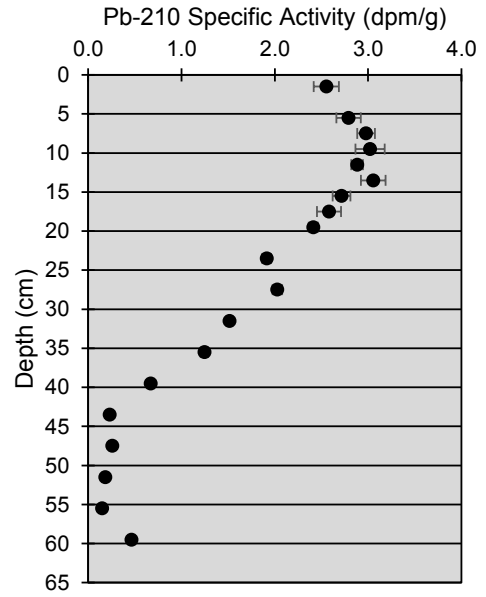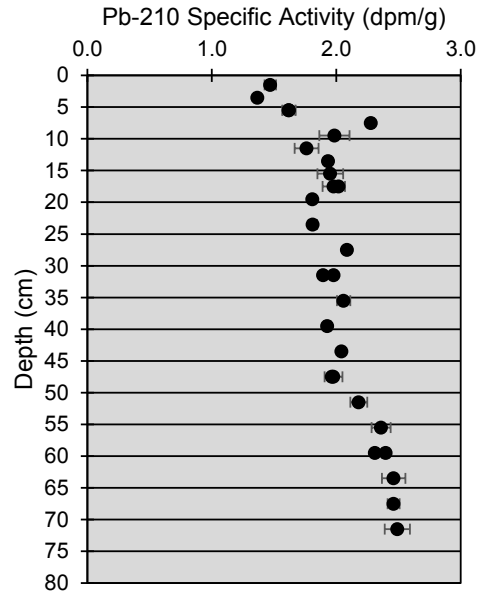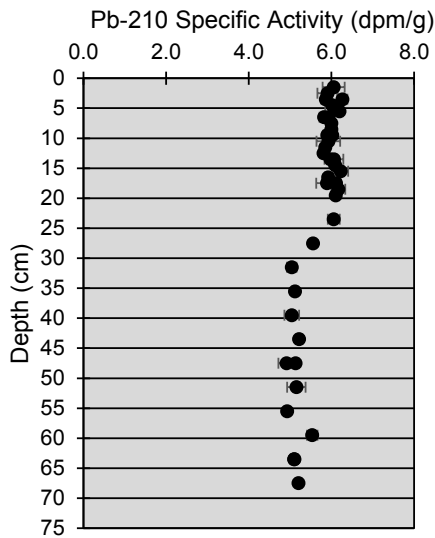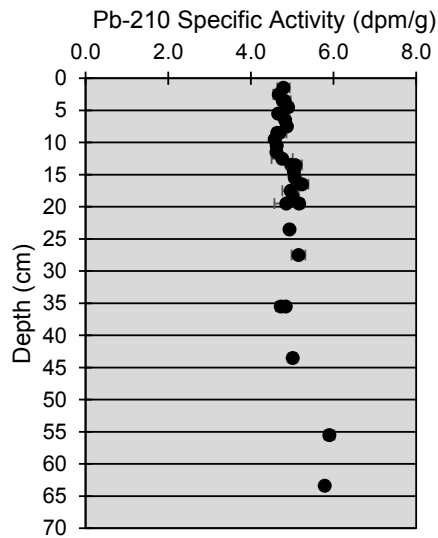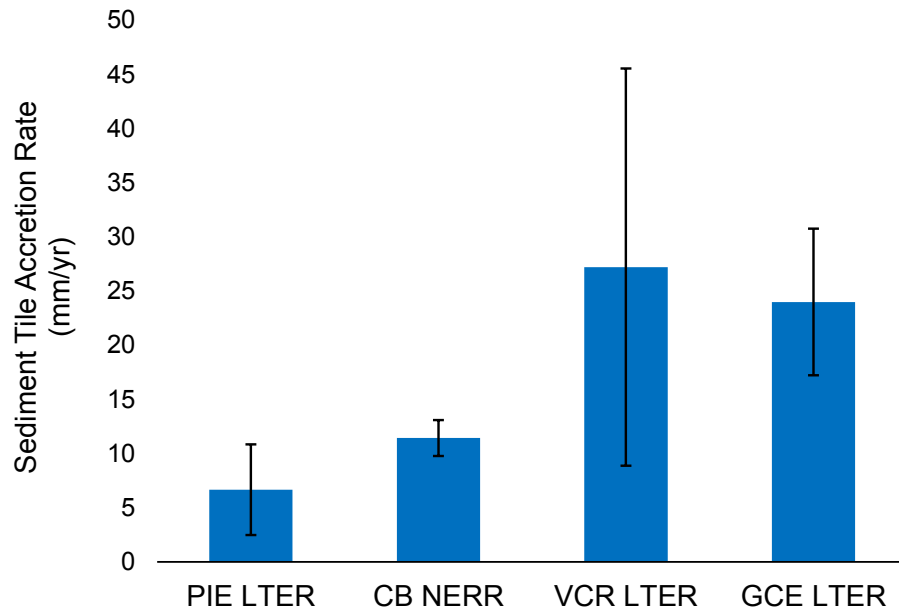
Supplementary Figure 3: Pb-210 total activity in sediment cores from the edge and interior of the four low marsh sites. Accretion rates of 6.6 mm yr^{-1} and 7.2 mm yr^{-1} were calculated for PIE LTER and CB NERR sites, respectively, whereas no accretion rate could be calculated for GCE LTER or VCR LTER.

Supplementary Figure 4: Vertical marsh accretion rate measured on top of sediment tiles and/or grids. Error bars represent one standard deviation. The rates shown for the VCR LTER and GCE LTER were used in lieu of radiochronological rates.

Supplementary Table 3: The three predictive empirical models used to calculate accretion are given with corresponding constants. The statistical measures are based on a linear regression between measured accretion and accretion predicted using the empirical model.

Model Type	Equation	Fitted Coefficients	RMSE	R^2	p-value
1. Simplest	$A = C_1 * SSC * TR$	C_1=0.22	21.3	0.89	<0.001
2. Logistic	$A = \left(\dfrac{C_1 - C_2}{1 + e^{C_3(TR-C_4)}} + C_2\right) * SSC$	C_1=1.10, C_2=0.18, C_3=-3.45, C_4=3.13	18.7	0.91	<0.001
3. Best Fit Linear	$A = C_1 * SSC + C_2 * TR + C_3 * SSC * TR$	C_1=-0.27, C_2=-10.1, C_3=0.32	18.1	0.92	<0.001
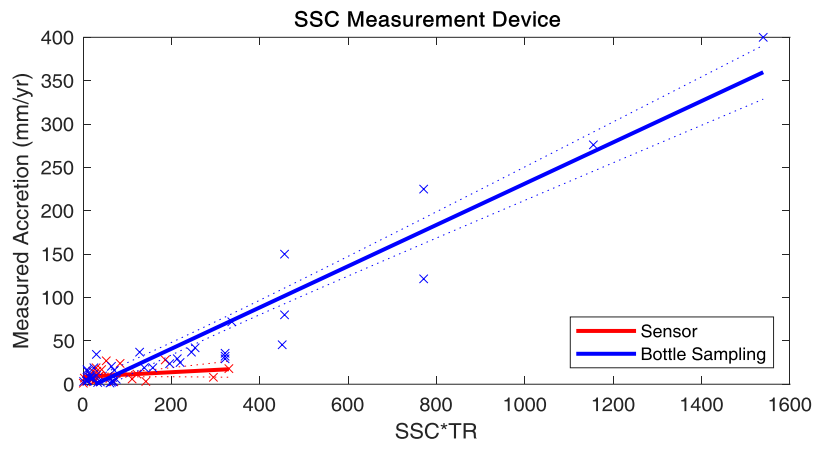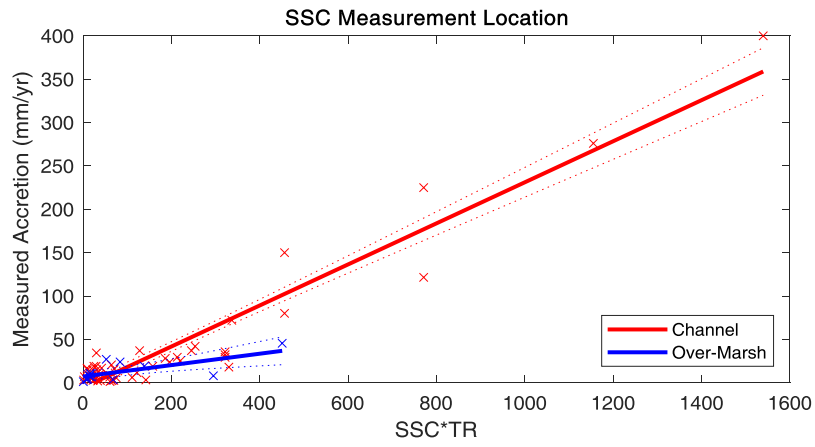
Supplementary Figure 5: Comparison of different SSC measurement methods. Note that channel sampling and bottle sampling are the dominant approaches.